Chapter 11
Aerodynamics

Antony Jameson
Stanford University, Stanford, CA, USA

1 FOCUS AND HISTORICAL BACKGROUND

1.1 Classical aerodynamics

This article surveys some of the principal developments of computational aerodynamics, with a focus on aeronautical applications. It is written with the perspective that computational mathematics is a natural extension of classical methods of applied mathematics, which has enabled the treatment of more complex, in particular nonlinear, mathematical models, and also the calculation of solutions in very complex geometric domains, not amenable to classical techniques such as the separation of variables.

Encyclopedia of Computational Mechanics, Edited by Erwin Stein, René de Borst and Thomas J.R. Hughes. Volume 3: *Fluids*.
 ISBN: 0-470-84699-2.

This is particularly true for aerodynamics. Efficient flight can be achieved only by establishing highly coherent flows. Consequently, there are many important applications where it is not necessary to solve the full Navier–Stokes equations in order to gain an insight into the nature of the flow, and useful predictions can be made with simplified mathematical models. It was already recognized by Prandtl (1904), and Schlichting and Gersten (1999), essentially contemporaneous with the first successful flights of the Wright brothers, that in flows at the large Reynolds numbers typical of powered flight, viscous effects are important chiefly in thin shear layers adjacent to the surface. While these boundary layers play a critical role in determining whether the flow will separate and how much circulation will be generated around a lifting surface, the equations of inviscid flow are a good approximation in the bulk of the flow field external to the boundary layer. In the absence of separation, a first estimate of the effect of the boundary layer is provided by regarding it as increasing the effective thickness of the body. This procedure can be justified by asymptotic analysis (Van Dyke, 1964; Ashley and Landahl, 1965).

The classical treatment of the external inviscid flow is based on Kelvin's theorem that in the absence of discontinuities the circulation around a material loop remains constant. Consequently, an initially irrotational flow remains irrotational. This allows us to simplify the equations further by representing the velocity as the gradient of a potential. If the flow is also regarded as incompressible, the governing equation reduces to Laplace's equation. These simplifications provided the basis for the classical airfoil theory of Glauert (1926) and Prandtl's wing theory (Ashley and Landahl, 1965; Prandtl and Tietjens, 1934). Supersonic flow over slender bodies at Mach numbers greater than two is also well represented by the linearized equations. Techniques for the solution of linearized flow were perfected in

the period 1935–1950, particularly by Hayes, who derived the supersonic area rule (Hayes, 1947).

Classical aerodynamic theory provided engineers with a good insight into the nature of the flow phenomena, and a fairly good estimate of the force on simple configurations such as an isolated wing, but could not predict the details of the flow over the complex configuration of a complete aircraft. Consequently, the primary tool for the development of aerodynamic configurations was the wind tunnel. Shapes were tested and modifications selected in the light of pressure and force measurements together with flow visualization techniques. In much the same way that Michelangelo, della Porta, and Fontana could design the dome of St. Peters through a good physical understanding of stress paths, so could experienced aerodynamicists arrive at efficient shapes through testing guided by good physical insight. Notable examples of the power of this method include the achievement of the Wright brothers in leaving the ground (after first building a wind tunnel), and more recently Whitcomb's discovery of the area rule for transonic flow, followed by his development of aft-loaded supercritical airfoils and winglets (Whitcomb, 1956, 1974, 1976). The process was expensive. More than 20 000 hours of wind-tunnel testing were expended in the development of some modern designs, such as the Boeing 747.

1.2 The emergence of computational aerodynamics and its application to transonic flow

Prior to 1960, computational methods were hardly used in aerodynamic analysis, although they were already widely used for structural analysis. The National Advisory Committee for Aeronautics (NACA) 6 series of airfoils had been developed during the forties, using hand computation to implement the Theodorsen method for conformal mapping (Theodorsen, 1931). The first major success in computational aerodynamics was the introduction of boundary integral methods by Hess and Smith (1962) to calculate potential flow over an arbitrary configuration. Generally known in the aeronautical community as panel methods, these continue to be used to the present day to make initial predictions of low speed aerodynamic characteristics of preliminary designs. It was the compelling need, however, both to predict transonic flow and to gain a better understanding of its properties and character that was a driving force for the development of computational aerodynamics through the period 1970 to 1990.

In the case of military aircraft capable of supersonic flight, the high drag associated with high g maneuvers forces them to be performed in the transonic regime. In the case of commercial aircraft, the importance of transonic flow stems from the Breguet range equation. This provides a good first estimate of range as

$$R = \frac{V}{sfc}\frac{L}{D}\log\frac{W_0 + W_f}{W_0} \tag{1}$$

Here V is the speed, L/D is the lift to drag ratio, sfc is the specific fuel consumption of the engines, W_0 is the landing weight, and W_f is the weight of the fuel burnt. The Breguet equation clearly exposes the multidisciplinary nature of the design problem. A lightweight structure is needed to minimize W_0. The specific fuel consumption is mainly the province of the engine manufacturers, and in fact, the largest advances during the last 30 years have been in engine efficiency. The aerodynamic designer should try to maximize VL/D. This means that the cruising speed should be increased until the onset of drag rise due to the formation of shock waves. Consequently, the best cruising speed is the transonic regime. The typical pattern of transonic flow over a wing section is illustrated in Figure 1.

Transonic flow had proved essentially intractable to analytic methods. Garabedian and Korn had demonstrated the feasibility of designing airfoils for shock-free flow in the transonic regime numerically by the method of complex characteristics (Bauer, Garabedian and Korn, 1972). Their method was formulated in the hodograph plane, and it required great skill to obtain solutions corresponding to physically realizable shapes. It was also known from Morawetz's theorem (Morawetz, 1956) that shock-free transonic solutions are isolated points.

A major breakthrough was accomplished by Murman and Cole (1971) with their development of type-dependent differencing in 1970. They obtained stable solutions by simply switching from central differencing in the subsonic zone to upwind differencing in the supersonic zone and using

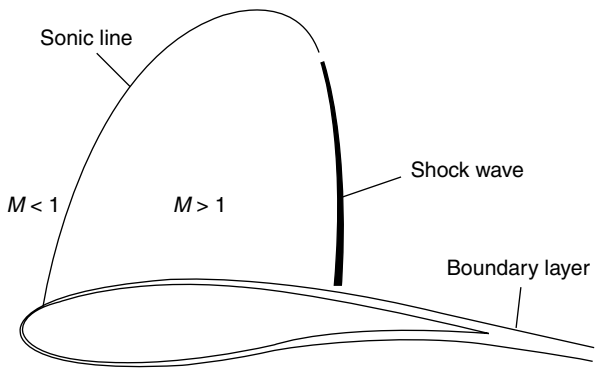

Figure 1. Transonic flow past an airfoil.

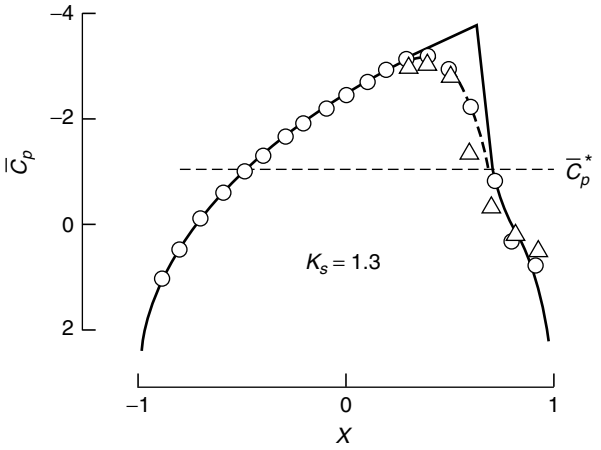

Figure 2. Scaled pressure coefficient on surface of a thin, circular-arc airfoil in transonic flow, compared with experimental data; solid line represents computational result.

a line-implicit relaxation scheme. Their discovery provided major impetus for the further development of computational fluid dynamics (CFD) by demonstrating that solutions for steady transonic flows could be computed economically. Figure 2 taken from their landmark paper illustrates the scaled pressure distribution on the surface of a symmetric airfoil. Efforts were soon underway to extend their ideas to more general transonic flows.

Numerical methods to solve transonic potential flow over complex configurations were essentially perfected during the period 1970 to 1982. The American Institute of Aeronautics and Astronautics (AIAA) First Computational Fluid Dynamics Conference, held in Palm Springs in July 1973, signified the emergence of CFD as an accepted tool for airplane design, and seems to mark the first use of the name CFD. The rotated difference scheme for transonic potential flow, first introduced by the author at this conference, proved to be a very robust method, and it provided the basis for the computer program flo22, developed with David Caughey during 1974 to 1975 to predict transonic flow past swept wings. At the time we were using the Control Data Corporation (CDC) 6600, which had been designed by Seymour Cray and was the world's fastest computer at its introduction, but had only 131 000 words of memory. This forced the calculation to be performed one plane at a time, with multiple transfers from the disk. Flo22 was immediately put into use at McDonnell Douglas. A simplified in-core version of flo22 is still in use at Boeing Long Beach today. Figure 3, shows the result of a recent calculation, using flo22, of transonic flow over the wing of a proposed aircraft to fly in the Martian atmosphere. The result was obtained with 100 iterations on a $192 \times 32 \times 32$ mesh in 7 seconds, using a typical modern workstation. When flo22 was first introduced at Long Beach, the calculations cost $3000 each. Nevertheless, they found it worthwhile to use it extensively for the aerodynamic design of the C17 military cargo aircraft.

In order to treat complete configurations, it was necessary to develop discretization formulas for arbitrary grids. An approach that proved successful (Jameson and Caughey, 1977), is to derive the discretization formulas from the Bateman variational principle that the integral of the pressure over the domain,

$$I = \int_D p \, \mathrm{d}\xi$$

is stationary (Jameson, 1978). The resulting scheme is essentially a finite element scheme using trilinear isoparametric elements. It can be stabilized in the supersonic zone by the introduction of artificial viscosity to produce an upwind bias. The 'hour-glass' instability that results from the use of one point integration scheme is suppressed by the introduction of higher-order coupling terms based on mixed derivatives. The flow solvers (flo27-30) based on this approach were subsequently incorporated in Boeing's A488 software, which was used in the aerodynamic design of Boeing commercial aircraft throughout the eighties (Rubbert, 1994).

In the same period, Perrier was focusing the research efforts at Dassault on the development of finite element methods using triangular and tetrahedral meshes, because he believed that if CFD software was to be really useful for aircraft design, it must be able to treat complete configurations. Although finite element methods were more computationally expensive, and mesh generation continued to present difficulties, finite element methods offered a route toward the achievement of this goal. The Dassault/INRIA group was ultimately successful, and they performed transonic potential flow calculations for complete aircraft such as the Falcon 50 in the early eighties (Bristeau *et al.*, 1985).

1.3 The development of methods for the Euler and Navier–Stokes equations

By the eighties, advances in computer hardware had made it feasible to solve the full Euler equations using software that could be cost-effective in industrial use. The idea of directly discretizing the conservation laws to produce a finite volume scheme had been introduced by MacCormack and Paullay (1972). Most of the early flow solvers tended to exhibit strong pre- or post-shock oscillations. Also, in a workshop held in Stockholm in 1979, (Rizzi and Viviand, 1979) it was apparent that none of the existing schemes converged to a steady state. These difficulties were resolved during the following decade.

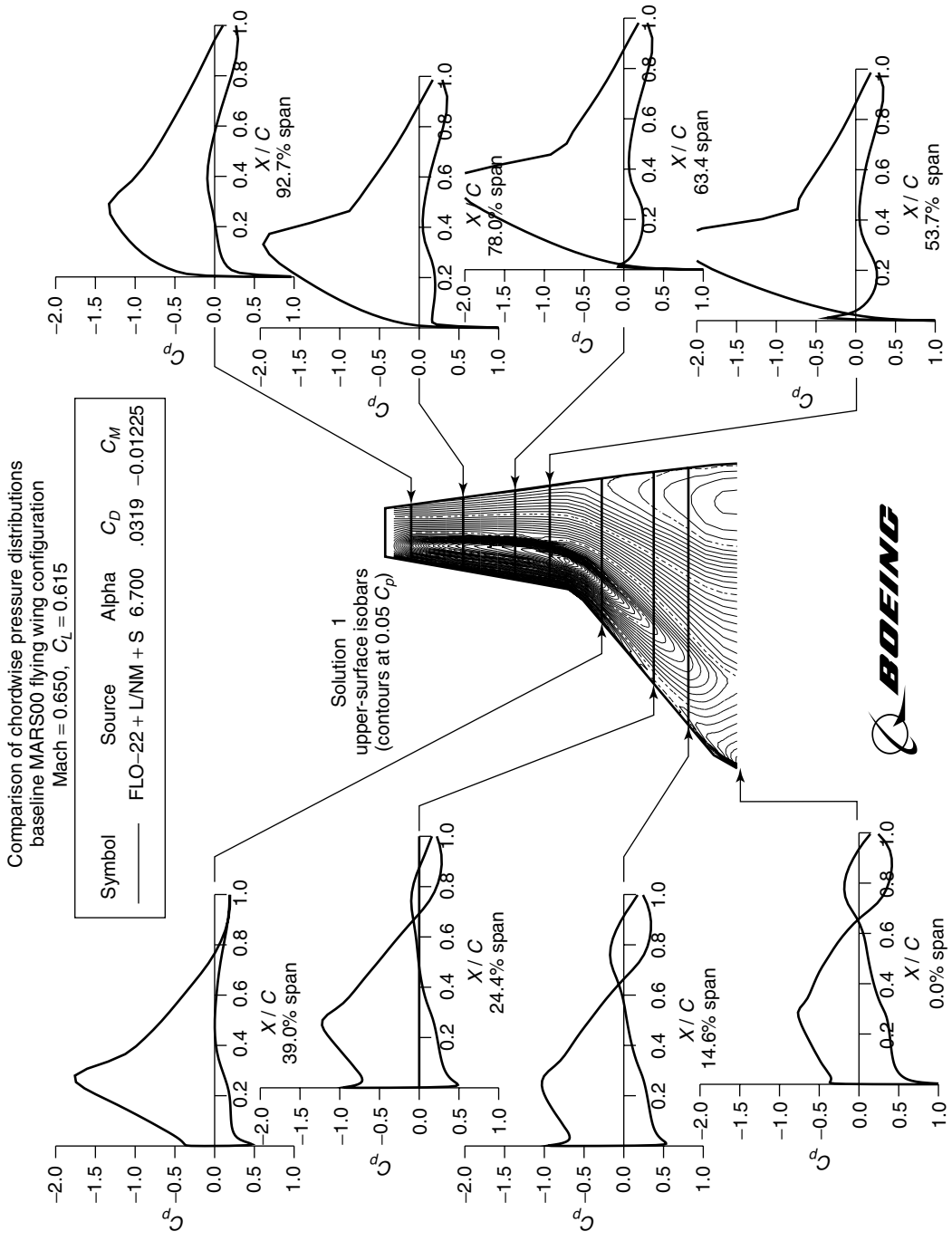

Figure 3. Pressure distribution over the wing of a Mars Lander using flo22 (supplied by John Vassberg).

The Jameson–Schmidt–Turkel (JST) scheme (Jameson, Schmidt, and Turkel, 1981), which used Runge–Kutta time stepping and a blend of second- and fourth-differences (both to control oscillations and to provide background dissipation), consistently demonstrated convergence to a steady state, with the consequence that it has remained one of the most widely used methods to the present day.

A fairly complete understanding of shock-capturing algorithms was achieved, stemming from the ideas of Godunov, Van Leer, Harten, and Roe. The issue of oscillation control and positivity had already been addressed by Godunov (1959) in his pioneering work in the 1950s (translated into English in 1959). He had introduced the concept of representing the flow as piecewise constant in each computational cell, and solving a Riemann problem at each interface, thus obtaining a first-order accurate solution that avoids nonphysical features such as expansion shocks. When this work was eventually recognized in the West, it became very influential. It was also widely recognized that numerical schemes might benefit from distinguishing the various wave speeds, and this motivated the development of characteristics-based schemes.

The earliest higher-order characteristics-based methods used flux vector splitting (Steger and Warming, 1981), but suffered from oscillations near discontinuities similar to those of central-difference schemes in the absence of numerical dissipation. The monotone upwind scheme for conservation laws (MUSCL) of Van Leer (1974) extended the monotonicity-preserving behavior of Godunov's scheme to higher order through the use of limiters. The use of limiters dates back to the flux-corrected transport (FCT) scheme of Boris and Book (1973). A general framework for oscillation control in the solution of nonlinear problems was provided by Harten's concept of total variation diminishing (TVD) schemes. It finally proved possible to give a rigorous justification of the JST scheme (Jameson, 1995a,b).

Roe's introduction of the concept of locally linearizing the equations through a mean value Jacobian (Roe, 1981) had a major impact. It provided valuable insight into the nature of the wave motions and also enabled the efficient implementation of Godunov-type schemes using approximate Riemann solutions. Roe's flux-difference splitting scheme has the additional benefit that it yields a single-point numerical shock structure for stationary normal shocks. Roe's and other approximate Riemann solutions, such as that due to Osher, have been incorporated in a variety of schemes of Godunov type, including the essentially nonoscillatory (ENO) schemes of Harten *et al.* (1987).

Solution methods for the Reynolds-averaged Navier–Stokes (RANS) equations had been pioneered in the seventies by MacCormack and others, but at that time they were extremely expensive. By the nineties, computer technology had progressed to the point where RANS simulations could be performed with manageable costs, and they began to be fairly widely used by the aircraft industry. The need for robust and reliable methods to predict hypersonic flows, which contain both very strong shock wave and near vacuum regions, gave a further impetus to the development of advanced shock-capturing algorithms for compressible viscous flow.

1.4 Overview of the article

The development of software for aerodynamic simulation can be broken down into five main steps.

1. The choice of a mathematical model that represents the physical phenomena that are important for the application;
2. mathematical analysis of the model to ensure existence and uniqueness of the solutions;
3. formulation of a stable and convergent discretization scheme;
4. implementation in software;
5. validation.

Thorough validation is difficult and time consuming. It should include verification procedures for program correctness and consistency checks. For example, does the numerical solution of a symmetric profile at zero angle of attack preserve the symmetry, with no lift? It should also include mesh refinement studies to verify convergence and, ideally, comparisons with the results of other computer programs that purport to solve the same equations. Finally, if it is sufficiently well established that the software provides an accurate solution of the chosen mathematical model, comparisons with experimental data should show whether the model adequately represents the true physics or establish its range of applicability.

This article is primarily focused on the third step, discretization. The complexity of predicting highly nonlinear transonic and hypersonic flows has forced the emergence of an entirely new class of numerical algorithms and a supporting body of theory, which is reviewed in this article. Section 2 presents a brief survey of the mathematical models of fluid flow that are relevant to different flight regimes. Section 3 surveys potential flow methods, which continue to be useful for preliminary design because of their low computational costs and rapid turn around. Section 4 focuses on the formulation of shock-capturing methods

for the Euler and RANS equations. Section 5 discusses alternative ways to discretize the equations in complex geometric domains using either structured or unstructured meshes. Section 6 discusses time-stepping schemes, including convergence acceleration techniques for steady flows and the formulation of accurate and efficient time-stepping techniques for unsteady flows. The article concludes with a discussion of methods to solve inverse and optimum shape-design problems.

2 MATHEMATICAL MODELS OF FLUID FLOW

The Navier–Stokes equations state the laws of conservation of mass, momentum, and energy for the flow of a gas in thermodynamic equilibrium. In the Cartesian tensor notation, let x_i be the coordinates, p, ρ, T, and E the pressure, density, temperature, and total energy, and u_i the velocity components. Each conservation equation has the form

$$\frac{\partial w}{\partial t} + \frac{\partial f_j}{\partial x_j} = 0 \tag{2}$$

For the mass equation

$$w = \rho, \quad f_j = \rho u_j \tag{3}$$

For the i momentum equation

$$w_i = \rho u_i, \quad f_{ij} = \rho u_i u_j + p\delta_{ij} - \sigma_{ij} \tag{4}$$

where σ_{ij} is the viscous stress tensor, which for a Newtonian fluid is proportional to the rate of strain tensor and the bulk dilatation. If μ and λ are the coefficients of viscosity and bulk viscosity, then

$$\sigma_{ij} = \mu\left(\frac{\partial u_i}{\partial x_j} + \frac{\partial u_j}{\partial x_i}\right) + \lambda\delta_{ij}\left(\frac{\partial u_k}{\partial x_k}\right) \tag{5}$$

Typically $\lambda = -2\mu/3$. For the energy equation

$$w = \rho E, \quad f_j = \rho H u_j - \sigma_{jk}u_k - \kappa\frac{\partial T}{\partial x_j} \tag{6}$$

where κ is the coefficient of heat conduction and H is the total enthalpy,

$$H = E + \frac{p}{\rho}$$

In the case of a perfect gas, the pressure is related to the density and energy by the equation of state

$$p = (\gamma - 1)\rho\left(E - \tfrac{1}{2}q^2\right) \tag{7}$$

where

$$q^2 = u_i u_i$$

and γ is the ratio of specific heats. The coefficient of thermal conductivity and the temperature satisfy the relations

$$k = \frac{c_p\mu}{Pr}, \quad T = \frac{p}{R\rho} \tag{8}$$

where c_p is the specific heat at constant pressure, R is the gas constant, and Pr is the Prandtl number. Also the speed of sound c is given by the ratio

$$c^2 = \frac{\gamma p}{\rho} \tag{9}$$

and a key dimensionless parameter governing the effects of compressibility is the Mach number

$$M = \frac{q}{c}$$

where q is the magnitude of the velocity.

If the flow is inviscid, the boundary condition that must be satisfied at a solid wall is

$$\mathbf{u}\cdot\mathbf{n} = u_i n_i = 0 \tag{10}$$

where $\mathbf{n}$ denotes the normal to the surface. Viscous flows must satisfy the 'no-slip' condition

$$\mathbf{u} = 0 \tag{11}$$

Viscous solutions also require a boundary condition for the energy equation. The usual practice in pure aerodynamic simulations is either to specify the isothermal condition

$$T = T_0 \tag{12}$$

or to specify the adiabatic condition

$$\frac{\partial T}{\partial n} = 0 \tag{13}$$

corresponding to zero heat transfer. The calculation of heat transfer requires an appropriate coupling to a model of the structure.

For an external flow, the flow variables should approach free-stream values

$$p = p_\infty, \quad \rho = \rho_\infty, \quad T = T_\infty, \quad \mathbf{u} = \mathbf{u}_\infty$$

for upstream at the inflow boundary. If any entropy is generated, the density for downstream at the outflow boundary cannot recover to ρ_∞ if the pressure recovers to p_∞. In fact, if trailing vortices persist downstream, the pressure does not recover to p_∞. In general, it is necessary to examine the incoming and outgoing waves at the outer boundaries of the flow domain. Boundary values should then only be imposed for quantities transported by the incoming waves. In a subsonic flow, there are four incoming waves at the inflow boundary, and one escaping acoustic wave. Correspondingly, four quantities should be specified. At the outflow boundary, there are four outgoing waves, so one quantity should be specified. One way to do this is to introduce Riemann invariants corresponding to a one-dimensional flow normal to the boundary, as will be discussed in Section 5.4. In a supersonic flow, all quantities should be fixed at the inflow boundary, while they should all be extrapolated at the outflow boundary. The proper specification of inflow and outflow boundary conditions is particularly important in the calculation of internal flows. Otherwise spurious wave reflections may severely corrupt the solution.

In smooth regions of the flow, the inviscid equations can be written in quasilinear form as

$$\frac{\partial w}{\partial t} + A_i \frac{\partial w}{\partial x_i} = 0 \tag{14}$$

where A_i are the Jacobians $\partial f_i / \partial w$. By transforming to the symmetrizing variables, which may be written in differential form as

$$\mathrm{d}\widetilde{w} = \left(\frac{\mathrm{d}p}{\rho c},\ \mathrm{d}u_1,\ \mathrm{d}u_2,\ \mathrm{d}u_3,\ \mathrm{d}p - c^2\,\mathrm{d}\rho \right)^T \tag{15}$$

the Jacobians assume the symmetric form

$$\tilde{A}_i = \begin{bmatrix} u_i & \delta_{i1}c & \delta_{i2}c & \delta_{i3}c & 0 \\ \delta_{i1}c & u_i & 0 & 0 & 0 \\ \delta_{i2}c & 0 & u_i & 0 & 0 \\ \delta_{i3}c & 0 & 0 & u_i & 0 \\ 0 & 0 & 0 & 0 & u_i \end{bmatrix} \tag{16}$$

where δ_{ij} are the Kronecker deltas. Equation (14) becomes

$$\frac{\partial \widetilde{w}}{\partial t} + \tilde{A}_i \frac{\partial \widetilde{w}}{\partial x_i} = 0 \tag{17}$$

The Jacobians for the conservative variables may now be expressed as

$$A_i = T \tilde{A}_i T^{-1} \tag{18}$$

where

$$T^{-1} = \frac{\partial \widetilde{w}}{\partial w} =$$

$$\begin{bmatrix} (\gamma-1)\dfrac{q^2}{2\rho c} & -(\gamma-1)\dfrac{u_1}{\rho c} & -(\gamma-1)\dfrac{u_2}{\rho c} & -(\gamma-1)\dfrac{u_3}{\rho c} & \dfrac{\gamma-1}{\rho c} \\ -\dfrac{u_1}{\rho} & \dfrac{1}{\rho} & 0 & 0 & 0 \\ -\dfrac{u_2}{\rho} & 0 & \dfrac{1}{\rho} & 0 & 0 \\ -\dfrac{u_3}{\rho} & 0 & 0 & \dfrac{1}{\rho} & 0 \\ (\gamma-1)\dfrac{q^2}{2} - c^2 & -(\gamma-1)u_1 & -(\gamma-1)u_2 & -(\gamma-1)u_3 & \gamma-1 \end{bmatrix}$$

and

$$T = \frac{\partial w}{\partial \widetilde{w}} = \begin{bmatrix} \dfrac{\rho}{c} & 0 & 0 & 0 & -\dfrac{1}{c^2} \\ \dfrac{\rho u_1}{c} & \rho & 0 & 0 & -\dfrac{u_1}{c^2} \\ \dfrac{\rho u_2}{c} & 0 & \rho & 0 & -\dfrac{u_2}{c^2} \\ \dfrac{\rho u_3}{c} & 0 & 0 & \rho & -\dfrac{u_3}{c^2} \\ \dfrac{\rho H}{c} & \rho u_1 & \rho u_2 & \rho u_3 & -\dfrac{q^2}{2c^2} \end{bmatrix} \tag{19}$$

The decomposition (17) clearly exposes the wave structure in solutions of the gas-dynamic equations. The wave speeds appear as the eigenvalues of the linear combination

$$\tilde{A} = n_i \tilde{A}_i \tag{20}$$

where $\mathbf{n}$ is a unit direction vector. They are

$$\left[q_n + c,\ q_n - c,\ q_n,\ q_n,\ q_n \right]^T \tag{21}$$

where $q_n = \mathbf{q} \cdot \mathbf{n}$. Corresponding to the fact that $\tilde{A}$ is symmetric, one can find a set of orthogonal eigenvectors, which may be normalized to unit length. Then one can express

$$\tilde{A} = \widetilde{M} \Lambda \widetilde{M}^{-1} \tag{22}$$

where Λ is diagonal, with the eigenvalues as its elements. The modal matrix $\widetilde{M}$ containing the eigenvectors as its

columns is

$$\widetilde{M} = \begin{bmatrix} \frac{1}{\sqrt{2}} & -\frac{1}{\sqrt{2}} & 0 & 0 & 0 \\ \frac{n_1}{\sqrt{2}} & \frac{n_1}{\sqrt{2}} & 0 & -n_3 & n_2 \\ \frac{n_2}{\sqrt{2}} & \frac{n_2}{\sqrt{2}} & n_3 & 0 & -n_1 \\ \frac{n_3}{\sqrt{2}} & \frac{n_3}{\sqrt{2}} & -n_2 & n_1 & 0 \\ 0 & 0 & n_1 & n_2 & n_3 \end{bmatrix} \tag{23}$$

and $\widetilde{M}^{-1} = \widetilde{M}^T$. The Jacobian matrix $A = n_i A_i$ now takes the form

$$A = M \Lambda M^{-1} \tag{24}$$

where

$$M = T\widetilde{M}, \quad M^{-1} = \widetilde{M}^T T^{-1} \tag{25}$$

In the design of difference schemes, it proves useful to introduce the absolute Jacobian matrix $|A|$, in which the eigenvalues are replaced by their absolute values, as will be discussed in Section 4.4.

Corresponding to the thermodynamic relation

$$\frac{\mathrm{d}p}{\rho} = \mathrm{d}h - T\,\mathrm{d}\mathcal{S}$$

where $\mathcal{S}$ is the entropy $\log(p/\rho^{\gamma-1})$, the last variable of $\mathrm{d}\widetilde{w}$ corresponds to $p\,\mathrm{d}\mathcal{S}$, since $c^2 = (\mathrm{d}p/\mathrm{d}\rho)$. It follows that in the absence of shock waves $\mathcal{S}$ is constant along streamlines. If the flow is isentropic, then $(\mathrm{d}p/\mathrm{d}\rho) \propto \rho^{\gamma-1}$, and the first variable can be integrated to give $2c/(\gamma-1)$. Then we may take the transformed variables as

$$\widetilde{w} = \left(\frac{2c}{\gamma - 1}, u_1, u_2, u_3, \mathcal{S} \right)^T \tag{26}$$

In the case of a one-dimensional flow, the equations for the Riemann invariants are recovered by adding and subtracting the equations for $2c/(\gamma-1)$ and u_1.

In order to calculate solutions for flows in complex geometric domains, it is often useful to introduce body-fitted coordinates through global, or, as in the case of isoparametric elements, local transformations. With the body now coinciding with a coordinate surface, it is much easier to enforce the boundary conditions accurately. Suppose that the mapping to computational coordinates (ξ_1, ξ_2, ξ_3) is defined by the transformation matrices

$$K_{ij} = \frac{\partial x_i}{\partial \xi_j}, \quad K_{ij}^{-1} = \frac{\partial \xi_i}{\partial x_j}, \quad J = \det(K) \tag{27}$$

The Navier–Stokes equations (2–6) become

$$\frac{\partial}{\partial t}(Jw) + \frac{\partial}{\partial \xi_i} F_i(w) = 0 \tag{28}$$

Here the transformed fluxes are

$$F_i = S_{ij} f_j \tag{29}$$

where

$$S = JK^{-1} \tag{30}$$

The elements of S are the cofactors of K, and in a finite volume discretization, they are just the face areas of the computational cells projected in the x_1, x_2, and x_3 directions. Using the permutation tensor ϵ_{ijk} we can express the elements of S as

$$S_{ij} = \frac{1}{2} \epsilon_{jpq} \epsilon_{irs} \frac{\partial x_p}{\partial \xi_r} \frac{\partial x_q}{\partial \xi_s} \tag{31}$$

Then

$$\frac{\partial}{\partial \xi_i} S_{ij} = \frac{1}{2} \epsilon_{jpq} \epsilon_{irs} \left(\frac{\partial^2 x_p}{\partial \xi_r \partial \xi_i} \frac{\partial x_q}{\partial \xi_s} + \frac{\partial x_p}{\partial \xi_r} \frac{\partial^2 x_q}{\partial \xi_s \partial \xi_i} \right) = 0 \tag{32}$$

Defining scaled contravariant velocity components as

$$U_i = S_{ij} u_j \tag{33}$$

the flux formulas may be expanded as

$$F_i = \begin{Bmatrix} \rho U_i \\ \rho U_i u_1 + S_{i1} p \\ \rho U_i u_2 + S_{i2} p \\ \rho U_i u_3 + S_{i3} p \\ \rho U_i H \end{Bmatrix} \tag{34}$$

If we choose a coordinate system so that the boundary is at $\xi_l = 0$, the wall boundary condition for inviscid flow is now

$$U_l = 0 \tag{35}$$

An indication of the relative magnitude of the inertial and viscous terms is given by the Reynolds number

$$Re = \frac{\rho U L}{\mu} \tag{36}$$

where U is a characteristic velocity and L a representative length. The viscosity of air is very small, and typical

Reynolds numbers for the flow past a component of an aircraft such as a wing are of the order of 10^7 or more, depending on the size and speed of the aircraft. In this situation, the viscous effects are essentially confined to thin boundary layers covering the surface. Boundary layers may nevertheless have a global impact on the flow by causing separation. Unfortunately, unless they are controlled by active means such as suction through a porous surface, boundary layers are unstable and generally become turbulent.

Using dimensional analysis, Kolmogorov's theory of turbulence (Kolmogorov, 1941) estimates the length scales of the smallest persisting eddies to be of order $(1/Re^{3/4})$ in comparison with the macroscopic length scale of the flow. Accordingly the computational requirements for the full simulation of all scales of turbulence can be estimated as growing proportionally to $Re^{9/4}$, and are clearly beyond the reach of current computers. Turbulent flows may be simulated by the RANS equations, where statistical averages are taken of rapidly fluctuating components. Denoting fluctuating parts by primes and averaging by an overbar, this leads to the appearance of Reynolds stress terms of the form $\overline{\rho u_i' u_j'}$, which cannot be determined from the mean values of the velocity and density. Estimates of these additional terms must be provided by a turbulence model. The simplest turbulence models augment the molecular viscosity by an eddy viscosity that crudely represents the effects of turbulent mixing, and is estimated with some characteristic length scale such as the boundary layer thickness. A rather more elaborate class of models introduces two additional equations for the turbulent kinetic energy and the rate of dissipation. Existing turbulence models are adequate for particular classes of flow for which empirical correlations are available, but they are generally not capable of reliably predicting more complex phenomena, such as shock wave–boundary layer interaction. The current status of turbulence modeling is reviewed by Wilcox (1998), Haase *et al.* (1997), Leschziner (2003), and Durbin (see **Chapter 10, this Volume**, *Reynolds averaged turbulence modeling*) in an article in this Encyclopedia.

Outside the boundary layer, excellent predictions can be made by treating the flow as inviscid. Setting $\sigma_{ij} = 0$ and eliminating heat conduction from equations (3, 4, and 6) yields the Euler equations for inviscid flow. These are a very useful model for predicting flows over aircraft. According to Kelvin's theorem, a smooth inviscid flow that is initially irrotational remains irrotational. This allows one to introduce a velocity potential ϕ such that $u_i = \partial\phi/\partial x_i$. The Euler equations for a steady flow now reduce to

$$\frac{\partial}{\partial x_i}\left(\rho\frac{\partial\phi}{\partial x_i}\right) = 0 \tag{37}$$

In a steady inviscid flow, it follows from the energy equation (6) and the continuity equation (3) that the total enthalpy is constant

$$H = \frac{c^2}{\gamma - 1} + \frac{1}{2}u_i u_i = H_\infty \tag{38}$$

where the subscript ∞ is used to denote the value in the far field. According to Crocco's theorem, vorticity in a steady flow is associated with entropy production through the relation

$$\mathbf{u} \times \boldsymbol{\omega} + T\nabla\mathcal{S} = \nabla H = 0$$

where $\mathbf{u}$ and $\boldsymbol{\omega}$ are the velocity and vorticity vectors, T is the temperature, and $\mathcal{S}$ is the entropy. Thus, the introduction of a velocity potential is consistent with the assumption of isentropic flow.

Substituting the isentropic relationship $p/\rho^\gamma = \text{constant}$, and the formula for the speed of sound, equation (38) can be solved for the density as

$$\frac{\rho}{\rho_\infty} = \left[1 + \frac{\gamma - 1}{2}M_\infty^2\left(1 - \frac{u_i u_i}{u_\infty^2}\right)\right]^{1/(\gamma-1)} \tag{39}$$

It can be seen from this equation that

$$\frac{\partial\rho}{\partial u_i} = -\frac{\rho u_i}{c^2} \tag{40}$$

and correspondingly in isentropic flow

$$\frac{\partial p}{\partial u_i} = \frac{\mathrm{d}p}{\mathrm{d}\rho}\frac{\partial\rho}{\partial u_i} = -\rho u_i \tag{41}$$

Substituting $(\partial\rho/\partial x_j) = (\partial\rho/\partial u_i)(\partial u_i/\partial x_j)$, the potential flow equation (37) can be expanded in quasilinear form as

$$c^2\frac{\partial^2\phi}{\partial x_i^2} - u_i u_j\frac{\partial^2\phi}{\partial x_i\partial x_j} = 0 \tag{42}$$

If the flow is locally aligned, say, with the x_1 axis, equation (42) reads as

$$(1 - M^2)\frac{\partial^2\phi}{\partial x_1^2} + \frac{\partial^2\phi}{\partial x_2^2} + \frac{\partial^2\phi}{\partial x_3^2} = 0 \tag{43}$$

where M is the Mach number u_1/c. The change from an elliptic to a hyperbolic partial differential equation as the flow becomes supersonic is evident.

The potential flow equation (42) also corresponds to the Bateman variational principle that the integral over the

domain of the pressure

$$I = \int_D p \, d\xi \tag{44}$$

is stationary. Here $d\xi$ denotes the volume element. Using the relation (41), a variation δp results in a variation

$$\delta I = \int_D \frac{\partial p}{\partial u_i} \delta u_i \, d\xi = - \int \rho u_i \frac{\partial}{\partial x_i} \delta\phi \, d\xi$$

or, on integrating by parts with appropriate boundary conditions

$$\delta I = \int_D \frac{\partial}{\partial x_i} \left(\rho \frac{\partial \phi}{\partial x_i} \right) \delta\phi \, d\xi$$

Then $\delta I = 0$ for an arbitrary variation $\delta\phi$ if equation (37) holds.

The equations of inviscid supersonic flow admit discontinuous solutions, both shock waves and contact discontinuities, which satisfy the Rankine Hugoniot jump conditions (Liepmann and Roshko, 1957). Only compression shock waves are admissible, corresponding to the production of entropy. Expansion shock waves cannot occur because they would correspond to a decrease in entropy.

Because shock waves generate entropy, they cannot be exactly modeled by the potential flow equations. The amount of entropy generated is proportional to $(M-1)^3$ where M is the Mach number upstream of the shock. Accordingly, weak solutions admitting isentropic jumps that conserve mass but not momentum are a good approximation to shock waves, as long as the shock waves are quite weak (with a Mach number < 1.3 for the normal velocity component upstream of the shock wave). Stronger shock waves tend to separate the flow, with the result that the inviscid approximation is no longer adequate. Thus this model is well balanced, and it has proved extremely useful for the prediction of the cruising performance of transport aircraft. An estimate of the pressure drag arising from shock waves is obtained because of the momentum deficit through an isentropic jump.

If one assumes small disturbances about a free stream in the x_i direction, and a Mach number close to unity, equation (43) can be reduced to the transonic small disturbance equation in which M^2 is estimated as

$$M_\infty^2 \left[1 - (\gamma + 1) \frac{\partial \phi}{\partial x_1} \right]$$

This is the simplest nonlinear model of compressible flow.

The final level of approximation is to linearize equation (43) by replacing M^2 by its free-stream value M_∞^2. In the subsonic case, the resulting Prandtl–Glauert equation can be reduced to Laplace's equation by scaling the x_i coordinate by $(1 - M_\infty^2)^{1/2}$. Irrotational incompressible flow satisfies the Laplace's equation, as can be seen by setting $\rho =$ constant, in equation (37). The relationships between some of the widely used mathematical models is illustrated in Figure 4. With limits on the available computing power, and the cost of the calculations, one has to make a trade-off between the complexity of the mathematical model and the complexity of the geometric configuration to be treated.

The computational requirements for aerodynamic simulation are a function of the number of operations required per mesh point, the number of cycles or time steps needed to reach a solution, and the number of mesh points needed to resolve the important features of the flow. Algorithms for the three-dimensional transonic potential flow equation require about 500 floating-point operations per mesh point per cycle. The number of operations required for an Euler simulation is in the range of 1000 to 5000 per time step, depending on the complexity of the algorithm. The number of mesh intervals required to provide an accurate representation of a two-dimensional inviscid transonic flow is of the order of 160 wrapping around the profile, and 32 normal to the airfoil. Correspondingly, about 200 000 mesh cells are sufficient to provide adequate resolution of three-dimensional inviscid transonic flow past a swept wing, and this number needs to be increased to provide a good simulation of a more complex configuration such as a complete aircraft. The requirements for viscous simulations by means of turbulence models are much more severe. Good resolution of a turbulent boundary layer needs about 32 intervals inside the boundary layer, with the result that a typical mesh for a two-dimensional Navier–Stokes calculation contains 512 intervals wrapping around the profile, and 64 intervals in the normal direction. A corresponding mesh for a swept wing would have, say, $512 \times 64 \times 256 \approx 8\,388\,608$ cells, leading to a calculation at the outer limits of current computing capabilities. The hierarchy of mathematical models is illustrated in Figure 5, while Figure 6 gives an indication of the boundaries of the complexity of problems which can be treated with different levels of computing power. The vertical axis indicates the geometric complexity, and the horizontal axis the equation complexity.

3 POTENTIAL FLOW METHODS

3.1 Boundary integral methods

The first major success in computational aerodynamics was the development of boundary integral methods for the solution of the subsonic linearized potential flow equation

$$(1 - M_\infty^2)\phi_{xx} + \phi_{yy} = 0 \tag{45}$$

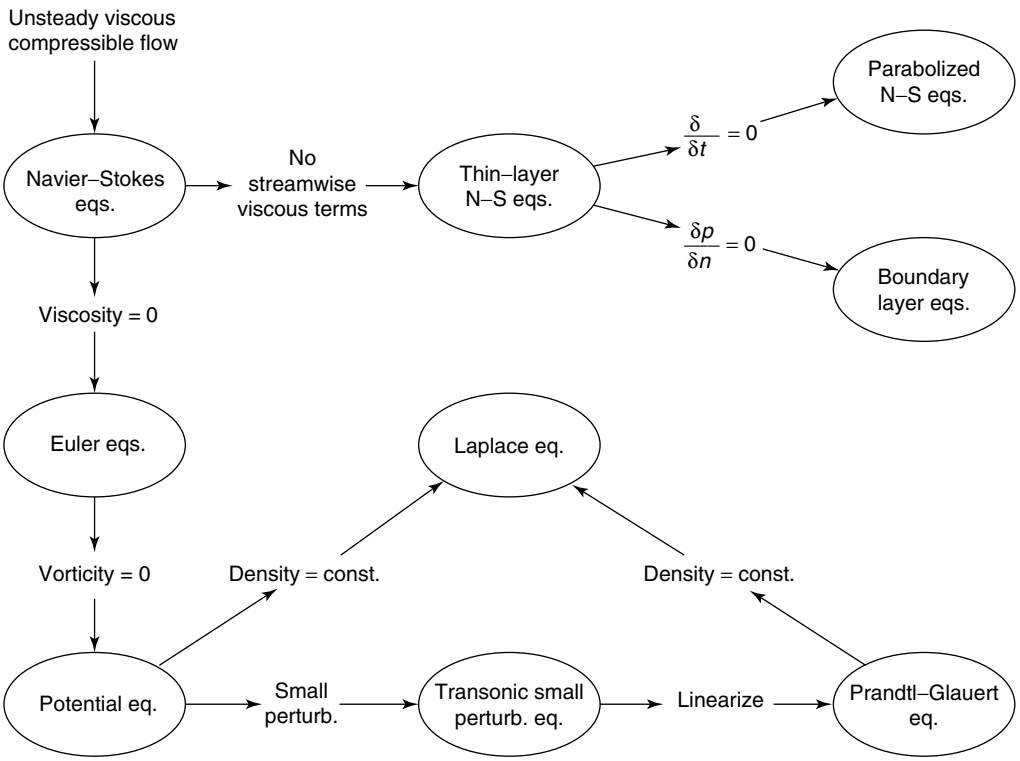

Figure 4. Equations of fluid dynamics for mathematical models of varying complexity. (Supplied by Luis Miranda, Lockheed Corporation.)

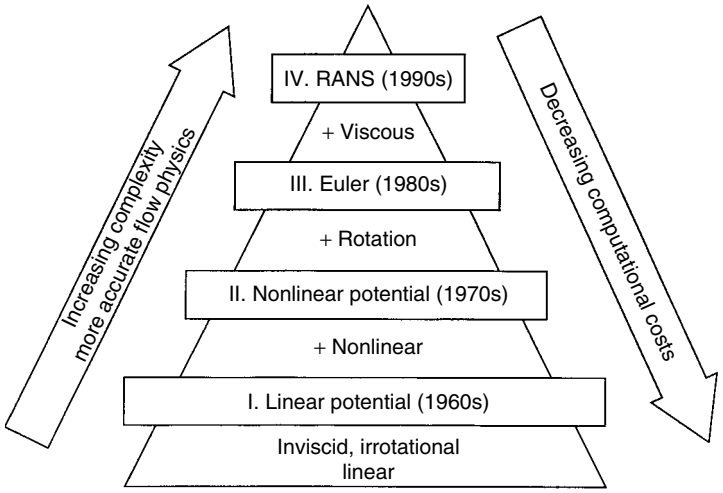

Figure 5. Hierarchy of fluid flow models.

This can be reduced to Laplace's equation by stretching the x coordinate by the factor $\sqrt{(1 - M_\infty^2)}$. Then, according to potential theory, the general solution can be represented in terms of a distribution of sources or doublets, or both sources and doublets, over the boundary surface. The boundary condition is that the velocity component normal to the surface is zero. Assuming, for example, a source distribution of strength $\sigma(Q)$ at the point Q of a surface S, this leads to the integral equation

$$2\pi\sigma_p - \iint_S \sigma(Q) n_p \cdot \nabla \left(\frac{1}{r}\right) = 0 \qquad (46)$$

where P is the point of evaluation, and r is the distance from P to Q. A similar equation can be found for a doublet distribution, and it usually pays to use a combination.

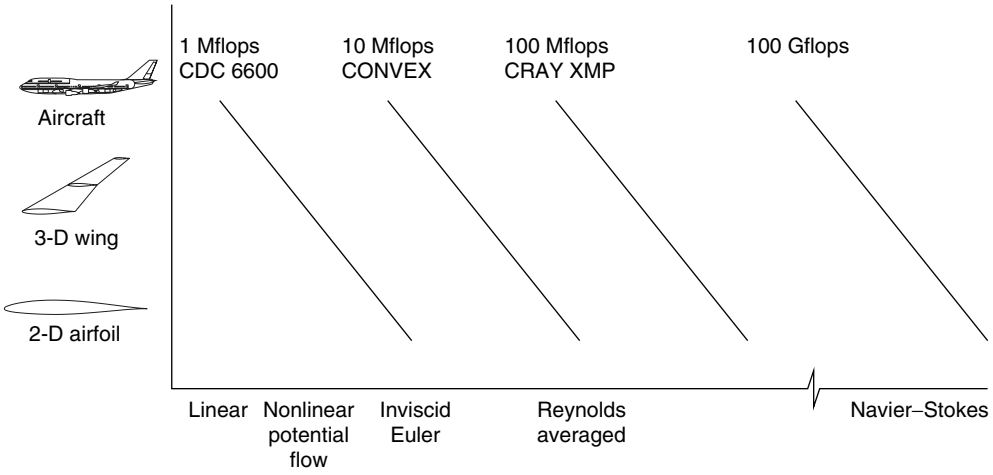

Figure 6. Complexity of the problems that can be treated with different classes of computer (1 flop = 1 floating-point operation per second; 1 Mflop = 10^6 flops; 1 Gflop = 10^9 flops). A color version of this image is available at http://www.mrw.interscience.wiley.com/ecm

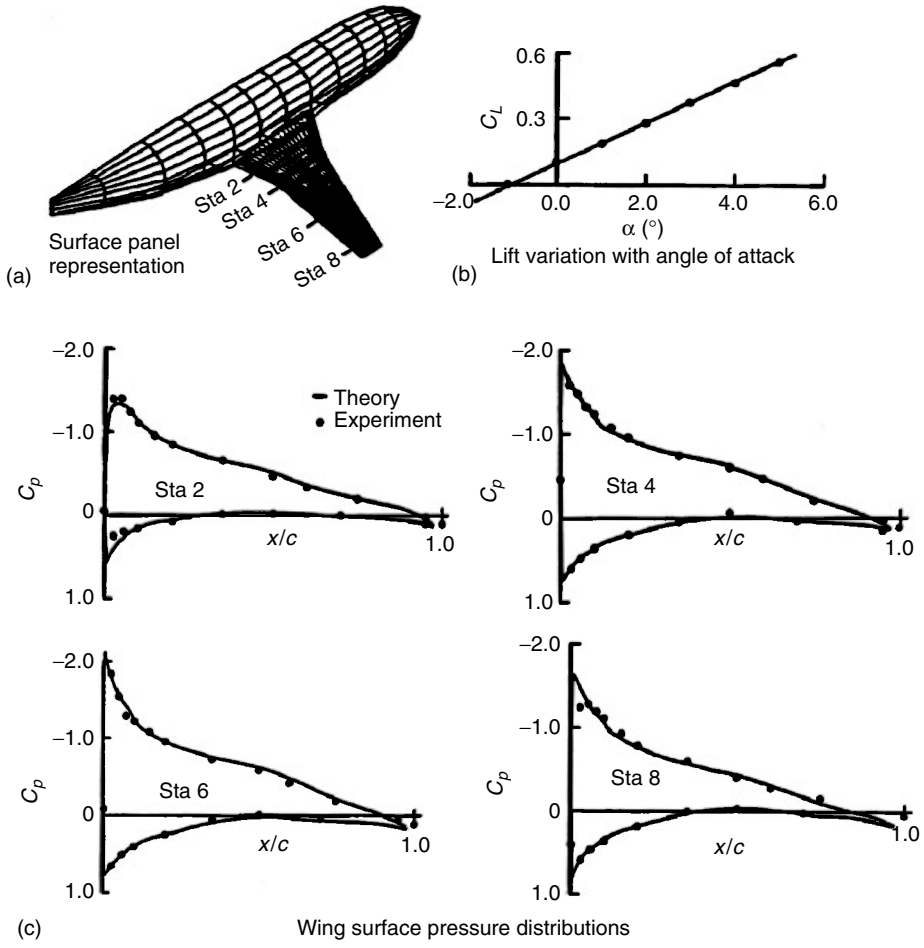

Figure 7. Panel method applied to Boeing 747. (Supplied by Paul Rubbert, the Boeing Company.)

Equation (46) can be reduced to a set of algebraic equations by dividing the surface into quadrilateral panels, assuming a constant source strength on each panel, and satisfying the condition of zero normal velocity at the center of each panel. This leads to N equations for the source strengths on N panels.

The first such method was introduced by Hess and Smith (1962). The method was extended to lifting flows, together with the inclusion of doublet distributions, by Rubbert and Saaris (1968). Subsequently higher-order panel methods (as these methods are generally called in the aircraft industry) have been introduced. A review has been given by Hunt (1978). An example of a calculation by a panel method is shown in Figure 7. The results are displayed in terms of the pressure coefficient defined as

$$c_p = \frac{p - p_\infty}{\frac{1}{2}\rho_\infty q_\infty^2}$$

Figure 8 illustrates the kind of geometric configuration that can be treated by panel methods.

In comparison with field methods, which solve for the unknowns in the entire domain, panel methods have the advantage that the dimensionality is reduced. Consider a three-dimensional flow field on an $n \times n \times n$ grid. This would be reduced to the solution of the source or doublet strengths on $N = O(n^2)$ panels. Since, however, every panel influences every other panel, the resulting equations have a dense matrix. The complexity of calculating the $N \times N$ influence coefficients is then $O(n^4)$. Also, $O(N^3) = O(n^6)$ operations are required for an exact solution. If one directly discretizes the equations for the three-dimensional domain, the number of unknowns is n^3, but the equations are sparse and can be solved with $O(n)$ iterations or even with a number of iterations independent of n if a multigrid method is used.

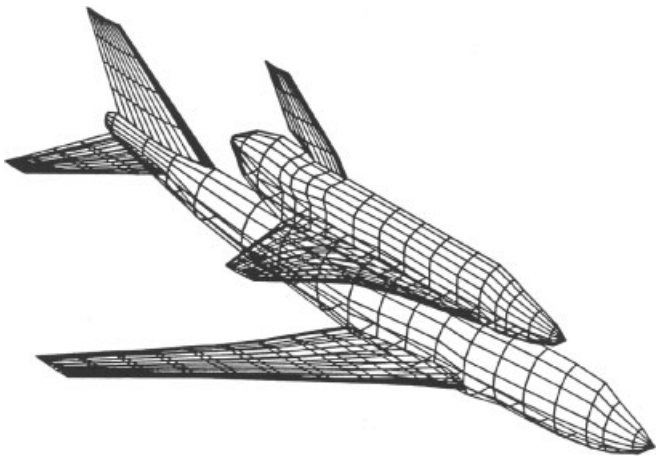

Figure 8. Panel method applied to flow around Boeing 747 and space shuttle. (Supplied by Allen Chen, the Boeing Company.)

Although the field methods appear to be potentially more efficient, the boundary integral method has the advantage that it is comparatively easy to divide a complex surface into panels, whereas the problem of dividing a three-dimensional domain into hexahedral or tetrahedral cells remains a source of extreme difficulty. Moreover the operation count for the solution can be reduced by iterative methods, while the complexity of calculating the influence coefficients can be reduced by agglomeration (Vassberg, 1997). Panel methods thus continue to be widely used both for the solution of flows at low Mach numbers for which compressibility effects are unimportant, and also to calculate supersonic flows at high Mach numbers, for which the linearized equation (45) is again a good approximation.

3.2 Formulation of the numerical method for transonic potential flow

The case of two-dimensional flow serves to illustrate the formulation of a numerical method for solving the transonic potential flow equation. With velocity components u, v and coordinates x, y equation (37) takes the form

$$\frac{\partial}{\partial x}(\rho u) + \frac{\partial}{\partial y}(\rho v) = 0 \tag{47}$$

The desired solution should have the property that ϕ is continuous, and the velocity components are piecewise continuous, satisfying equation (47) at points where the flow is smooth, together with the jump condition,

$$[\rho v] - \frac{\mathrm{d}y}{\mathrm{d}x}[\rho v] = 0 \tag{48}$$

across a shock wave, where [ ] denotes the jump, and $(\mathrm{d}y/\mathrm{d}x)$ is the slope of the discontinuity. That is to say, ϕ should be a weak solution of the conservation law (47), satisfying the condition,

$$\iint (\rho u \psi_x + \rho v \psi_y)\, \mathrm{d}x\, \mathrm{d}y = 0 \tag{49}$$

for any smooth test function ψ, which vanishes in the far field.

The general method to be described stems from the idea introduced by Murman and Cole (1971), and subsequently improved by Murman (1974), of using type-dependent differencing, with central-difference formulas in the subsonic zone, where the governing equation is elliptic, and upwind difference formulas in the supersonic zone,

where it is hyperbolic. The resulting directional bias in the numerical scheme corresponds to the upwind region of dependence of the flow in the supersonic zone. If we consider the transonic flow past a profile with fore-and-aft symmetry such as an ellipse, the desired solution of the potential flow equation is not symmetric. Instead it exhibits a smooth acceleration over the front half of the profile, followed by a discontinuous compression through a shock wave. However, the solution of the potential flow equation (42) is invariant under a reversal of the velocity vector, $u_i = -\phi_{x_i}$. Corresponding to the solution with a compression shock, there is a reverse flow solution with an expansion shock, as illustrated in Figure 9. In the absence of a directional bias in the numerical scheme, the fore-and-aft symmetry would be preserved in any solution that could be obtained, resulting in the appearance of improper discontinuities.

Since the quasilinear form does not distinguish between conservation of mass and momentum, difference approximations to it will not necessarily yield solutions that satisfy the jump condition unless shock waves are detected and special difference formulas are used in their vicinity. If we treat the conservation law (47), on the other hand, and preserve the conservation form in the difference approximation, we can ensure that the proper jump condition is satisfied. Similarly, we can obtain proper solutions of the small-disturbance equation by treating it in the conservation form.

The general method of constructing a difference approximation to a conservation law of the form

$$f_x + g_y = 0$$

is to preserve the flux balance in each cell, as illustrated in Figure 10. This leads to a scheme of the form

$$\frac{F_{i+\frac{1}{2},j} - F_{i-\frac{1}{2},j}}{\Delta x} + \frac{G_{i,j+\frac{1}{2}} - G_{i,j-\frac{1}{2}}}{\Delta y} = 0 \qquad (50)$$

where F and G should converge to f and g in the limit as the mesh width tends to zero. Suppose, for example, that

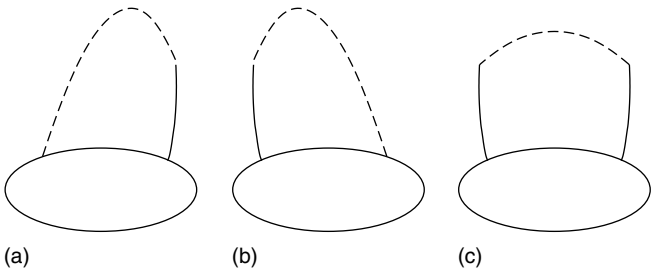

Figure 9. Alternative solutions for an ellipse. (a) Compression shock, (b) expansion shock, (c) symmetric shock.

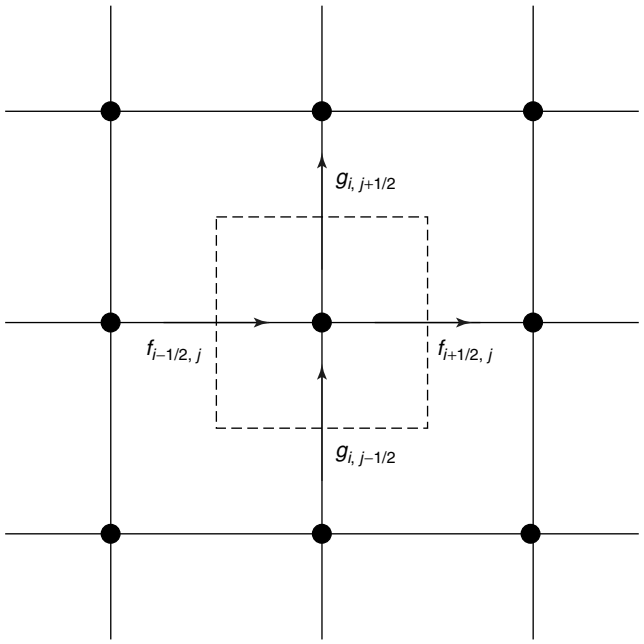

Figure 10. Flux balance of difference scheme in conservation form. A color version of this image is available at http://www.mrw.interscience.wiley.com/ecm

equation (50) represents the conservation law (47). Then on multiplying by a test function ψ_{ij} and summing by parts, there results an approximation to the integral (49). Thus, the condition for a proper weak solution is satisfied. Some latitude is allowed in the definitions of F and G, since it is only necessary that $F = f + O(\Delta x)$ and $G = g + O(\Delta x)$. In constructing a difference approximation, we can therefore introduce an artificial viscosity of the form

$$\frac{\partial P}{\partial x} + \frac{\partial Q}{\partial y}$$

provided that P and Q are of order Δx. Then, the difference scheme is an approximation to the modified conservation law

$$\frac{\partial}{\partial x}(f + P) + \frac{\partial}{\partial y}(g + Q) = 0$$

which reduces to the original conservation law in the limit as the mesh width tends to zero.

This formulation provides a guideline for constructing type-dependent difference schemes in conservation form. The dominant term in the discretization error introduced by the upwind differencing can be regarded as an artificial viscosity. We can, however, turn this idea around. Instead of using a switch in the difference scheme to introduce an artificial viscosity, we can explicitly add an artificial viscosity, which produces an upwind bias in the difference

scheme at supersonic points. Suppose that we have a central-difference approximation to the differential equation in conservation form. Then the conservation form will be preserved as long as the added viscosity is also in conservation form. The effect of the viscosity is simply to alter the conserved quantities by terms proportional to the mesh width Δx, which vanish in the limit as the mesh width approaches zero, with the result that the proper jump conditions must be satisfied. By including a switching function in the viscosity to make it vanish in the subsonic zone, we can continue to obtain the sharp representation of shock waves that results from switching the difference scheme.

There remains the problem of finding a convergent iterative scheme for solving the nonlinear difference equations that result from the discretization. Suppose that in the $(n+1)$st cycle the residual R_{ij} at the point $i\Delta x,\ j\Delta y$ is evaluated by inserting the result $\phi_{ij}^{(n)}$ of the nth cycle in the difference approximation. Then, the correction $C_{ij} = \phi_{ij}^{(n+1)} - \phi_{ij}^{(n)}$ is to be calculated by solving an equation of the form

$$NC + \sigma R = 0 \tag{51}$$

where N is a discrete linear operator and σ is a scaling function. In a relaxation method, N is restricted to a lower triangular or block triangular form so that the elements of C can be determined sequentially. In the analysis of such a scheme, it is helpful to introduce a time-dependent analogy. The residual R is an approximation to $L\phi$, where L is the operator appearing in the differential equation. If we consider C as representing $\Delta t \phi_t$, where t is an artificial time coordinate, and $N\Delta t$ is an approximation to a differential operator D, then equation (51) is an approximation to

$$D\phi_t + \sigma L\phi = 0 \tag{52}$$

Thus, we should choose N so that this is a convergent time-dependent process.

With this approach, the formulation of a relaxation method for solving a transonic flow is reduced to three main steps.

- Construct a central-difference approximation to the differential equation.
- Add a numerical viscosity to produce the desired directional bias in the hyperbolic region.
- Add time-dependent terms to embed the steady state equation in a convergent time-dependent process.

Methods constructed along these lines have proved extremely reliable. Their main shortcoming is a rather slow rate of convergence. In order to speed up the convergence, we can extend the class of permissible operators N.

3.3 Solution of the transonic small-disturbance equation

3.3.1 Murman difference scheme

The basic ideas can conveniently be illustrated by considering the solution of the transonic small-disturbance equation (Ashley and Landahl, 1965)

$$\left[1 - M_\infty^2 - (\gamma+1)M_\infty^2\phi_x\right]\phi_{xx} + \phi_{yy} = 0 \tag{53}$$

The treatment of the small-disturbance equation is simplified by the fact that the characteristics are locally symmetric about the x direction. Thus, the desired directional bias can be introduced simply by switching to upwind differencing in the x direction at all supersonic points. To preserve the conservation form, some care must be exercised in the method of switching as illustrated in Figure 11. Let p_{ij} be

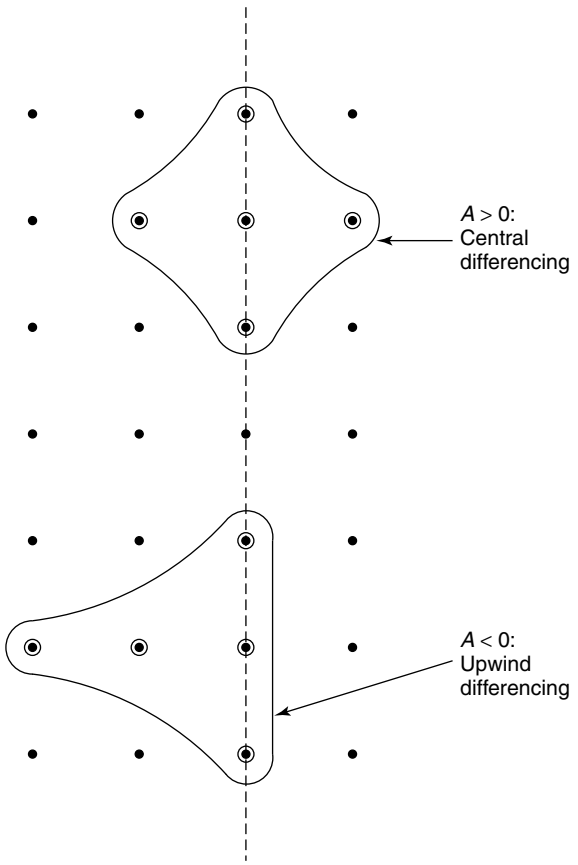

Figure 11. Murman–Cole difference scheme: $A\phi_{xx} + \phi_{yy} = 0$. A color version of this image is available at http://www.mrw.interscience.wiley.com/ecm

a central-difference approximation to the x derivatives at the point $i\Delta x$, $j\Delta y$:

$$p_{ij} = (1 - M_\infty^2)\frac{\phi_{i+1,j} - \phi_{ij} - (\phi_{ij} - \phi_{i-1,j})}{\Delta x^2} - (\gamma + 1)M_\infty^2 \frac{(\phi_{i+1,j} - \phi_{ij})^2 - (\phi_{ij} - \phi_{i-1,j})^2}{2\Delta x^3} = A_{ij}\frac{\phi_{i+1,j} - 2\phi_{ij} + \phi_{i-1,j}}{\Delta x^2} \tag{54}$$

where

$$A_{ij} = (1 - M_\infty^2) - (\gamma + 1)M_\infty^2 \frac{\phi_{i+1,j} - \phi_{i-1,j}}{2\Delta x} \tag{55}$$

Also, let q_{ij} be a central-difference approximation to ϕ_{yy}:

$$q_{ij} = \frac{\phi_{i,j+1} - 2\phi_{ij} + \phi_{i,j-1}}{\Delta y^2} \tag{56}$$

Define a switching function μ with the value unity at supersonic points and zero at subsonic points:

$$\mu_{ij} = 0 \quad \text{if } A_{ij} > 0; \quad \mu_{ij} = 1 \quad \text{if } A_{ij} < 0 \tag{57}$$

Then, the original scheme of Murman and Cole (1971) can be written as

$$p_{ij} + q_{ij} - \mu_{ij}(p_{ij} - p_{i-1,j}) = 0 \tag{58}$$

Let

$$P = \Delta x \frac{\partial}{\partial x}\left[(1 - M_\infty^2)\phi_x - \frac{\gamma + 1}{2}M_\infty^2 {\phi_x}^2\right] = \Delta x A \phi_{xx}$$

where A is the nonlinear coefficient defined by equation (55). Then, the added terms are an approximation to

$$-\mu\frac{\partial P}{\partial x} = -\mu\Delta x A \phi_{xxx} \tag{59}$$

This may be regarded as an artificial viscosity of order Δx, which is added at all points of the supersonic zone. Since the coefficient $-A$ of $\phi_{xxx} = u_{xx}$ is positive in the supersonic zone, it can be seen that the artificial viscosity includes a term similar to the viscous terms in the Navier–Stokes equation.

Since μ is not constant, the artificial viscosity is not in conservation form, with the result that the difference scheme does not satisfy the conditions stated in the previous section for the discrete approximation to converge to a weak solution satisfying the proper jump conditions. To correct this, all that is required is to recast the artificial viscosity in a divergence form as $(\partial/\partial x)(\mu P)$. This leads to Murman's fully conservative scheme (Murman, 1974)

$$p_{ij} + q_{ij} - \mu_{ij}p_{ij} + \mu_{i-1,j}p_{i-1,j} = 0 \tag{60}$$

At points where the flow enters and leaves the supersonic zone, μ_{ij} and $\mu_{i-1,j}$ have different values, leading to special parabolic and shock-point equations

$$q_{ij} = 0$$

and

$$p_{ij} + p_{i-1,j} + q_{ij} = 0$$

With the introduction of these special operators, it can be verified by directly summing the difference equations at all points of the flow field that the correct jump conditions are satisfied across an oblique shock wave.

3.3.2 *Solution of the difference equations by relaxation*

The nonlinear difference equations (54–57, and 58 or 60) may be solved by a generalization of the line relaxation method for elliptic equations. At each point we calculate the coefficient A_{ij} and the residual R_{ij} by substituting the result ϕ_{ij} of the previous cycle in the difference equations. Then we set $\phi_{ij}^{(n+1)} = \phi_{ij}^{(n)} + C_{ij}$, where the correction C_{ij} is determined by solving the linear equations

$$\frac{C_{i,j+1} - 2C_{i,j} + C_{i,j-1}}{\Delta y^2} + (1 - \mu_{i,j})A_{i,j}\frac{-(2/\omega)C_{i,j} + C_{i-1,j}}{\Delta x^2} + \mu_{i-1,j}A_{i-1,j}\frac{C_{i,j} - 2C_{i-1,j} + C_{i-2,j}}{\Delta x^2} + R_{i,j} = 0 \tag{61}$$

on each successive vertical line. In these equations, ω is the overrelaxation factor for subsonic points, with a value in the range 1 to 2. In a typical line relaxation scheme for an elliptic equation, provisional values $\tilde{\phi}_{ij}$ are determined on the line $x = i\Delta x$ by solving the difference equations with the latest available values $\phi_{i-1,j}^{(n+1)}$ and $\phi_{i+1,j}^{(n)}$ inserted at points on the adjacent lines. Then, new values $\phi_{i,j}^{(n+1)}$ are determined by the formula

$$\phi_{ij}^{(n+1)} = \phi_{ij}^{(n)} + \omega(\tilde{\phi}_{ij} - \phi_{ij}^{(n)})$$

By eliminating $\tilde{\phi}_{ij}$, we can write the difference equations in terms of $\phi_{ij}^{(n+1)}$ and $\phi_{ij}^{(n)}$. Then, it can be seen that ϕ_{yy} would

be represented by $(1/\omega)\delta_y^2\phi^{(n+1)} + [1-(1/\omega)]\delta_y^2\phi^{(n)}$ in such a process, where δ_y^2 denotes the second central-difference operator. The appropriate procedure for treating the upwind difference formulas in the supersonic zone, however, is to march in the flow direction, so that the values $\phi_{ij}^{(n+1)}$ on each new column can be calculated from the values $\phi_{i-2,j}^{(n+1)}$ and $\phi_{i-1,j}^{(n+1)}$ already determined on the previous columns. This implies that ϕ_{yy} should be represented by $\delta_y^2\phi^{(n+1)}$ in the supersonic zone, leading to a discontinuity at the sonic line. The correction formula (61) is derived by modifying this process to remove this discontinuity. New values $\phi_{ij}^{(n+1)}$ are used instead of provisional values $\tilde{\phi}_{ij}$ to evaluate ϕ_{yy}, at both supersonic and subsonic points. At supersonic points, ϕ_{xx} is also evaluated using new values. At subsonic points, ϕ_{xx} is evaluated from $\phi_{i-1,j}^{(n+1)}$, $\phi_{i+1,j}^{(n)}$ and a linear combination of $\phi_{ij}^{(n+1)}$ and $\phi_{ij}^{(n)}$. In the subsonic zone, the scheme acts like a line relaxation scheme, with a comparable rate of convergence. In the supersonic zone, it is equivalent to a marching scheme, once the coefficients A_{ij} have been evaluated. Since the supersonic difference scheme is implicit, no limit is imposed on the step length Δx as A_{ij} approaches zero near the sonic line.

3.3.3 *Nonunique solutions of the difference equations for one-dimensional flow*

Some of the properties of the Murman difference formulas are clarified by considering a uniform flow in a parallel channel. Then $\phi_{yy} = 0$, and with a suitable normalization of the potential, the equation reduces to

$$\frac{\partial}{\partial x}\left(\frac{\phi_x^2}{2}\right) = 0 \tag{62}$$

with ϕ and ϕ_x given at $x = 0$, and ϕ given at $x = L$. The supersonic zone corresponds to $\phi_x > 0$. Since ϕ_x^2 is constant, ϕ_x simply reverses sign at a jump. Provided we enforce the entropy condition that ϕ_x decreases through a jump, there is a unique solution with a single jump whenever $\phi_x(0) > 0$ and $\phi(0) + L\phi_x(0) \geq \phi(L) \geq \phi(0) - L\phi_x(0)$.

Let $u_{i+1/2} = (\phi_{i+1} - \phi_i)/\Delta x$ and $u_i = (u_{i+1/2} + u_{i-1/2})/2$. Then, the fully conservative difference equations can be written as

Elliptic:

$$u_{i+\frac{1}{2}}^2 = u_{i-\frac{1}{2}}^2 \quad \text{when } u_i \leq 0 \quad u_{i-1} \leq 0 \tag{a}$$

Hyperbolic:

$$u_{i-\frac{1}{2}}^2 = u_{i-\frac{3}{2}}^2 \quad \text{when } u_i > 0 \quad u_{i-1} > 0 \tag{b}$$

Shock Point:

$$u_{i+\frac{1}{2}}^2 = u_{i-\frac{3}{2}}^2 \quad \text{when } u_i \leq 0 \quad u_{i-1} > 0 \tag{c}$$

Parabolic:

$$0 = 0 \quad \text{when } u_i > 0 \quad u_{i-1} < 0 \tag{d}$$

These admit the correct solution, illustrated in Figure 12(a) with a constant slope on the two sides of the shock. The shock-point operator allows a single link with an intermediate slope, corresponding to the shock lying in the middle of a mesh cell.

The nonconservative difference scheme omits the shock-point operator, with the result that it admits solutions of the type illustrated in Figure 12(b), with the shock too far forward and the downstream velocity too close to the sonic speed (zero with the present normalization). The direct switch in the difference scheme from (b) to (a) allows a break in the slope as long as the downstream slope is negative. The magnitude of the downstream slope cannot exceed the magnitude of the upstream slope, however, because then $u_{i-1} < 0$, and accordingly the elliptic operator would be used at the point $(i-1)\Delta x$. Thus, the nonconservative

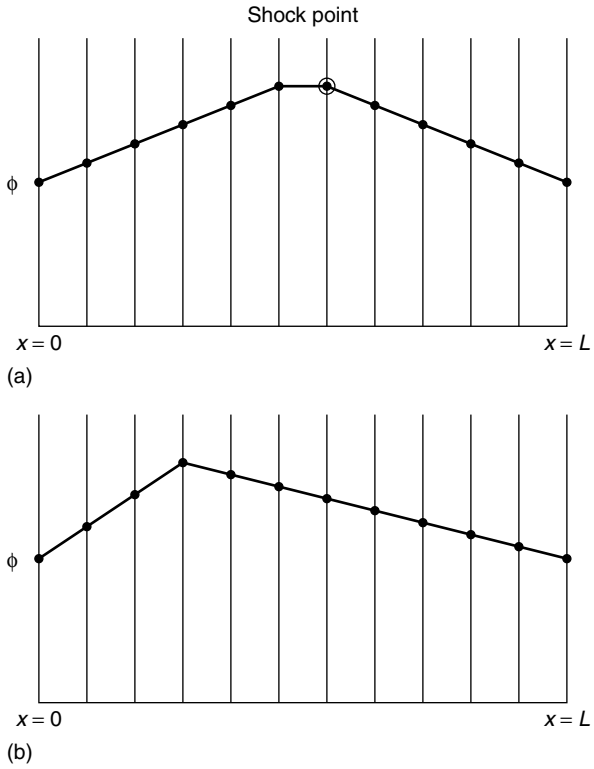

Figure 12. One-dimensional flow in a channel. • – value of ϕ at node i. A color version of this image is available at http://www.mrw.interscience.wiley.com/ecm

scheme enforces the weakened shock condition,

$$\phi_i - \phi_{i-2} > \phi_i - \phi_{i+2} > 0$$

which allows solutions ranging from the point at which the downstream velocity is barely subsonic up to the point at which the shock strength is correct. When the downstream velocity is too close to sonic speed, there is an increase in the mass flow. Thus, the nonconservative scheme may introduce a source at the shock wave.

The fully conservative difference equations also admit, however, various improper solutions. Figure 13(a) illustrates a sawtooth solution with u^2 constant everywhere except in one cell ahead of a shock point. Figure 13(b) illustrates another improper solution in which the shock is too far forward. At the last interior point, there is then an expansion shock that is admitted by the parabolic operator. Since the difference equations have more than one root, we must depend on the iterative scheme to find the desired root. The scheme should ideally be designed so that the correct solution is stable under a small perturbation and improper solutions are unstable. Using a scheme similar to equation (61), the instability of the sawtooth solution has been confirmed in numerical experiments. The solutions with an expansion shock at the downstream boundary are stable, on the other hand, if the compression shock is too far forward by more than the width of a mesh cell. Thus there is a continuous range of stable improper solutions, while the correct solution is an isolated stable equilibrium point.

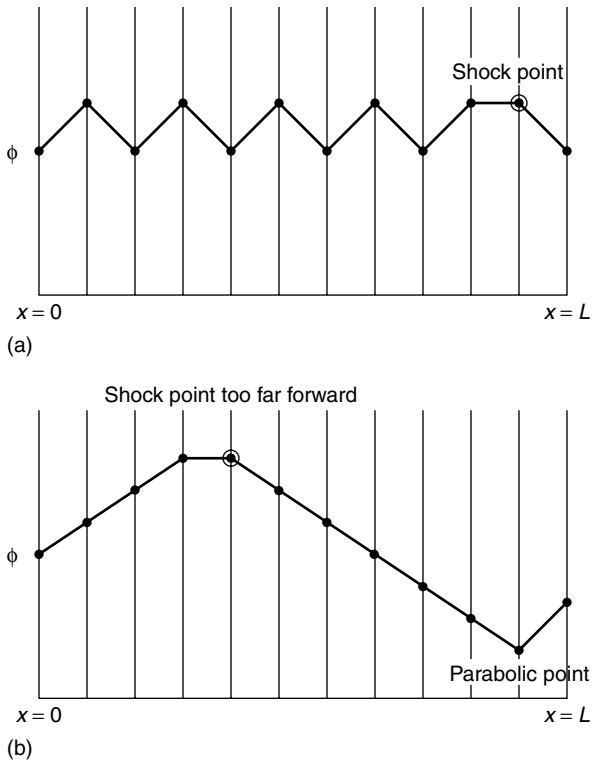

Figure 13. One-dimensional flow in a channel (a) sawtooth solution and (b) solution with downstream parabolic point. A color version of this image is available at http://www.mrw.interscience.wiley.com/ecm

3.4 Solution of the exact potential flow equation

3.4.1 Difference schemes for the exact potential flow equation in quasilinear form

It is less easy to construct difference approximations to the potential flow equation with a correct directional bias, because the upwind direction is not known in advance. Following Jameson (1974), the required rotation of the upwind differencing at any particular point can be accomplished by introducing an auxiliary Cartesian coordinate system that is locally aligned with the flow at that point. If s and n denote the local stream-wise and normal directions, then the transonic potential flow equation becomes

$$(c^2 - q^2)\phi_{ss} + c^2\phi_{nn} = 0 \tag{63}$$

Since u/q and v/q are the local direction cosines, ϕ_{ss} and ϕ_{nn} can be expressed in the original coordinate system as

$$\phi_{ss} = \frac{1}{q^2}\left(u^2\phi_{xx} + 2uv\phi_{xy} + v^2\phi_{yy}\right) \tag{64}$$

and

$$\phi_{nn} = \frac{1}{q^2}\left(v^2\phi_{xx} - 2uv\phi_{xy} + u^2\phi_{yy}\right) \tag{65}$$

Then, at subsonic points, central-difference formulas are used for both ϕ_{ss} and ϕ_{nn}. At supersonic points, central-difference formulas are used for ϕ_{nn}, but upwind difference formulas are used for the second derivatives contributing to ϕ_{ss}, as illustrated in Figure 14.

At a supersonic point at which $u > 0$ and $v > 0$, for example, ϕ_{ss} is constructed from the formulas

$$\begin{aligned}
\phi_{xx} &= \frac{\phi_{ij} - 2\phi_{i-1,j} + \phi_{i-2,j}}{\Delta x^2} \\
\phi_{xy} &= \frac{\phi_{ij} - \phi_{i-1,j} - \phi_{i,j-1} + \phi_{i-1,j-1}}{\Delta x \Delta y} \\
\phi_{yy} &= \frac{\phi_{ij} - 2\phi_{i,j-1} + \phi_{i,j-2}}{\Delta y^2}
\end{aligned} \tag{66}$$

It can be seen that the rotated scheme reduces to a form similar to the scheme of Murman and Cole for the small-disturbance equation if either $u = 0$ or $v = 0$. The upwind difference formulas can be regarded as approximations

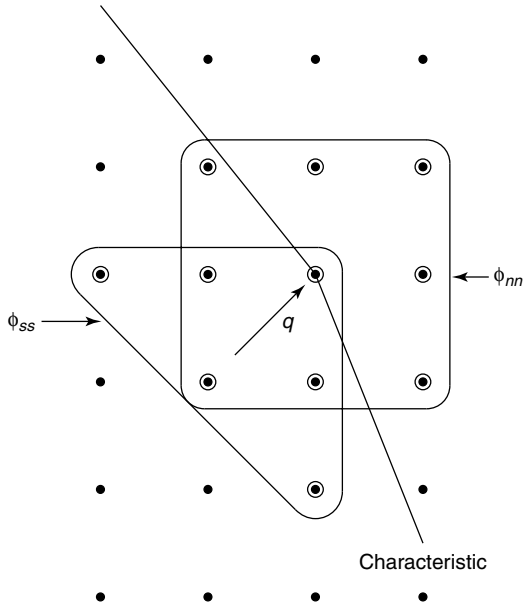

Figure 14. Rotated difference scheme.

to $\phi_{xx} - \Delta x \phi_{xxx}$, $\phi_{xy} - (\Delta x/2)\phi_{xxy} - (\Delta y/2)\phi_{xyy}$, and $\phi_{yy} - \Delta y \phi_{yyy}$. Thus at supersonic points, the scheme introduces an effective artificial viscosity

$$\left(1 - \frac{c^2}{q^2}\right)\left[\Delta x\left(u^2 u_{xx} + uvv_{xx}\right) + \Delta y\left(uvu_{yy} + v^2 v_{yy}\right)\right] \tag{67}$$

which is symmetric in x and y.

3.4.2 *Difference schemes for the exact potential flow equation in conservation form*

In the construction of a discrete approximation to the conservation form of the potential flow equation, it is convenient to accomplish the switch to upwind differencing by the explicit addition of an artificial viscosity. Thus, we solve an equation of the form

$$S_{ij} + T_{ij} = 0 \tag{68}$$

where T_{ij} is the artificial viscosity, which is constructed as an approximation to an expression in divergence form $\partial P/\partial x + \partial Q/\partial y$, where P and Q are appropriate quantities with a magnitude proportional to the mesh width. The central-difference approximation is constructed in the natural manner as

$$S_{ij} = \frac{(\rho u)_{i+\frac{1}{2},j} - (\rho u)_{i-\frac{1}{2},j}}{\Delta x} + \frac{(\rho v)_{i,j+\frac{1}{2}} - (\rho v)_{i,j-\frac{1}{2}}}{\Delta y} \tag{69}$$

Consider first the case in which the flow in the supersonic zone is aligned with the x coordinate, so that it is sufficient to restrict the upwind differencing to the x derivatives. In a smooth region of the flow, the first term of S_{ij} is an approximation to

$$\frac{\partial}{\partial x}(\rho u) = \rho\left(1 - \frac{u^2}{c^2}\right)\phi_{xx} - \frac{\rho u v}{c^2}\phi_{xy}$$

We wish to construct T_{ij} so that ϕ_{xx} is effectively represented by an upwind difference formula when $u > c$. Define the switching function

$$\mu = \min\left[0, \rho\left(1 - \frac{u^2}{c^2}\right)\right] \tag{70}$$

Then set

$$T_{ij} = \frac{P_{i+\frac{1}{2},j} - P_{i-\frac{1}{2},j}}{\Delta x} \tag{71}$$

where

$$P_{i+\frac{1}{2},j} = -\frac{\mu_{ij}}{\Delta x}[\phi_{i+1,j} - 2\phi_{ij} + \phi_{i-1,j} - \epsilon(\phi_{ij} - 2\phi_{i-1,j} + \phi_{i-2,j})] \tag{72}$$

The added terms are an approximation to $\partial P/\partial x$, where

$$P = -\mu[(1-\epsilon)\Delta x \phi_{xx} + \epsilon \Delta x^2 \phi_{xxx}]$$

Thus, if $\epsilon = 0$, the scheme is first-order accurate; but if $\epsilon = 1 - \lambda \Delta x$ and λ is a constant, the scheme is second-order accurate. Also, when $\epsilon = 0$ the viscosity cancels the term $\rho(1 - u^2/c^2)\phi_{xx}$ and replaces it by its value at the adjacent upwind point.

In this scheme, the switch to upwind differencing is introduced smoothly because the coefficient $\mu \to 0$ as $u \to c$. If the first term in S_{ij} were simply replaced by the upwind difference formula

$$\frac{(\rho u)_{i-\frac{1}{2},j} - (\rho u)_{i-\frac{3}{2},j}}{\Delta x}$$

the switch would be less smooth because there would also be a sudden change in the representation of the term $(\rho u v/c^2)\phi_{xy}$, which does not necessarily vanish when $u = c$. A scheme of this type proved to be unstable in numerical tests.

The treatment of flows that are not well aligned with the coordinate system requires the use of a difference scheme in which the upwind bias conforms to the local flow direction. The desired bias can be obtained by modeling the added terms T_{ij} on the artificial viscosity of the rotated difference

scheme for the quasilinear form described in the previous section. Since equation (47) is equivalent to equation (63) multiplied by ρ/c^2, P and Q should be chosen so that $\partial P/\partial x + \partial Q/\partial y$ contains terms similar to equation (67) multiplied by ρ/c^2. The following scheme has proved successful. Let μ be a switching function that vanishes in the subsonic zone:

$$\mu = \max\left[0, \left(1 - \frac{c^2}{q^2}\right)\right] \tag{73}$$

Then, P and Q are defined as approximations to

$$-\mu\left[(1-\epsilon)u\Delta x\rho_x + \epsilon u\Delta x^2\rho_{xx}\right]$$

and

$$-\mu[(1-\epsilon)v\Delta y\rho_y + \epsilon v\Delta y^2\rho_{yy}]$$

where the parameter ϵ controls the accuracy in the same way as in the simple scheme. If $\epsilon = 0$, the scheme is first-order accurate, and at a supersonic point where $u > 0$ and $v > 0$, P then approximates

$$-\Delta x\left(1 - \frac{c^2}{q^2}\right)u\rho_x = \Delta x\frac{\rho}{c^2}\left(1 - \frac{c^2}{q^2}\right)(u^2u_x + uvv_x)$$

When this formula and the corresponding formula for Q are inserted in $\partial P/\partial x + \partial Q/\partial y$, it can be verified that the terms containing the highest derivatives of ϕ are the same as those in equation (67) multiplied by ρ/c^2. In the construction of P and Q, the derivatives of P are represented by upwind difference formulas. Thus, the formula for the viscosity finally becomes

$$T_{ij} = \frac{P_{i+\frac{1}{2},j} - P_{i-\frac{1}{2},j}}{\Delta x} + \frac{Q_{i,j+\frac{1}{2}} - Q_{i,j-\frac{1}{2}}}{\Delta y} \tag{74}$$

where if $u_{i+1/2,j} > 0$, then

$$P_{i+\frac{1}{2},j} = u_{i+\frac{1}{2},j}\mu_{ij}\left[\rho_{i+\frac{1}{2},j} - \rho_{i-\frac{1}{2},j} - \epsilon\left(\rho_{i-\frac{1}{2},j} - \rho_{i-\frac{3}{2},j}\right)\right]$$

and if $u_{i+1/2,j} < 0$, then

$$P_{i+\frac{1}{2},j} = u_{i+\frac{1}{2},j}\mu_{i+1,j}\left[\rho_{i+\frac{1}{2},j} - \rho_{i+\frac{3}{2},j} - \epsilon\left(\rho_{i+\frac{3}{2},j} - \rho_{i+\frac{5}{2},j}\right)\right]$$

while $Q_{i,j+1/2}$ is defined by a similar formula.

3.4.3 Analysis of the relaxation method

Both the nonconservative rotated difference scheme and the difference schemes in conservation form lead to difference equations that are not amenable to solution by marching in the supersonic zone, and a rather careful analysis is needed to ensure the convergence of the iterative scheme. For this purpose, it is convenient to introduce the time-dependent analogy proposed in Section 3.2. Thus, we regard the iterative scheme as an approximation to the artificial time-dependent equation (52). It was shown by Garabedian (1956) that this method can be used to estimate the optimum relaxation factor for an elliptic problem.

To illustrate the application of the method, consider the standard difference scheme for Laplace's equation. Typically, in a point overrelaxation scheme, a provisional value $\tilde{\phi}_{ij}$ is obtained by solving

$$\frac{\phi^{(n+1)}_{i-1,j} - 2\tilde{\phi}_{ij} + \phi^{(n)}_{i+1,j}}{\Delta x^2} + \frac{\phi^{(n+1)}_{i,j-1} - 2\tilde{\phi}_{ij} + \phi^{(n)}_{i,j+1}}{\Delta y^2} = 0$$

Then the new value $\phi^{(n+1)}_{ij}$ is determined by the formula

$$\phi^{(n+1)}_{ij} = \phi^{(n)}_{ij} + \omega\left(\tilde{\phi}_{ij} - \phi^{(n)}_{ij}\right)$$

where ω is the overrelaxation factor. Eliminating $\tilde{\phi}_{ij}$, this is equivalent to calculating the correction $C_{ij} = \phi^{(n+1)}_{ij} - \phi^{(n)}_{ij}$ by solving

$$\tau_1(C_{ij} - C_{i-1,j}) + \tau_2(C_{ij} - C_{i,j-1}) + \tau_3 C_{i,j} = R_{ij} \tag{75}$$

where R_{ij} is the residual, and

$$\tau_1 = \frac{1}{\Delta x^2}$$
$$\tau_2 = \frac{1}{\Delta y^2}$$
$$\tau_3 = \left(\frac{2}{\omega} - 1\right)\left(\frac{1}{\Delta x^2} + \frac{1}{\Delta y^2}\right)$$

Equation (75) is an approximation to the wave equation

$$\tau_1\Delta t\Delta x\phi_{xt} + \tau_2\Delta t\Delta y\phi_{yt} + \tau_3\Delta t\phi_t = \phi_{xx} + \phi_{yy}$$

This is damped if $\tau_3 > 0$, and to maximize the rate of convergence, the relaxation factor ω should be chosen to give an optimal amount of damping.

If we consider the potential flow equation (63) at a subsonic point, these considerations suggest that the scheme (75), where the residual R_{ij} is evaluated from the difference

approximation described in Section 3.4.1, will converge if

$$\tau_1 \geq \frac{c^2 - u^2}{\Delta x^2}, \quad \tau_2 \geq \frac{c^2 - v^2}{\Delta y^2}, \quad \tau_3 > 0$$

Similarly, the scheme

$$\tau_1(C_{ij} - C_{i-1,j}) + \tau_2(C_{i,j+1} - 2C_{ij} + C_{i,j-1}) + \tau_3 C_{i,j} = R_{ij} \tag{76}$$

which requires the simultaneous solution of the corrections on each vertical line, can be expected to converge if

$$\tau_1 \geq \frac{c^2 - u^2}{\Delta x^2}, \quad \tau_2 = \frac{c^2 - v^2}{\Delta y^2}, \quad \tau_3 > 0$$

At supersonic points, schemes similar to (75) or (76) are not necessarily convergent (Jameson, 1974). If we introduce a locally aligned Cartesian coordinate system and divide through by c^2, the general form of the equivalent time-dependent equation is

$$\left(M^2 - 1\right)\phi_{ss} - \phi_{nn} + 2\alpha\phi_{st} + 2\beta\phi_{nt} + \gamma\phi_t = 0 \tag{77}$$

where M is the local Mach number, and s and n are the stream-wise and normal directions. The coefficients α, β, and γ depend on the coefficients of the elements of C on the left-hand side of (75) and (76). The substitution

$$T = t - \frac{\alpha s}{M^2 - 1} + \beta n$$

reduces this equation to the diagonal form

$$(M^2 - 1)\phi_{ss} - \phi_{nn} - \left(\frac{\alpha^2}{M^2 - 1} - \beta^2\right)\phi_{TT} + \gamma\phi_T = 0$$

Since the coefficients of ϕ_{nn} and ϕ_{ss} have opposite signs when $M > 1$, T cannot be the time-like direction at a supersonic point. Instead, either s or n is time-like, depending on the sign of the coefficient of ϕ_{TT}. Since s is the time-like direction of the steady state problem, it ought also to be the time-like direction of the unsteady problem. Thus, when $M > 1$, the relaxation scheme should be designed so that α and β satisfy the compatibility condition

$$\alpha > \beta\sqrt{M^2 - 1} \tag{78}$$

The characteristics of the unsteady equation (77) satisfy

$$(M^2 - 1)(t^2 + 2\beta nt) - 2\alpha st - (\beta s - \alpha n)^2 = 0$$

Thus, the characteristic cone touches the s–n plane. As long as condition (78) holds with $\alpha > 0$ and $\beta > 0$, it slants upstream in the reverse time direction, as illustrated in Figure 15. To ensure that the iterative scheme has the proper region of dependence, the flow field should be swept in a direction such that the updated region always includes the upwind line of tangency between the characteristic cone and the s–n plane.

A von Neumann analysis (Jameson, 1974) indicates that the coefficient of ϕ_t should be zero at supersonic points, reflecting the fact that t is not a time-like direction. The mechanism of convergence in the supersonic zone can be inferred from Figure 15. An equation of the form of (78) with constant coefficients reaches a steady state because with advancing time the cone of dependence ceases to intersect the initial time plane. Instead, it intersects a surface containing the Cauchy data of the steady state problem. The rate of convergence is determined by the backward inclination of the most retarded characteristic

$$t = \frac{2\alpha s}{M^2 - 1}, \qquad n = -\frac{\beta}{\alpha}s$$

and is maximized by using the smallest permissible coefficient α for the term in ϕ_{st}. In the subsonic zone, on the other hand, the cone of dependence contains the t axis, and it is important to introduce damping to remove the influence of the initial data.

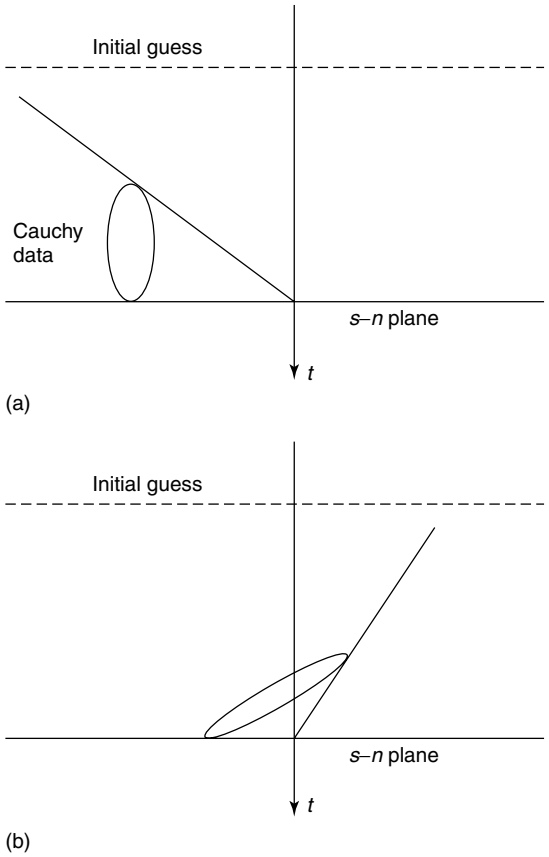

Figure 15. Characteristic cone of equivalent time-dependent equation. (a) Supersonic, (b) subsonic.

3.5 Treatment of complex geometric configurations

An effective approach to the treatment of two-dimensional flows over complex profiles is to map the exterior domain conformally onto the unit disk (Jameson, 1974). Equation (47) is then written in polar coordinates as

$$\frac{\partial}{\partial\theta}\left(\frac{\rho}{r}\phi_\theta\right)+\frac{\partial}{\partial r}(r\rho\phi_r)=0 \tag{79}$$

where the modulus h of the mapping function enters only in the calculation of the density from the velocity

$$\mathbf{q}=\frac{\nabla\phi}{h} \tag{80}$$

The Kutta condition is enforced by adding circulation such that $\nabla\phi=0$ at the trailing edge. This procedure is very accurate. Figure 16 shows a numerical verification of Morawetz's theorem that a shock-free transonic flow is an isolated point, and that arbitrary small changes in boundary conditions will lead to the appearance of shock waves (Morawetz, 1956).These calculations were performed by the author's program flo6.

Applications to complex three-dimensional configurations require a more flexible method of discretization, such as that provided by the finite element method. Jameson and Caughey proposed a scheme using isoparametric bilinear or trilinear elements (Jameson and Caughey, 1977; Jameson, 1978). The discrete equations can most conveniently be derived from the Bateman variational principle. In the scheme of Jameson and Caughey, I is approximated as

$$I=\sum p_k V_k$$

where p_k is the pressure at the center of the kth cell and V_k is its area (or volume), and the discrete equations are obtained by setting the derivative of I with respect to the nodal values of potential to zero. Artificial viscosity is added to give an upwind bias in the supersonic zone, and an iterative scheme is derived by embedding the steady state equation in an artificial time-dependent equation. Several widely used codes (flo27, flo28, flo30) have been developed using this scheme. Figure 17 shows a result for a swept wing.

An alternative approach to the treatment of complex configurations has been developed by Bristeau *et al.* (1980a,b). Their method uses a least squares formulation of the problem, together with an iterative scheme derived with the aid of optimal control theory. The method could be used in conjunction with a subdivision into either quadrilaterals or triangles, but in practice triangulations have been used.

The simplest conceivable least squares formulation calls for the minimization of the objective function

$$I=\int_S \psi^2\,\mathrm{d}S$$

where ψ is the residual of equation (47) and S is the domain of the calculation. The resulting minimization problem could be solved by a steepest descent method in which

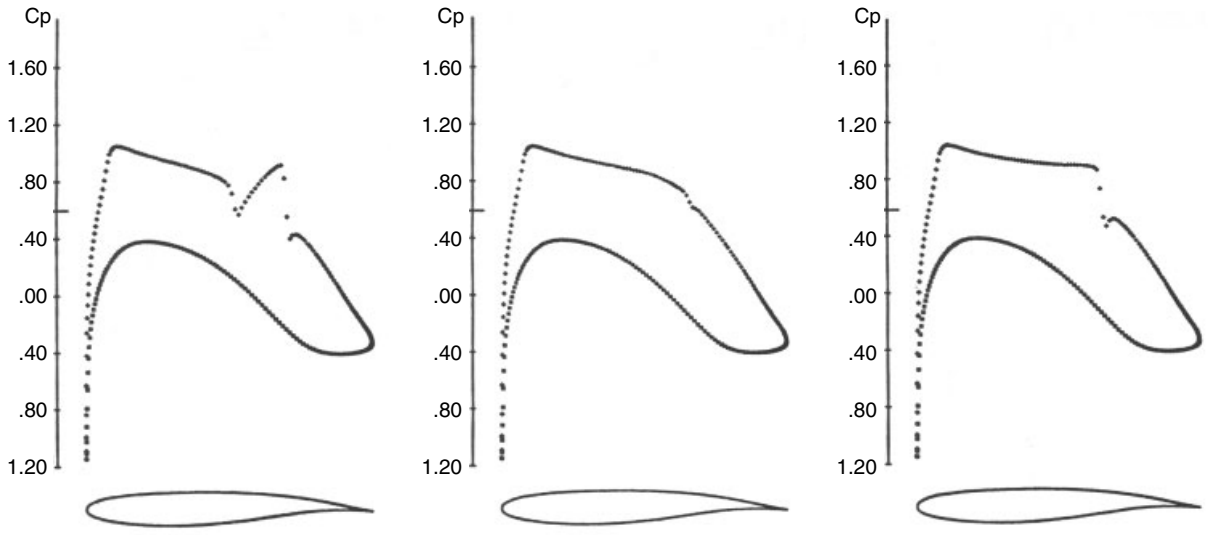

Figure 16. Sensitivity of a shock-free solution.

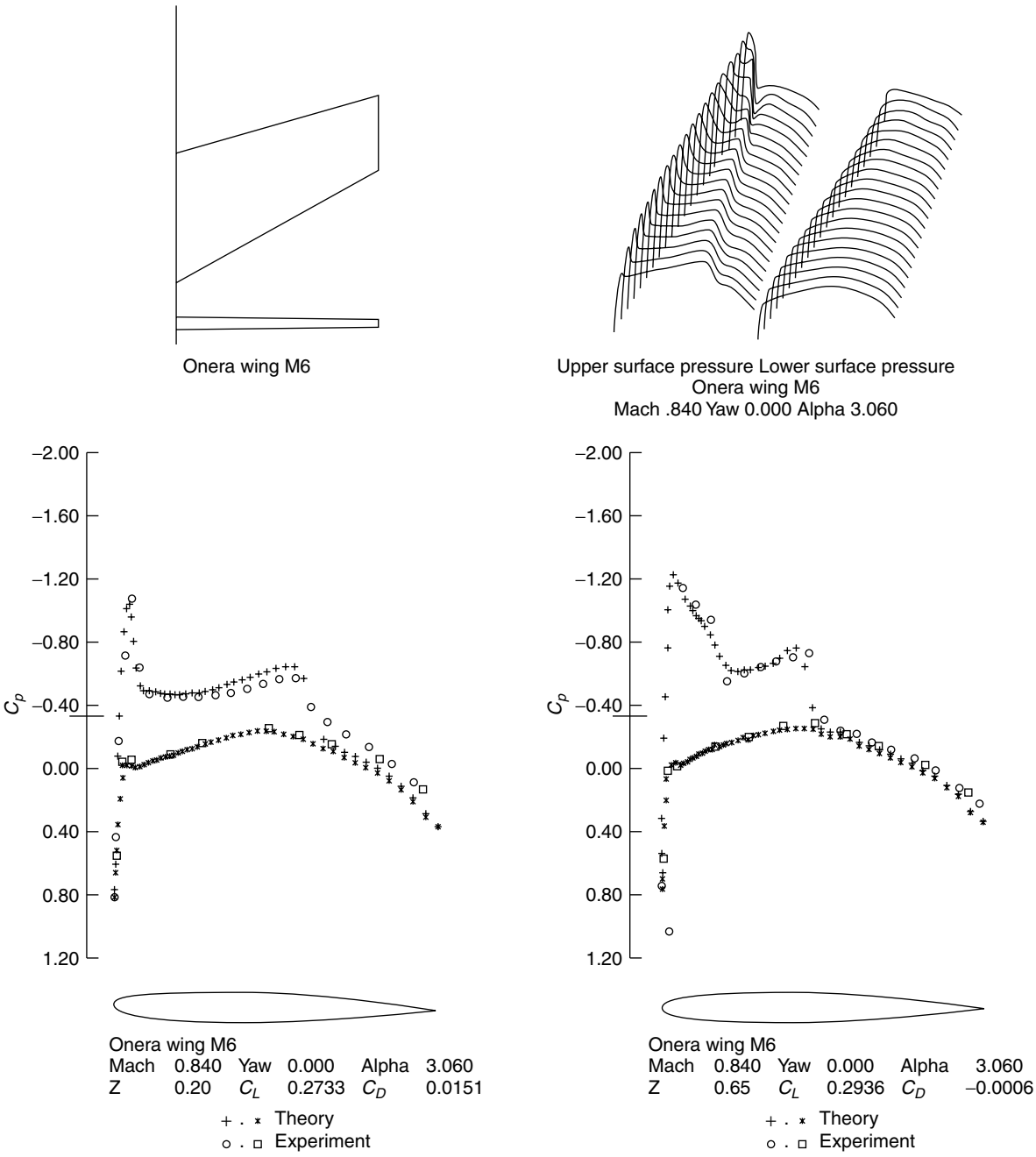

Figure 17. Swept wing.

the potential is repeatedly modified by a correction $\delta\phi$ proportional to $(\partial I/\partial\phi)$. Such a method would be very slow. In fact, it simulates a time-dependent equation of the form

$$\phi_t = -L^* L\phi$$

where L is the differential operator in equation (47), and L^* is its adjoint. Much faster convergence can be obtained by the introduction of a more sophisticated objective function

$$I = \int_S \nabla\psi^2 \, \mathrm{d}S$$

where the auxiliary function ϕ is calculated from

$$\nabla^2\psi = \nabla \cdot (\rho\nabla\phi)$$

Let g be the value of $(\partial\phi/\partial n)$ specified on the boundary C of the domain. Then, this equation can be replaced by the corresponding variational form

$$\int_S \nabla\psi \cdot \nabla v \, dS = \int_S \rho \nabla \cdot \nabla v \, dS - \int_C g v \, dS$$

which must be satisfied by ψ for all differentiable test functions v. This formulation, which is equivalent to the use of an H^{-1} norm in Sobolev space, reduces the calculation of the potential to the solution of an optimal control problem, with ϕ as the control function and ψ as the state function. It leads to an iterative scheme that calls for solutions of Poisson equations twice in each cycle. A further improvement can be realized by the use of a conjugate gradient method instead of a simple steepest descent method.

The least squares method in its basic form allows expansion shocks. In early formulations, these were eliminated by penalty functions. Subsequently, it was found best to use upwind biasing of the density. The method has been extended at Avions Marcel Dassault to the treatment of extremely complex three-dimensional configurations, using a subdivision of the domain into tetrahedra (Bristeau *et al.*, 1985).

4 SHOCK-CAPTURING ALGORITHMS FOR THE EULER AND NAVIER–STOKES EQUATIONS

4.1 Overview

The development of nonoscillatory shock-capturing schemes has been a prime focus of algorithms in research in compressible flow. This section presents the theory for the general Euler equations describing inviscid flow. In order to develop the theory systematically, the strategy adopted here is first to develop a theory for the one-dimensional scalar conservation law. This provides a theoretical framework for the design of nonoscillatory schemes based on the introduction of appropriate measures of oscillation. The criterion preferred here is that local extrema should not be allowed to increase. This leads to the concept of local extremum diminishing (LED) schemes, which is closely related to the concept of TVD schemes introduced by Harten (1983). This theory provides a platform for the generalization to the system constituted by the one-dimensional gas dynamics equations, where the focus becomes the appropriate formulation of the numerical flux across cell interfaces. Finally, the treatment of multidimensional systems is considered, including the treatment of complex geometric domains on arbitrary meshes. The theory of nonoscillatory schemes is substantially simplified by the use of the semidiscrete form in which only the spatial derivatives are discretized to produce a system of ordinary differential equation. This allows the design of time-stepping schemes to be treated as a separate issue.

4.2 The need for oscillation control and upwinding

The need for oscillation control is already evident from a consideration of the linear advection equation

$$\frac{\partial u}{\partial t} + a\frac{\partial u}{\partial x} = 0$$

which represents a right running wave of the wave speed a as positive. Consider a semidiscrete scheme with central differencing on a uniform mesh with an interval Δx:

$$\frac{\partial v_j}{\partial t} + a D_x v = 0$$

where

$$D_x v_j = \frac{1}{2\Delta x}(v_{j+1} - v_{j-1})$$

Suppose that $v_j = (-1)^j$ as illustrated in Figure 18. Then (dv_j/dt) is zero at every mesh point, so the odd–even mode is a stationary solution. Consider also the propagation of a step as a right running wave (Figure 19). Then at a crest j, $D_x v_j < 0$, and with $a > 0$, $(dv_j/dt) > 0$, leading to an immediate overshoot. This motivates the use of an upwind space discretization

$$D_x v_j = \frac{1}{\Delta x}(v_j - v_{j-1})$$

for which $D_x v_j = 0$ at the crest.

Upwind schemes are subject, however, to limitations that need to be considered. The Iserles Barrier theorem (Iserles, 1981) states that the maximum order of accuracy of a stable semidiscrete scheme with r points upwind and s points downwind (as illustrated in Figure 20) is

$$\min(r + s, 2r, 2s + 2)$$

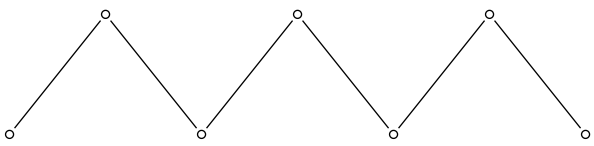

Figure 18. Stationary odd–even mode.

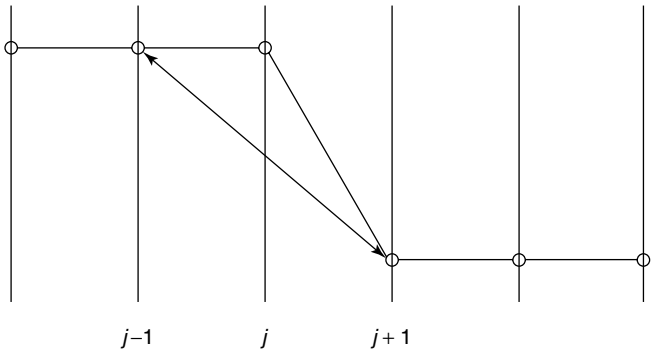

Figure 19. Propagation of a step discontinuity. A color version of this image is available at http://www.mrw.interscience.wiley.com/ecm

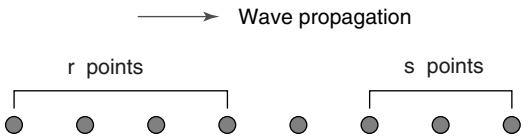

Figure 20. Stencil for a multipoint scheme. A color version of this image is available at http://www.mrw.interscience.wiley.com/ecm

Thus, the maximum order of accuracy of a purely upwind scheme ($s = 0$) is two, a result also established by Engquist and Osher (1981).

4.3 Nonoscillatory shock-capturing schemes with positive coefficients

4.3.1 Local extremum diminishing (LED) schemes

Clearly, a systematic formulation of oscillation control is needed. The most direct approach is directly to consider the conditions under which extrema can be prevented from growing in the discrete solution (Jameson, 1986a). Consider a general semidiscrete scheme of the form

$$\frac{\mathrm{d}}{\mathrm{d}t}v_j = \sum_{k\neq j} c_{jk}(v_k - v_j) \tag{81}$$

A maximum cannot increase and a minimum cannot decrease if the coefficients c_{jk} are nonnegative, since at a maximum $v_k - v_j \leq 0$, and at a minimum $v_k - v_j \geq 0$. Thus, the condition

$$c_{jk} \geq 0, \quad k \neq j \tag{82}$$

is sufficient to ensure stability in the maximum norm. Moreover, if the scheme has a compact stencil, so that $c_{jk} = 0$ when j and k are not nearest neighbors, a local maximum cannot increase and local minimum cannot decrease. This LED property prevents the birth and growth of oscillations. The one-dimensional conservation law

$$\frac{\partial u}{\partial t} + \frac{\partial}{\partial x} f(u) = 0 \tag{83}$$

provides a useful model for analysis. In this case, waves are propagated with a speed $a(u) = (\partial f/\partial u)$, and the solution is constant along the characteristics $(\mathrm{d}x/\mathrm{d}t) = a(u)$. Thus, the LED property is satisfied by the true solution. In fact, the total variation

$$TV(u) = \int_{-\infty}^{\infty} \left|\frac{\partial u}{\partial x}\right| \mathrm{d}x$$

of a solution of this equation does not increase, provided that any discontinuity appearing in the solution satisfies an entropy condition (Lax, 1973b). Harten proposed that difference schemes ought to be designed so that the discrete total variation cannot increase (Harten, 1983). If the end values are fixed, the total variation can be expressed as

$$TV(u) = 2\left(\sum \text{maxima} - \sum \text{minima}\right)$$

Thus, an LED scheme is also TVD. The converse is not necessarily true, since it is possible for adjacent maxima and minima to be shifted an equal amount, say upwards, so that the total variation is unchanged, while the local maximum is increased. Positivity conditions of the type expressed in equations (81) and (82) lead to diagonally dominant schemes and are the key to the elimination of improper oscillations. The positivity conditions may be realized by the introduction of diffusive terms or by the use of upwind biasing in the discrete scheme. Unfortunately, they may also lead to severe restrictions on accuracy unless the coefficients have a complex nonlinear dependence on the solution.

4.3.2 Artificial diffusion and upwinding for a one-dimensional scalar conservation law

Following the pioneering work of Godunov (1959), a variety of dissipative and upwind schemes designed to have good shock-capturing properties have been developed during the past two decades (Steger and Warming, 1981; Boris and Book, 1973; Van Leer, 1974, 1982; Roe, 1981; Osher and Solomon, 1982; Harten, 1983; Osher and Chakravarthy, 1984; Sweby, 1984; Anderson, Thomas and Van Leer, 1985; Jameson, 1985a; Yee, 1985a; Hughes, Franca and Mallet, 1986; Woodward and Colella, 1984; Barth and Jespersen, 1989; Barth and Frederickson, 1990; Barth,

1994). The principles underlying the formulation of these schemes can conveniently be illustrated by the case of the one-dimensional scalar conservation law (83). Suppose that this is represented by the three-point semidiscrete scheme

$$\frac{\mathrm{d}v_j}{\mathrm{d}t} = c^+_{j+\frac{1}{2}}(v_{j+1} - v_j) + c^-_{j-\frac{1}{2}}(v_{j-1} - v_j)$$

According to equations (81) and (82), this scheme is LED if

$$c^+_{j+\frac{1}{2}} \geq 0, \qquad c^-_{j-\frac{1}{2}} \geq 0 \tag{84}$$

A conservative semidiscrete approximation to the one-dimensional conservation law (83) can be derived by subdividing the line into cells. Then the evolution of the value v_j in the jth cell is given by

$$\Delta x \frac{\mathrm{d}v_j}{\mathrm{d}t} + h_{j+\frac{1}{2}} - h_{j-\frac{1}{2}} = 0 \tag{85}$$

where $h_{j+1/2}$ is an estimate of the flux between cells j and $j+1$. Defining $f_j = f(v_j)$, the simplest estimate is the arithmetic average $(f_{j+1} + f_j)/2$, but this leads to a scheme that does not satisfy the positivity conditions (84). To correct this, one may add a dissipative term and set

$$h_{j+\frac{1}{2}} = \tfrac{1}{2}(f_{j+1} + f_j) - d_{j+\frac{1}{2}} \tag{86}$$

Here $d_{j+1/2}$ takes the form $\alpha_{j+1/2}(v_{j+1} - v_j)$, and then $d_{j+1/2} - d_{j-1/2}$ approximates the first-order diffusive term $\Delta x(\partial/\partial x)\alpha(\partial v/\partial x)$. In order to estimate the required value of the coefficient $\alpha_{j+1/2}$, let $a_{j+1/2}$ be a numerical estimate of the wave speed $(\partial f/\partial u)$,

$$a_{j+\frac{1}{2}} = \begin{cases} \dfrac{f_{j+1} - f_j}{v_{j+1} - v_j} & \text{if} v_{j+1} \neq v_j \\ \left.\dfrac{\partial f}{\partial v}\right|_{v=v_j} & \text{if} v_{j+1} = v_j \end{cases} \tag{87}$$

Then,

$$h_{j+\frac{1}{2}} - h_{j-\frac{1}{2}} = -\left(\alpha_{j+\frac{1}{2}} - \tfrac{1}{2}a_{j+\frac{1}{2}}\right)\Delta v_{j+\frac{1}{2}} + \left(\alpha_{j-\frac{1}{2}} + \tfrac{1}{2}a_{j-\frac{1}{2}}\right)\Delta v_{j-\frac{1}{2}}$$

where

$$\Delta v_{j+\frac{1}{2}} = v_{j+1} - v_j$$

and the LED condition (84) is satisfied if

$$\alpha_{j+\frac{1}{2}} \geq \tfrac{1}{2}\left|a_{j+\frac{1}{2}}\right| \tag{88}$$

If one takes

$$\alpha_{j+\frac{1}{2}} = \tfrac{1}{2}\left|a_{j+\frac{1}{2}}\right|$$

one obtains the first-order upwind scheme

$$h_{j+\frac{1}{2}} = \begin{cases} f_j & \text{if } a_{j+\frac{1}{2}} > 0 \\ f_{j+1} & \text{if } a_{j+\frac{1}{2}} < 0 \end{cases}$$

This is the least diffusive first-order scheme that satisfies the LED condition. In this sense, upwinding is a natural approach to the construction of nonoscillatory schemes.

If one considers the normalized one-dimensional transonic small-disturbance equation (62) with an artificial time-dependent term

$$\phi_{xt} + \frac{\partial}{\partial x}\left(\frac{\phi_x^2}{2}\right)$$

it is apparent, on setting $u = \phi_x$, that the first-order upwind scheme is equivalent to the Murman–Cole scheme.

Another important requirement of discrete schemes is that they should exclude nonphysical solutions that do not satisfy appropriate entropy conditions (Lax, 1973b), which require the convergence of characteristics toward admissible discontinuities. This places more stringent bounds on the minimum level of numerical viscosity (Majda and Osher, 1979; Tadmor, 1984; Osher, 1984; Osher and Tadmor, 1988). In the case that the numerical flux function is strictly convex, Aiso has proved (Aiso, 1993) that it is sufficient that

$$\alpha_{j+\frac{1}{2}} > \max\left\{\tfrac{1}{2}\left|a_{j+\frac{1}{2}}\right|, \epsilon\ \mathrm{sign}(v_{j+1} - v_j)\right\}$$

for $\epsilon > 0$. Thus, the numerical viscosity should be rounded out and not allowed to reach zero at a point where the wave speed $a(u) = (\partial f/\partial u)$ approaches zero. This justifies, for example, Harten's entropy fix (Harten, 1983).

Higher-order schemes generally have larger stencils and coefficients of varying sign, which are not compatible with the conditions (82) for an LED scheme. It is also known that schemes that satisfy these conditions are at best first-order accurate in the neighborhood of an extremum. A widely used approach to the computation of higher-order nonoscillatory schemes is to introduce antidiffusive terms in a controlled manner. It also proves useful in

the following development to introduce the concept of essentially local extremum diminishing (ELED) schemes. These are defined to be schemes that satisfy the condition that in the limit as the mesh width $\Delta x \to 0$, local maxima are nonincreasing and local minima are nondecreasing.

4.3.3 *High resolution switched schemes: Jameson–Schmidt–Turkel (JST) scheme*

An early attempt to produce a high-resolution scheme is the JST scheme (Jameson, Schmidt, and Turkel, 1981). Suppose that antidiffusive terms are introduced by subtracting neighboring differences to produce a third-order diffusive flux

$$d_{j+\frac{1}{2}} = \alpha_{j+\frac{1}{2}} \left\{ \Delta v_{j+\frac{1}{2}} - \tfrac{1}{2}\left(\Delta v_{j+\frac{3}{2}} + \Delta v_{j-\frac{1}{2}}\right) \right\} \tag{89}$$

which is an approximation to $(1/2)\alpha\Delta x^3(\partial^3 v/\partial x^3)$. The positivity condition (82) is violated by this scheme. It proves that it generates substantial oscillations in the vicinity of shock waves, which can be eliminated by switching locally to the first-order scheme. The JST scheme therefore introduces blended diffusion of the form

$$\begin{aligned} d_{j+\frac{1}{2}} = {} & \epsilon^{(2)}_{j+\frac{1}{2}} \Delta v_{j+\frac{1}{2}} \\ & - \epsilon^{(4)}_{j+\frac{1}{2}} \left(\Delta v_{j+\frac{3}{2}} - 2\Delta v_{j+\frac{1}{2}} + \Delta v_{j-\frac{1}{2}}\right) \end{aligned} \tag{90}$$

The idea is to use variable coefficients $\epsilon^{(2)}_{j+1/2}$ and $\epsilon^{(4)}_{j+1/2}$, which produce a low level of diffusion in regions where the solution is smooth, but prevent oscillations near discontinuities. If $\epsilon^{(2)}_{j+1/2}$ is constructed so that it is of order Δx^2 where the solution is smooth, while $\epsilon^{(4)}_{j+1/2}$ is of order unity, both terms in $d_{j+1/2}$ will be of order Δx^3.

The JST scheme has proved very effective in practice in numerous calculations of complex steady flows, and conditions under which it could be a TVD scheme have been examined by Swanson and Turkel (1992). An alternative statement of sufficient conditions on the coefficients $\epsilon^{(2)}_{j+1/2}$ and $\epsilon^{(4)}_{j+1/2}$ for the JST scheme to be LED is as follows (Jameson, 1995a):

Theorem 1 (Positivity of the JST scheme) *Suppose that whenever either v_{j+1} or v_j is an extremum, the coefficients of the JST scheme satisfy*

$$\epsilon^{(2)}_{j+\frac{1}{2}} \geq \tfrac{1}{2}\left|\alpha_{j+\frac{1}{2}}\right|, \quad \epsilon^{(4)}_{j+\frac{1}{2}} = 0 \tag{91}$$

Then the JST scheme is local extremum diminishing (LED).

Proof. We need only consider the rate of change of v at extremal points. Suppose that v_j is an extremum. Then,

$$\epsilon^{(4)}_{j+\frac{1}{2}} = \epsilon^{(4)}_{j-\frac{1}{2}} = 0$$

and the semidiscrete scheme (85) reduces to

$$\begin{aligned} \Delta x \frac{\mathrm{d}v_j}{\mathrm{d}t} = {} & \left(\epsilon^{(2)}_{j+\frac{1}{2}} - \frac{1}{2} a_{j+\frac{1}{2}}\right) \Delta v_{j+\frac{1}{2}} \\ & - \left(\epsilon^{(2)}_{j-\frac{1}{2}} + \frac{1}{2} a_{j-\frac{1}{2}}\right) \Delta v_{j-\frac{1}{2}} \end{aligned}$$

and each coefficient has the required sign. □

In order to construct $\epsilon^{(2)}_{j-1/2}$ and $\epsilon^{(4)}_{j-1/2}$ with the desired properties, define

$$R(u, v) = \begin{cases} \left| \dfrac{u - v}{|u| + |v|} \right|^q & \text{if } u \neq 0 \text{ or } v \neq 0 \\ 0 & \text{if } u = v = 0 \end{cases} \tag{92}$$

where q is a positive integer. Then, $R(u, v) = 1$ if u and v have opposite signs. Otherwise $R(u, v) < 1$. Now set

$$Q_j = R\left(\Delta v_{j+\frac{1}{2}}, \Delta v_{j-\frac{1}{2}}\right), \quad Q_{j+\frac{1}{2}} = \max(Q_j, Q_{j+1})$$

and

$$\epsilon^{(2)}_{j+\frac{1}{2}} = \alpha_{j+\frac{1}{2}} Q_{j+\frac{1}{2}}, \quad \epsilon^{(4)}_{j+\frac{1}{2}} = \tfrac{1}{2}\alpha_{j+\frac{1}{2}}\left(1 - Q_{j+\frac{1}{2}}\right) \tag{93}$$

In the case of an extremum, $R = 1$ and thus $Q_{j+1/2} = 1$, making $\epsilon^{(2)}_{j+1/2} = \alpha_{j+1/2}$ and $\epsilon^{(4)}_{j+1/2} = 0$.

4.3.4 *Symmetric limited positive (SLIP) scheme*

An alternative route to high resolution without oscillation is to introduce flux limiters to guarantee the satisfaction of the positivity condition (82). The use of limiters dates back to the work of Boris and Book (1973). A particularly simple way to introduce limiters, proposed by the author in 1984 (Jameson, 1985a), is to use flux limited dissipation. In this scheme, the third-order diffusion defined by equation (89) is modified by the insertion of limiters that produce an equivalent three-point scheme with positive coefficients. The original scheme (Jameson, 1985a) can be improved in the following manner so that less restrictive flux limiters are required. Let $L(u, v)$ be a limited average of u and v with the following properties:

P1. $L(u, v) = L(v, u)$,
P2. $L(\alpha u, \alpha v) = \alpha L(u, v)$,
P3. $L(u, u) = u$,
P4. $L(u, v) = 0$ if u and v have opposite signs; otherwise $L(u, v)$ has the same sign as u and v.

Properties (P1–P3) are natural properties of an average. Property (P4) is needed for the construction of an LED or TVD scheme.

It is convenient to introduce the notation

$$\phi(r) = L(1, r) = L(r, 1)$$

where according to (P4) $\phi(r) \geq 0$. It follows from (P2) on setting $\alpha = (1/u)$ or $(1/v)$ that

$$L(u, v) = \phi\left(\frac{v}{u}\right) u = \phi\left(\frac{u}{v}\right) v$$

Also, it follows on setting $v = 1$ and $u = r$ that

$$\phi(r) = r\phi\left(\frac{1}{r}\right)$$

Thus, if there exists $r < 0$ for which $\phi(r) > 0$, then $\phi(1/r) < 0$. The only way to ensure that $\phi(r) \geq 0$ is to require $\phi(r) = 0$ for all $r < 0$, corresponding to property (P4).

Now one defines the diffusive flux for a scalar conservation law as

$$d_{j+\frac{1}{2}} = \alpha_{j+\frac{1}{2}} \left\{ \Delta v_{j+\frac{1}{2}} - L\left(\Delta v_{j+\frac{3}{2}}, \Delta v_{j-\frac{1}{2}}\right)\right\} \qquad (94)$$

Set

$$r^+ = \frac{\Delta v_{j+\frac{3}{2}}}{\Delta v_{j-\frac{1}{2}}}, \quad r^- = \frac{\Delta v_{j-\frac{3}{2}}}{\Delta v_{j+\frac{1}{2}}}$$

and correspondingly

$$L\left(\Delta v_{j+\frac{3}{2}}, \Delta v_{j-\frac{1}{2}}\right) = \phi(r^+)\Delta v_{j-\frac{1}{2}}$$
$$L\left(\Delta v_{j-\frac{3}{2}}, \Delta v_{j+\frac{1}{2}}\right) = \phi(r^-)\Delta v_{j+\frac{1}{2}}$$

Then,

$$\Delta x \frac{\mathrm{d}v_j}{\mathrm{d}t} = \left\{\alpha_{j+\frac{1}{2}} - \frac{1}{2}a_{j+\frac{1}{2}} + \alpha_{j-\frac{1}{2}}\phi(r^-)\right\}\Delta v_{j+\frac{1}{2}} - \left\{\alpha_{j-\frac{1}{2}} + \frac{1}{2}a_{j-\frac{1}{2}} + \alpha_{j+\frac{1}{2}}\phi(r^+)\right\}\Delta v_{j-\frac{1}{2}} \qquad (95)$$

Thus, the scheme satisfies the LED condition if $\alpha_{j+1/2} \geq (1/2)|a_{j+1/2}|$ for all j, and $\phi(r) \geq 0$, which is assured by property (P4) on L. At the same time, it follows from property (P3) that the first-order diffusive flux is canceled when Δv is smoothly varying and of constant sign. Schemes constructed by this formulation will be referred to as *symmetric limited positive* (SLIP) schemes. This result may be summarized as

Theorem 2 (Positivity of the SLIP scheme) *Suppose that the discrete conservation law (85) contains a limited diffusive flux as defined by equation (94). Then the positivity condition (88), together with the properties (P1–P4) for limited averages, are sufficient to ensure satisfaction of the LED principle that a local maximum cannot increase and a local minimum cannot decrease.*

A variety of limiters may be defined that meet the requirements of properties (P1–P4). Define

$$S(u, v) = \tfrac{1}{2}\{\mathrm{sign}(u) + \mathrm{sign}(v)\}$$

which vanishes as u and v have opposite signs. Then two limiters that are appropriate are the following well-known schemes:

1. Minmod:

$$L(u, v) = S(u, v)\min(|u|, |v|)$$

2. Van Leer:

$$L(u, v) = S(u, v)\frac{2|u||v|}{|u| + |v|}$$

In order to produce a family of limiters, which contains these as special cases, it is convenient to set

$$L(u, v) = \tfrac{1}{2}D(u, v)(u + v)$$

where $D(u, v)$ is a factor that should deflate the arithmetic average and become zero if u and v have opposite signs. Take

$$D(u, v) = 1 - R(u, v) = 1 - \left|\frac{u - v}{|u| + |v|}\right|^q \qquad (96)$$

where $R(u, v)$ is the same function that was introduced in the JST scheme and q is a positive integer. Then $D(u, v) = 0$ if u and v have opposite signs. Also if $q = 1$, $L(u, v)$ reduces to minmod, while if $q = 2$, $L(u, v)$ is equivalent to Van Leer's limiter. By increasing q, one can generate a sequence of limited averages that approach a limit defined

by the arithmetic mean truncated to zero when u and v have opposite signs.

When the terms are regrouped, it can be seen that with this limiter the SLIP scheme is exactly equivalent to the JST scheme, with the switch defined as

$$Q_{j+\frac{1}{2}} = R\left(\Delta v_{j+\frac{3}{2}}, \Delta v_{j+\frac{1}{2}}\right)$$
$$\epsilon^{(2)}_{j+\frac{1}{2}} = \alpha_{j+\frac{1}{2}} Q_{j+\frac{1}{2}}$$
$$\epsilon^{(4)}_{j+\frac{1}{2}} = \alpha_{j+\frac{1}{2}}\left(1 - Q_{j+\frac{1}{2}}\right)$$

This formulation thus unifies the JST and SLIP schemes. The SLIP construction, however, provides a convenient framework for the construction of LED schemes on unstructured meshes (Jameson, 1995a).

4.3.5 *Essentially local extremum diminishing (ELED) scheme with soft limiter*

The limiters defined by the formula (96) have the disadvantage that they are active at a smooth extrema, reducing the local accuracy of the scheme to first order. In order to prevent this, the SLIP scheme can be relaxed to give an ELED scheme, which is second-order accurate at smooth extrema by the introduction of a threshold in the limited average. Therefore, redefine $D(u, v)$ as

$$D(u, v) = 1 - \left|\frac{u - v}{\max(|u| + |v|, \epsilon\Delta x^r)}\right|^q \qquad (97)$$

where $r = (3/2)$, $q \geq 2$, and ϵ is a dimensional parameter that must be chosen to be consistent with the solution variable in equation (83). This reduces to the previous definition if $|u| + |v| > \epsilon\Delta x^r$.

In any region where the solution is smooth, $\Delta v_{j+3/2} - \Delta v_{j-1/2}$ is of order Δx^2. In fact, if there is a smooth extremum in the neighborhood of v_j or v_{j+1}, a Taylor series expansion indicates that $\Delta v_{j+3/2}$, $\Delta v_{j+1/2}$, and $\Delta v_{j-1/2}$ are each individually of order Δx^2, since $(\mathrm{d}v/\mathrm{d}x) = 0$ at the extremum. It may be verified that second-order accuracy is preserved at a smooth extremum if $q \geq 2$. On the other hand, the limiter acts in the usual way if $|\Delta v_{j+3/2}|$ or $|\Delta v_{j-3/2}| > \epsilon\Delta x^r$, and it may also be verified that in the limit $\Delta x \to 0$ local maxima are nonincreasing and local minima are nondecreasing (Jameson, 1995a). Thus, the scheme is ELED.

The effect of the 'soft limiter' is not only to improve the accuracy: the introduction of a threshold below which extrema of small amplitude are accepted also usually results in a faster rate of convergence to a steady state, and decreases the likelihood of limit cycles in which the limiter interacts unfavorably with the corrections produced by the updating scheme. In a scheme recently proposed by Venkatakrishnan, a threshold is introduced precisely for this purpose (Venkatakrishnan, 1993).

4.3.6 *Upstream limited positive (USLIP) schemes*

By adding the antidiffusive correction purely from the upstream side, one may derive a family of upstream limited positive (USLIP) schemes. Corresponding to the original SLIP scheme defined by equation (94), a USLIP scheme is obtained by setting

$$d_{j+\frac{1}{2}} = \alpha_{j+\frac{1}{2}}\left\{\Delta v_{j+\frac{1}{2}} - L\left(\Delta v_{j+\frac{1}{2}}, \Delta v_{j-\frac{1}{2}}\right)\right\}$$

if $a_{j+1/2} > 0$, or

$$d_{j+\frac{1}{2}} = \alpha_{j+\frac{1}{2}}\left\{\Delta v_{j+\frac{1}{2}} - L\left(\Delta v_{j+\frac{1}{2}}, \Delta v_{j+\frac{3}{2}}\right)\right\}$$

if $a_{j+1/2} < 0$. If $\alpha_{j+1/2} = (1/2)|a_{j+1/2}|$, one recovers a standard high-resolution upwind scheme in semidiscrete form. Consider the case that $a_{j+1/2} > 0$ and $a_{j-1/2} > 0$. If one sets

$$r^+ = \frac{\Delta v_{j+\frac{1}{2}}}{\Delta v_{j-\frac{1}{2}}}, \quad r^- = \frac{\Delta v_{j-\frac{3}{2}}}{\Delta v_{j-\frac{1}{2}}}$$

the scheme reduces to

$$\Delta x \frac{\mathrm{d}v_j}{\mathrm{d}t} = -\frac{1}{2}\left\{\phi(r^+)a_{j+\frac{1}{2}} + \left(2 - \phi(r^-)\right)a_{j-\frac{1}{2}}\right\}\Delta v_{j-\frac{1}{2}}$$

To assure the correct sign to satisfy the LED criterion, the flux limiter must now satisfy the additional constraint that $\phi(r) \leq 2$.

The USLIP formulation is essentially equivalent to standard upwind schemes (Osher and Solomon, 1982; Sweby, 1984). Both the SLIP and USLIP constructions can be implemented on unstructured meshes (Jameson, 1993, 1995a). The antidiffusive terms are then calculated by taking the scalar product of the vectors defining an edge with the gradient in the adjacent upstream and downstream cells.

4.3.7 *Higher-order schemes*

The JST and SLIP constructions are perhaps the simplest way to implement schemes of second-order accuracy. It should be noted that the finite volume discretization defined by equation (85) is an exact statement of the evolution of the cell-average values v_j if the interface fluxes

$h_{j+1/2}$ are exact, and consequently the generally preferred interpretation is to regard v_j as denoting the cell average and not the point value. The distinction is not important for second-order accurate schemes because for a smooth solution the difference between the cell average and the pointwise value at the cell centroid is $O(\Delta x^2)$, but it is important for the construction of third or higher-order accurate schemes.

One approach to the construction of progressively more accurate LED schemes is to define the numerical flux as a combination of low- and high-order fluxes $f_{L_{j+1/2}}$ and $f_{H_{j+1/2}}$. Then the difference $f_{H_{j+1/2}} - f_{L_{j+1/2}}$ is applied to as a correction $f_{C_{j+1/2}}$, which is limited in the neighborhood of extrema to preserve the LED property. Accordingly,

$$h_{j+\frac{1}{2}} = f_{L_{j+\frac{1}{2}}} + f_{C_{j+\frac{1}{2}}}$$

where

$$f_{C_{j+\frac{1}{2}}} = B_{j+\frac{1}{2}}\left(f_{H_{j+\frac{1}{2}}} - f_{L_{j+\frac{1}{2}}}\right)$$

and the limiter $B_{j+1/2}$ is determined from local scope comparisons. This approach has been proposed by Zalesak (1979) and Jameson (1995a).

4.3.8 Reconstruction

Any scheme of third- or higher-order accuracy must construct the numerical flux $h_{j+1/2}$ from a stencil of more than two points. To extend the SLIP scheme defined by equations (85, 86, and 94), for example, to a higher-order accuracy, it is necessary to replace $(1/2)(f_{j+1} + f_j)$ by a combination over the cells from $j-1$ to $j+2$. An alternative approach that has been widely adopted is to construct the flux $h_{j+1/2}$ as a function of two values labeled v_L and v_R, which may be regarded as estimates of $v_{j+1/2}$ biased to the left and right,

$$h_{j+\frac{1}{2}} = h(v_L, v_R)$$

Now the desired order of accuracy p is attained by constructing v_L and v_R so that they both differ from the true value of the solution at the interface by $O(\Delta x^p)$. Thus, the formulation of higher-order schemes is reduced to the 'reconstruction' of sufficiently accurate point values v_L and v_R from stencils of cell average values (or possible point values) centered at j and $j+1$, while an upwind bias can be introduced by the way in which $h(v_L, v_R)$ is evaluated from v_L and v_R, depending on the wave speed. For a simple upwind scheme

$$h(v_L, v_R) = \begin{cases} f(v_L) & \text{if } a_{j+\frac{1}{2}} > 0 \\ f(v_R) & \text{if } a_{j+\frac{1}{2}} < 0 \end{cases} \tag{98}$$

In the SLIP scheme, as another example, equation (94) can be rewritten as

$$d_{j+\frac{1}{2}} = \alpha_{j+\frac{1}{2}}(v_R - v_L)$$

where for a second-order scheme

$$v_L = v_j + \tfrac{1}{2}L\left(\Delta v_{j+\frac{3}{2}}, \Delta v_{j-\frac{1}{2}}\right)$$
$$v_R = v_{j+1} - \tfrac{1}{2}L\left(\Delta v_{j+\frac{3}{2}}, \Delta v_{j+\frac{1}{2}}\right) \tag{99}$$

Accordingly, setting $f_L = f(v_L)$ and $f_R = f(v_R)$, the SLIP scheme may be formulated as

$$h_{j+\frac{1}{2}} = \tfrac{1}{2}(f_R + f_L) - \alpha_{j+\frac{1}{2}}(v_R - v_L) \tag{100}$$

Numerical tests by the author have shown that on smooth meshes the substitution $(1/2)(f_R + f_L)$ for $(1/2)(f_{j+1} + f_j)$ makes a negligible difference.

However, the use of reconstruction, which was first introduced by Van Leer in his MUSCL scheme (Van Leer, 1974) as a way to extend Godunov's method (Godunov, 1959) to second-order accuracy, has the advantage that it neatly separates the design of flux functions with nonoscillatory shock-capturing properties from the construction of higher-order interpolation and time-stepping schemes. It proves particularly useful both for the treatment of systems of equations (considered in Section 4.4) and for discretization on arbitrary meshes (considered in Section 5).

4.3.9 ENO and WENO schemes

Schemes using reconstruction still require the use of limiters near extrema to maintain the LED or TVD property. In order to alleviate this difficulty, Harten, Osher, Engquist, and Chakaravarthy proposed the idea of 'essentially nonoscillatory' (ENO) schemes (Harten *et al.*, 1987). These use an adaptive stencil for the reconstruction of v_L and v_R designed to find the least oscillatory interpolant of a given order of accuracy. To construct $v_{L_{j+1/2}}$, for example, with rth-order accuracy, one would examine the interpolants of r stencils, each spanning r cells, symmetrically arranged around cell j, as illustrated in Figure 21. In order to measure which interpolant is least oscillatory, we can introduce the divided differences for each stencil. For a function $V(x)$

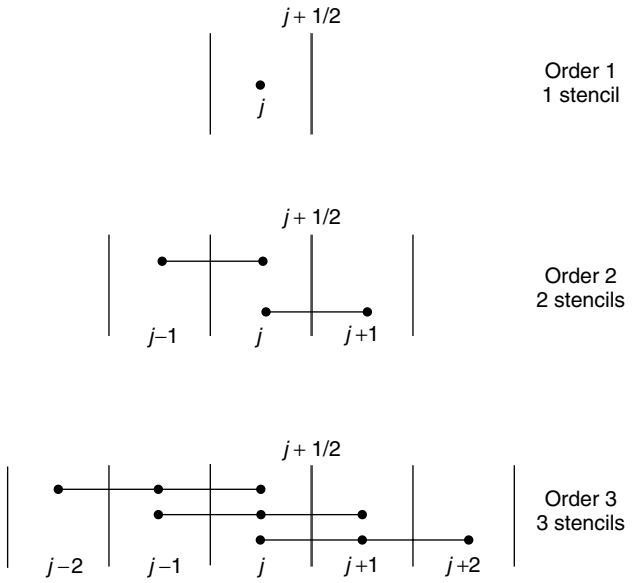

Figure 21. Stencils for reconstruction of $v_{L_{j+1/2}}$. A color version of this image is available at http://www.mrw.interscience.wiley.com/ecm

defined at the points $x_0, x_1, \ldots, x_r$, the divided differences are defined recursively as

$$V[x_0] = V(x_0)$$
$$V[x_0, x_1] = \frac{V[x_1] - V[x_0]}{x_1 - x_0}$$
$$V[x_0, x_1, x_2] = \frac{V[x_1, x_2] - V[x_0, x_1]}{x_2 - x_0} \qquad (101)$$

Then, if $V(x)$ is smooth in the stencil $[x_0, x_2]$, the rth divided difference is proportional to the rth derivative at a point ξ within the stencil

$$V[x_0, \ldots, x_r] = \frac{1}{r!} V^{(r)}(\xi)$$

while if $V(x)$ is discontinuous

$$V[x_0, \ldots, x_r] = O\frac{1}{(\Delta x^r)}$$

Accordingly, the divided differences provide a measure of the smoothness of $V(x)$ in the stencil.

The ENO scheme builds up successively higher-order interpolants to the primitive function $V(x)$ defined as

$$V_{x+\frac{1}{2}} = \int_{-\infty}^{x_{j+1/2}} v(\xi)\, \mathrm{d}\xi = \sum_{i=-\infty}^{j} \bar{v}_i \Delta x_i$$

where $\bar{v}_i$ is the average value of $v(x)$ in cell i. Then the derivative of the Lagrange interpolation polynomial $P(x)$ over an r-cell stencil satisfies

$$P'(x) = V'(x) + O(\Delta x^r)$$

with the result that $P'(x_{j+1/2})$ provides the desired rth-order reconstruction of $v_{j+1/2}$.

The reconstruction procedure starts with a stencil consisting of the single cell j. At each step, a higher-order interpolant is formed by adding a cell to the left or right of the previous stencil. We choose whichever of the two new candidate stencils has the smaller absolute value of the divided difference thus arriving at the least oscillatory interpolants of any given order. Alternative reconstruction procedures to generate interpolants from point values have also been worked out.

The original ENO schemes have the drawback that very small changes in the solution could cause sudden changes in the adaptive stencils. In steady flow calculations, this could lead to limit cycles that prevent complete convergence. If the initial data was an odd–even mode $v_j = (-1)^j$, for example, all divided differences would be equal in magnitude and the choice of adaptive stencils would be random.

These deficiencies are remedied by the weighted essentially non-oscillatory (WENO) schemes originally developed by Liu, Osher and Chan (1994), and Jiang and Shu (1996). Instead of picking one stencil at each stage, the WENO schemes use a weighted average of the r possible r-cell stencils symmetrically arranged about cell j for the reconstruction of v_L at the interface $j + 1/2$, and about cell $j + 1$ for the reconstruction of v_R. Referring to Figure 21, it can be seen that these span $2r - 1$ cells, with the consequence that the weights can be chosen to recover $(2r - 1)$th-order accurate estimates of v_L and v_R.

Suppose that the r cell interpolants for the stencils $(j + k - r + 1, \ldots, j + k), k = 0, \ldots, r - 1$ are q_k^r, and the optimal $(2r - 1)$th-order accurate combination is

$$\hat{v}_L = \sum_{k=0}^{r-1} C_k q_k^r \qquad (102)$$

with weights C_k such that

$$\sum_{k=0}^{r-1} C_k = 1 \qquad (103)$$

In order to find a less oscillatory interpolant when the solution is not smooth, we replace these weights with weights ω_k, which are deflated if the interpolant q_k^r is oscillatory. For this purpose, we introduce a measure IS_k of the smoothness of q_k^r. Then, the weights ω_k may be

defined as

$$\omega_k = \frac{\alpha_k}{\alpha_0 + \cdots + \alpha_{r-1}} \tag{104}$$

where

$$\alpha_k = \frac{C_k^r}{(\epsilon + IS_k)^p}, \quad k = 0, 1, \ldots, r-1 \tag{105}$$

These definitions ensure that

$$\sum_{k=0}^{r-1} \omega_k = 1$$

The quantity ϵ is a small tolerance (>0) to ensure that α_k is defined as $IS_k = 0$. Jiang and Shu recommend a formula based on the divided differences for the smoothness indicator IS_k and the value $p = 2$ for the power in equation (105).

WENO schemes have been widely adopted and shown to give excellent results for unsteady flows with shock waves and contact discontinuities, such as flows in shock tubes (Jiang and Shu, 1996). Their extension to multidimensional flows on unstructured grids has been worked out, but is very complex.

4.4 Systems of conservation laws: flux splitting and flux-difference splitting

Steger and Warming (1981) first showed how to generalize the concept of upwinding to the system of conservation laws

$$\frac{\partial w}{\partial t} + \frac{\partial}{\partial x} f(w) = 0 \tag{106}$$

by the concept of flux splitting. Suppose that the flux is split as $f = f^+ + f^-$, where $(\partial f^+/\partial w)$ and $(\partial f^-/\partial w)$ have positive and negative eigenvalues. Then the first-order upwind scheme is produced by taking the numerical flux to be

$$h_{j+\frac{1}{2}} = f_j^+ + f_{j+1}^-$$

This can be expressed in viscosity form as

$$\begin{aligned} h_{j+\frac{1}{2}} &= \tfrac{1}{2}(f_{j+1}^+ + f_j^+) - \tfrac{1}{2}(f_{j+1}^+ - f_j^+) \\ &\quad + \tfrac{1}{2}(f_{j+1}^- + f_j^-) + \tfrac{1}{2}(f_{j+1}^- - f_j^-) \\ &= \tfrac{1}{2}(f_{j+1} + f_j) - d_{j+\frac{1}{2}} \end{aligned}$$

where the diffusive flux is

$$d_{j+\frac{1}{2}} = \tfrac{1}{2}\Delta(f^+ - f^-)_{j+\frac{1}{2}} \tag{107}$$

Roe derived the alternative formulation of flux-difference splitting (Roe, 1981) by distributing the corrections due to the flux difference in each interval upwind and downwind to obtain

$$\Delta x \frac{\mathrm{d}w_j}{\mathrm{d}t} + (f_{j+1} - f_j)^- + (f_j - f_{j-1})^+ = 0$$

where now the flux difference $f_{j+1} - f_j$ is split. The corresponding diffusive flux is

$$d_{j+\frac{1}{2}} = \tfrac{1}{2}\left(\Delta f^+_{j+\frac{1}{2}} - \Delta f^-_{j+\frac{1}{2}}\right)$$

Following Roe's derivation, let $A_{j+1/2}$ be a mean value Jacobian matrix exactly satisfying the condition

$$f_{j+1} - f_j = A_{j+\frac{1}{2}}(w_{j+1} - w_j) \tag{108}$$

$A_{j+1/2}$ may be calculated by substituting the weighted averages

$$\begin{aligned} u &= \frac{\sqrt{\rho_{j+1}}u_{j+1} + \sqrt{\rho_j}u_j}{\sqrt{\rho_{j+1}} + \sqrt{\rho_j}} \\ H &= \frac{\sqrt{\rho_{j+1}}H_{j+1} + \sqrt{\rho_j}H_j}{\sqrt{\rho_{j+1}} + \sqrt{\rho_j}} \end{aligned} \tag{109}$$

into the standard formulas for the Jacobian matrix $A = (\partial f/\partial w)$. A splitting according to characteristic fields is now obtained by decomposing $A_{j+1/2}$ as

$$A_{j+\frac{1}{2}} = M\Lambda M^{-1} \tag{110}$$

where the columns of M are the eigenvectors of $A_{j+1/2}$ and Λ is a diagonal matrix of the eigenvalues as defined in equations (14–25). Now the corresponding diffusive flux is

$$d_{j+\frac{1}{2}} = \tfrac{1}{2}\left|A_{j+\frac{1}{2}}\right|(w_{j+1} - w_j)$$

where

$$\left|A_{j+\frac{1}{2}}\right| = M|\Lambda|M^{-1}$$

and $|\Lambda|$ is the diagonal matrix containing the absolute values of the eigenvalues.

4.5 Alternative splittings

Characteristic splitting has the advantages that it introduces the minimum amount of diffusion to exclude the growth of local extrema of the characteristic variables and that with the Roe linearization it allows a discrete shock structure with a single interior point. To reduce the computational complexity, one may replace $|A|$ by αI, where if α is at least equal to the spectral radius $\max|\lambda(A)|$, the positivity conditions will still be satisfied. Then the first-order scheme simply has the scalar diffusive flux

$$d_{j+\frac{1}{2}} = \tfrac{1}{2}\alpha_{j+\frac{1}{2}}\Delta w_{j+\frac{1}{2}} \tag{111}$$

The JST scheme with scalar diffusive flux captures shock waves with about 3 interior points, and it has been widely used for transonic flow calculations because it is both robust and computationally inexpensive.

An intermediate class of schemes can be formulated by defining the first-order diffusive flux as a combination of differences of the state and flux vectors

$$d_{j+\frac{1}{2}} = \tfrac{1}{2}\alpha^*_{j+\frac{1}{2}}c(w_{j+1} - w_j) + \tfrac{1}{2}\beta_{j+\frac{1}{2}}(f_{j+1} - f_j) \tag{112}$$

where the speed of sound c is included in the first term to make $\alpha^*_{j+1/2}$ and $\beta_{j+1/2}$ dimensionless. Schemes of this class are fully upwind in supersonic flow if one takes $\alpha^*_{j+1/2} = 0$ and $\beta_{j+1/2} = \text{sign}(M)$ when the absolute value of the Mach number M exceeds 1. The flux vector f can be decomposed as

$$f = uw + f_p \tag{113}$$

where

$$f_p = \begin{pmatrix} 0 \\ p \\ up \end{pmatrix} \tag{114}$$

Then

$$f_{j+1} - f_j = \bar{u}(w_{j+1} - w_j) + \bar{w}(u_{j+1} - u_j) + f_{p_{j+1}} - f_{p_j} \tag{115}$$

where $\bar{u}$ and $\bar{w}$ are the arithmetic averages

$$\bar{u} = \tfrac{1}{2}(u_{j+1} + u_j), \quad \bar{w} = \tfrac{1}{2}(w_{j+1} + w_j)$$

Thus these schemes are closely related to schemes that introduce separate splittings of the convective and pressure terms, such as the wave-particle scheme (Rao and Deshpande, 1991; Balakrishnan and Deshpande, 1991), the advection upwind splitting method (AUSM) (Liou and Steffen, 1993; Wada and Liou, 1994), and the convective upwind and split pressure (CUSP) scheme (Jameson, 1993).

In order to examine the shock-capturing properties of these various schemes, consider the general case of a first-order diffusive flux of the form

$$d_{j+\frac{1}{2}} = \tfrac{1}{2}\alpha_{j+\frac{1}{2}}B_{j+\frac{1}{2}}(w_{j+1} - w_j) \tag{116}$$

where the matrix $B_{j+1/2}$ determines the properties of the scheme and the scaling factor $\alpha_{j+1/2}$ is included for convenience. All the previous schemes can be obtained by representing $B_{j+1/2}$ as a polynomial in the matrix $A_{j+1/2}$ defined by equation (108). Schemes of this class were considered by Van Leer (1974). According to the Cayley-Hamilton theorem, a matrix satisfies its own characteristic equation. Therefore the third and higher powers of A can be eliminated, and there is no loss of generality in limiting $B_{j+1/2}$ to a polynomial of degree 2,

$$B_{j+\frac{1}{2}} = \alpha_0 I + \alpha_1 A_{j+\frac{1}{2}} + \alpha_2 A^2_{j+\frac{1}{2}} \tag{117}$$

Scalar diffusion is represented by the first term, while using the substitution (108), the intermediate (CUSP) scheme is represented by a two-term expansion. The characteristic upwind scheme for which $B_{j+1/2} = |A_{j+1/2}|$ is obtained by substituting $A_{j+1/2} = T\Lambda T^{-1}$, $A^2_{j+1/2} = T\Lambda^2 T^{-1}$. Then α_0, α_1, and α_2 are determined from the three equations

$$\alpha_0 + \alpha_1\lambda_k + \alpha_2\lambda_k^2 = |\lambda_k|, \quad k = 1, 2, 3$$

The same representation remains valid for three-dimensional flow because $A_{j+1/2}$ still has only three distinct eigenvalues u, $u + c$, and $u - c$.

4.6 Analysis of stationary discrete shocks

The ideal model of a discrete shock is illustrated in Figure 22. Suppose that w_L and w_R are left and right states that satisfy the jump conditions for a stationary shock, and that the corresponding fluxes are $f_L = f(w_L)$ and $f_R = f(w_R)$. Since the shock is stationary, $f_L = f_R$. The ideal discrete shock has constant states w_L to the left and w_R to the right, and a single point with an intermediate value w_A. The intermediate value is needed to allow the discrete solution to correspond to a true solution in which the shock wave does not coincide with an interface between two mesh cells.

Schemes corresponding to one, two, or three terms in equation (117) are examined in Jameson (1995b). The analysis of these three cases shows that a discrete shock

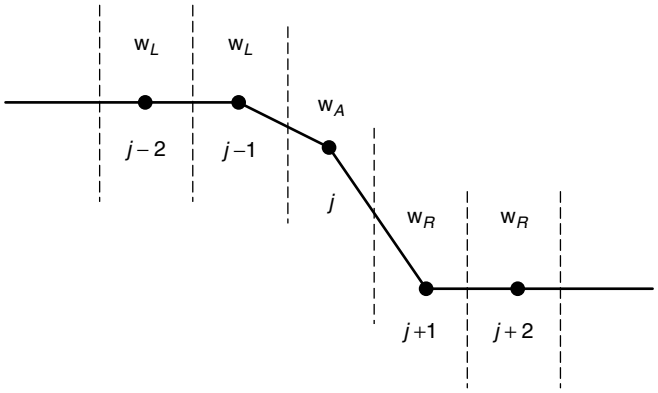

Figure 22. Shock structure for single interior point.

structure with a single interior point is supported by artificial diffusion that satisfies the two conditions that

1. it produces an upwind flux if the flow is determined to be supersonic through the interface,
2. it satisfies a generalized eigenvalue problem for the exit from the shock of the form

$$\left(A_{AR} - \alpha_{AR} B_{AR}\right)\left(w_R - w_A\right) = 0 \qquad (118)$$

where A_{AR} is the linearized Jacobian matrix and B_{AR} is the matrix defining the diffusion for the interface AR. This follows from the equilibrium condition $h_{RA} = h_{RR}$ for the cell $j+1$ in Figure 22. These two conditions are satisfied by both the characteristic scheme and also the CUSP scheme, provided that the coefficients of convective diffusion and pressure differences are correctly balanced. Scalar diffusion does not satisfy the first condition. In the case of the CUSP scheme (112), equation (118) reduces to

$$\left(A_{RA} + \frac{\alpha^* c}{1+\beta}\right)\left(w_R - w_A\right) = 0$$

Thus $w_R - w_A$ is an eigenvector of the Roe matrix A_{RA}, and $-[\alpha^* c/(1+\beta)]$ is the corresponding eigenvalue. Since the eigenvalues are u, $u+c$, and $u-c$, the only choice that leads to positive diffusion when $u > 0$ is $u - c$, yielding the relationship

$$\alpha^* c = (1+\beta)(c-u), \quad 0 < u < c$$

This leads to a one-parameter family of schemes that support the ideal shock structure. The term $\beta(f_R - f_A)$ contributes to the diffusion of the convective terms. Allowing for the split (113), the total effective coefficient of convective diffusion is $\alpha c = \alpha^* c + \beta\overline{u}$. A CUSP scheme with low numerical diffusion is then obtained by taking $\alpha = |M|$, leading to the coefficients illustrated in Figure 23.

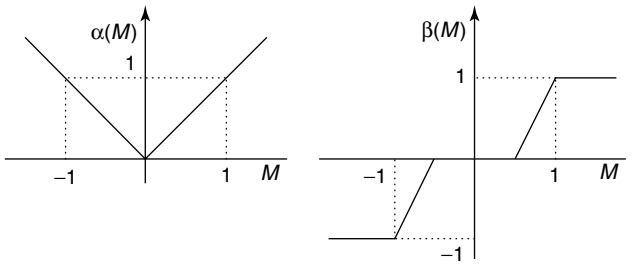

Figure 23. Diffusion coefficients.

4.7 CUSP and characteristic schemes admitting constant total enthalpy in steady flow

In steady flow, the stagnation enthalpy H is constant, corresponding to the fact that the energy and mass conservation equations are consistent when the constant factor H is removed from the energy equation. Discrete and semidiscrete schemes do not necessarily satisfy this property. In the case of a semidiscrete scheme expressed in viscosity form, equations (85) and (86), a solution with constant H is admitted if the viscosity for the energy equation reduces to the viscosity for the continuity equation with ρ replaced by ρH. When the standard characteristic decomposition (110) is used, the viscous fluxes for ρ and ρH that result from composition of the fluxes for the characteristic variables do not have this property, and H is not constant in the discrete solution. In practice, there is an excursion of H in the discrete shock structure that represents a local heat source. In very high speed flows, the corresponding error in the temperature may lead to a wrong prediction of associated effects such as chemical reactions.

The source of the error in the stagnation enthalpy is the discrepancy between the convective terms

$$u\begin{pmatrix}\rho\\ \rho u\\ \rho H\end{pmatrix}$$

in the flux vector, which contain ρH, and the state vector, which contains ρE. This may be remedied by introducing a modified state vector

$$w_h = \begin{pmatrix}\rho\\ \rho u\\ \rho H\end{pmatrix}$$

Then one introduces the linearization

$$f_R - f_L = A_h(w_{h_R} - w_{h_L})$$

Table 1. Shock wave at Mach 20.

I	ρ	H	p	M
19	1.0000	283.5000	1.0000	20.0000
20	1.0000	283.5000	1.0000	20.0000
21	1.0000	283.5000	1.0000	20.0000
22	4.1924	283.4960	307.4467	0.7229
23	5.9259	283.4960	466.4889	0.3804
24	5.9259	283.4960	466.4889	0.3804
25	5.9259	283.4960	466.4889	0.3804

Here A_h may be calculated in the same way as the standard Roe linearization. Introduce the weighted averages defined by equation (109). Then

$$A_h = \begin{pmatrix} 0 & 1 & 0 \\ -\dfrac{\gamma+1}{\gamma}\dfrac{u^2}{2} & \dfrac{\gamma+1}{\gamma}u & \dfrac{\gamma-1}{\gamma} \\ -uH & H & u \end{pmatrix}$$

The eigenvalues of A_h are u, λ^+, and λ^-, where

$$\lambda^{\pm} = \frac{\gamma+1}{2\gamma}u \pm \sqrt{\left(\frac{\gamma+1}{2\gamma}u\right)^2 + \frac{c^2-u^2}{\gamma}} \qquad (119)$$

Now both CUSP and characteristic schemes that preserve constant stagnation enthalpy in steady flow can be constructed from the modified Jacobian matrix A_h (Jameson, 1995b). These schemes also produce a discrete shock structure with one interior point in steady flow. Then one arrives at four variations with this property, which can conveniently be distinguished as the E- and H-CUSP schemes, and the E- and H-characteristic schemes.

Table 1 shows the result for a shock wave at Mach 20, using the H-CUSP scheme. The SLIP–JST construction was used with the limiter defined by equation (97), and $q = 3$. The table shows the values of ρ, u, H, p, M, and the entropy $S = \log(p/\rho\gamma) - \log(p_L/\rho_L^{\gamma})$. A perfect one point shock structure is displayed. The entropy is zero to 4 decimal places upstream of the shock, exhibits a slight excursion at the interior point, and is constant to 4 decimal places downstream of the shock.

5 DISCRETIZATION SCHEME FOR FLOWS IN COMPLEX MULTIDIMENSIONAL DOMAINS

5.1 Structured and unstructured meshes

In order to simulate multidimensional flow over complex configurations, the first choice that must be made is the nature of the mesh used to divide the flow field into discrete subdomains. The principal alternatives are Cartesian meshes, body-fitted curvilinear meshes, and unstructured tetrahedral meshes. Each of these approaches has some advantages that have led to their use. The Cartesian mesh minimizes the complexity of the algorithm at interior points and facilitates the use of high-order discretization procedures, at the expense of greater complexity, and possibly a loss of accuracy, in the treatment of boundary conditions at curved surfaces. This difficulty may be alleviated by using mesh refinement procedures near the surface. With their aid, schemes that use Cartesian meshes have recently been developed to treat very complex configurations (Melton, Pandya and Steger, 1993; Samant *et al.*, 1987; Berger and LeVeque, 1989; Landsberg *et al.*, 1993; Aftosmis, Melton and Berger, 1995).

Body-fitted meshes have been widely used and are particularly well suited to the treatment of viscous flow because they readily allow the mesh to be compressed near the body surface. With this approach, the problem of mesh generation itself has proved to be a major pacing item. The most commonly used procedures are algebraic transformations (Baker, 1986; Eiseman, 1979; Eriksson, 1982; Smith, 1983), methods based on the solution of elliptic equations, pioneered by Thompson, Thames and Mastin (1974), Thompson, Warsi and Mastin (1982), and Sorenson (1986, 1988), and methods based on the solution of hyperbolic equations marching out from the body (Steger and Chaussee, 1980). In order to treat very complex configurations, it generally proves expedient to use a multiblock procedure (Weatherill and Forsey, 1985; Sawada and Takanashi, 1987), with separately generated meshes in each block, which may then be patched at block faces, or allowed to overlap, as in the Chimera scheme (Benek, Buning and Steger, 1985; Benek, Donegan and Suhs, 1987). It remains both difficult and time consuming to generate a structured mesh for a complex configuration such as a complete aircraft, perhaps with its high-lift system deployed. The use of overset meshes facilitates the treatment of complex geometries, but automatic generation of structured meshes remains out of reach, and in current practice, the definition of a sufficiently accurate geometry model and mesh generation pose a major bottleneck in the industrial application of CFD.

The alternative is to use unstructured tetrahedral or polyhedral meshes. This alleviates (but not entirely eliminates) the difficulty of mesh generation, and facilitates adaptive mesh refinement. This approach has been gaining acceptance, as it is becoming apparent that it can lead to a speedup and reduction in the cost of mesh generation that more than offsets the increased complexity and cost of the flow simulations. Two competing procedures for generating

triangulations that have both proved successful are Delaunay triangulation (Delaunay, 1934; Barth, 1994), based on concepts introduced at the beginning of the century by Voronoi (1908), and the advancing front method (Lohner and Parikh, 1988).

5.2 Finite difference, finite volume, and finite element schemes

Associated with the choice of mesh type is the formulation of the discretization procedure. The finite difference method, which requires the use of a Cartesian or a structured curvilinear mesh, directly approximates the differential operators appearing in equations (27–30). In the finite volume method (MacCormack and Paullay, 1972), the discretization is accomplished by dividing the domain of the flow into a large number of small subdomains and applying the conservation laws in the integral form

$$\frac{\partial}{\partial t}\int_{\Omega} w \, \mathrm{d}V + \int_{\partial\Omega} \mathbf{f} \cdot \mathrm{d}\mathbf{S} = 0$$

Here $\mathbf{f}$ is the flux appearing in equation (2) and $\mathrm{d}\mathbf{S}$ is the directed surface element of the boundary $\partial\Omega$ of the domain Ω. The use of the integral form has the advantage that no assumption of the differentiability of the solutions is implied, with the result that it remains a valid statement for a subdomain containing a shock wave. In general, the subdomains could be arbitrary, but it is convenient to use either hexahedral cells in a body conforming curvilinear mesh or tetrahedrons in an unstructured mesh.

Alternative discretization schemes may be obtained by storing flow variables at either the cell centers or the vertices. These variations are illustrated in Figure 24 for the two-dimensional case. With a cell-centered scheme, the discrete conservation law takes the form

$$\frac{\mathrm{d}}{\mathrm{d}t} wV + \sum_{\text{faces}} \mathbf{f} \cdot \mathbf{S} = 0 \tag{120}$$

where V is the cell volume, and $\mathbf{f}$ is now a numerical estimate of the flux vector through each face. $\mathbf{f}$ may be evaluated from values of the flow variables in the cells separated by each face, using upwind biasing to allow for the directions of wave propagation. With hexahedral cells, equation (120) is very similar to a finite difference scheme in curvilinear coordinates. The transformed flux (33) corresponds to the dot product of the flux $\mathbf{f}$ with a vector face area $\mathbf{S}_j$ in the j coordinate direction, while in equation (27) J represents the transformation of the cell volume. The finite volume form (120) has the advantages that it is valid for both structured and unstructured meshes, and that it assures that a uniform flow exactly satisfies the equations, because $\sum_{\text{faces}} \mathbf{S} = 0$ for a closed control volume. Finite difference schemes do not necessarily satisfy this constraint because of the discretization errors in evaluating the transformation matrix $(\partial\xi_i/\partial x_j)$, which must then be inverted.

A cell-vertex finite volume scheme can be derived by taking the union of the cells surrounding a given vertex as the control volume for that vertex (Hall, 1985; Jameson, 1986b; Radespiel, Rossow and Swanson, 1989). In equation (120), V is now the sum of the volumes of the surrounding cells, while the flux balance is evaluated over the outer faces of the polyhedral control volume. In the absence of upwind biasing, the flux vector is evaluated by averaging over the corners of each face. This has the advantage of remaining accurate on an irregular or unstructured mesh. An alternative route to the discrete equations is provided by the finite element method.

Whereas the finite difference and finite volume methods approximate the differential and integral operators, the finite element method proceeds by inserting an approximate solution into the exact equations. On multiplying by a test function ϕ and integrating by parts over space, one obtains the weak form

$$\frac{\partial}{\partial t}\iiint_{\Omega} \phi w \, \mathrm{d}\Omega = \iiint_{\Omega} \mathbf{f} \cdot \nabla\phi \, \mathrm{d}\Omega - \iint_{\partial\Omega} \phi \mathbf{f} \cdot \mathrm{d}\mathbf{S} \tag{121}$$

which is also valid in the presence of discontinuities in the flow. In the Galerkin method, the approximate solution is expanded in terms of the same family of functions as those from which the test functions are drawn. By choosing test functions with local support, separate equations are obtained for each node. For example, if a tetrahedral mesh is used, and ϕ is piecewise linear, with a nonzero value

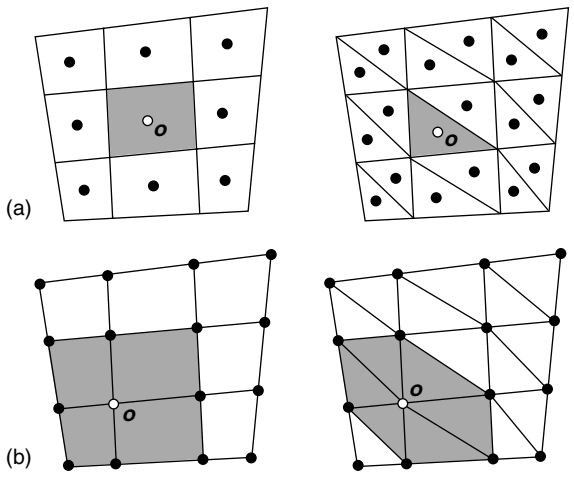

Figure 24. Discretizations on quadrilateral and triangular meshes. Shaded area is the control volume for the solution at location O. (a) Cell centered scheme, (b) vertex scheme.

only at a single node, the equations at each node have a stencil that contains only the nearest neighbors. In this case, the finite element approximation corresponds closely to a finite volume scheme. If a piecewise linear approximation to the flux **f** is used in the evaluation of the integrals on the right-hand side of equation (121), these integrals reduce to formulas that are identical to the flux balance of the finite volume scheme.

Thus the finite difference and finite volume methods lead to essentially similar schemes on structured meshes, while the finite volume method is essentially equivalent to a finite element method with linear elements when a tetrahedral mesh is used. Provided that the flow equations are expressed in the conservation law form (2), all three methods lead to an exact cancellation of the fluxes through interior cell boundaries, so that the conservative property of the equations is preserved. The important role of this property in ensuring correct shock jump conditions was pointed out by Lax and Wendroff (l960).

5.3 Wall boundary condition

Different treatments of the wall boundary condition are required for vertex and cell-centered schemes. In either case, assuming local body-fitted coordinates the tangency condition (10) for inviscid flow implies that there is no convective flux across the boundary, say $\xi_l = 0$. If the flow variables are stored at the vertices, their updated values at boundary vertices may no longer satisfy (10). A simple procedure is to correct the surface velocities by a projection in which the normal component of the velocity is set to zero.

In the case of a cell-centered scheme, the surface velocity does not explicitly appear in the discrete equations While there is no convective flux across the boundary faces, sketched in Figure 25 for the two-dimensional case, it is necessary to determine the pressure on these faces. An accurate estimate can be obtained by using the normal pressure gradient to extrapolate the pressure at the wall from its value in the boundary cell. The tangency condition (10) implies that

$$\frac{\partial}{\partial t}(\rho \mathbf{u} \cdot \mathbf{n}) = 0 \tag{122}$$

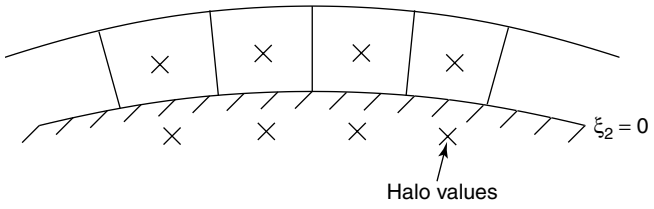

Figure 25. Boundary cells.

Combining the momentum equations, we find that

$$n_i \frac{\partial}{\partial x_j}(\rho u_i u_j) + n_i \frac{\partial p}{\partial x_i} = \frac{\partial}{\partial x_j}(\rho n_i u_i u_j) - \rho u_i u_j \frac{\partial n_i}{\partial x_j} + n_i \frac{\partial p}{\partial x_i} = 0 \tag{123}$$

where the first term vanishes by the tangency condition. Thus,

$$\frac{\partial p}{\partial n} = \rho u_i u_j \frac{\partial n_i}{\partial x_j} \tag{124}$$

Here the normal pressure gradient balances the centrifugal terms induced by the curvature of the wall.

The computational grid is not necessarily orthogonal, so in the discrete equations, one should estimate the pressure gradient in the direction of the radial mesh lines. Under a local coordinate transformation

$$\frac{\partial (J \rho u_i)}{\partial t} + \frac{\partial}{\partial \xi_j}(S_{jk} \rho u_i u_k + S_{ji} p) = 0 \tag{125}$$

where on a wall $\xi_l = 0$,

$$u_i S_{li} = 0 \tag{126}$$

Then

$$\begin{aligned} 0 &= \frac{\partial (J \rho u_i S_{li})}{\partial t} \\ &= S_{li} \frac{\partial}{\partial \xi_j}(S_{jk} \rho u_i u_k + S_{ji} p) \\ &= \frac{\partial}{\partial \xi_j}(S_{li} S_{jk} \rho u_i u_k) - S_{jk} \rho u_i u_k \frac{\partial S_{li}}{\partial \xi_j} \\ &\quad + S_{li} S_{ji} \frac{\partial p}{\partial \xi_j} + S_{li} p \frac{\partial S_{ji}}{\partial \xi_j} \end{aligned} \tag{127}$$

where the first term vanishes by (126) and the last term vanishes by the identity (32). Thus the pressure gradients satisfy the relation

$$S_{li} S_{ji} \frac{\partial p}{\partial \xi_j} = \rho u_i u_k S_{jk} \frac{\partial S_{li}}{\partial \xi_j} \tag{128}$$

where for $j = l$, $u_k S_{jk} = 0$. This allows the pressure gradient $(\partial p / \partial \xi_l)$ in the radial direction to be evaluated from the gradients in the tangential direction and the wall curvature. In order to allow the same equations to be used on calculating the flux across both interior and boundary faces, it is a common practice to extrapolate the pressure to halo cells beyond the boundary.

5.4 Far-field boundary condition

The rate of convergence to a steady state will be impaired if outgoing waves are reflected back into the flow from the outer boundaries. The treatment of the far-field boundary condition is based on the introduction of Riemann invariants for a one-dimensional flow normal to the boundary. Let subscripts ∞ and e denote free-stream values and values extrapolated from the interior cells adjacent to the boundary, and let q_n and c be the velocity component normal to the boundary and the speed of sound. Assuming that the flow is subsonic at infinity, we introduce fixed and extrapolated Riemann invariants

$$R_\infty = q_{n_\infty} - \frac{2c_\infty}{\gamma - 1}$$

and

$$R_e = q_{n_e} + \frac{2c_e}{\gamma - 1}$$

corresponding to incoming and outgoing waves. These may be added and subtracted to give

$$q_n = \tfrac{1}{2}\left(R_e + R_\infty\right)$$

and

$$c = \frac{\gamma - 1}{4}\left(R_e - R_\infty\right)$$

where q_n and c are the actual normal velocity component and speed of sound to be specified in the far field. At an outflow boundary, the tangential velocity components and entropy are extrapolated from the interior, while at an inflow boundary, they are specified as having free-stream values. These quantities provide a complete definition of the flow in the far field. If the flow is supersonic in the far field, all the flow quantities are specified at an inflow boundary, and they are all extrapolated from the interior at an outflow boundary.

5.5 Discretization on a tetrahedral mesh

The successful use of unstructured meshes is contingent on the formulation of sufficiently accurate discretization procedures. It also poses a variety of problems related to data structures and indirect addressing. Jameson, Baker, and Weatherill derived a finite element approximation by applying the Galerkin method to the weak form of the equations, using linear trial solutions and test functions (Jameson, Baker and Weatherill, 1986a). With some simplifications, it proves to be equivalent to balancing mass, momentum, and energy in polyhedral control volumes. Each of these control volumes is formed by the union of the tetrahedra meeting at a common vertex (Figure 26). Accordingly equation (2) can be approximated on a tetrahedral mesh by first writing the flux balance for each tetrahedron assuming the fluxes (F) to vary linearly over each face. Then at any given mesh point one considers the rate of change of w for a control volume consisting of the union of the tetrahedra meeting at a common vertex. The flux balance equation (120) now assumes the form

$$\frac{\mathrm{d}}{\mathrm{d}t}\left(\sum_k V_k w\right) + \sum_k R_k = 0 \tag{129}$$

where V_k is the volume of the kth tetrahedron meeting at a given mesh point and R_k is the flux of that tetrahedron.

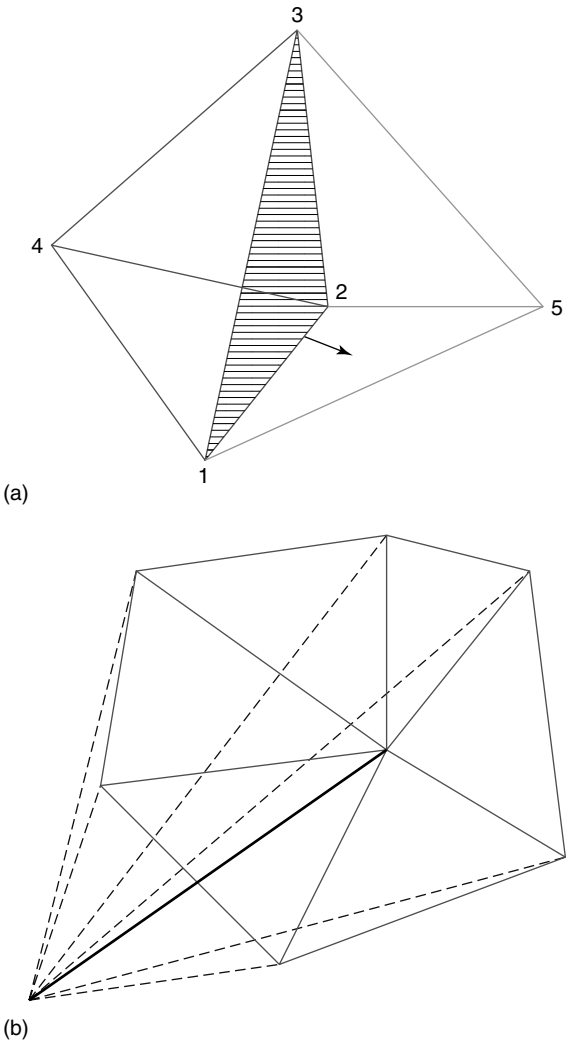

Figure 26. Face-based and edge-based data structures for flux evaluation with tetrahedral elements. A color version of this image is available at http://www.mrw.interscience.wiley.com/ecm

It turns out that the flux balance can be broken down into contributions of fluxes through faces in a very elegant way (Figure 26). This decomposition reduces the evaluation of the Euler equations to a single main loop over the faces. When the flux balances of the neighboring tetrahedra are summed, all contributions across interior faces cancel. Referring to Figure 26, which illustrates a portion of a three-dimensional mesh, it may be seen that with a tetrahedral mesh, each face is a common external boundary of exactly two control volumes. Therefore, each internal face can be associated with a set of 5 mesh points consisting of its corners 1, 2 and 3, and the vertices 4 and 5 of the two control volumes on either side of the common face. It is now possible to generate the approximation in equation (129), by presetting the flux balance at each mesh point to zero and then performing a single loop over the faces. For each face, one first calculates the fluxes of mass, momentum, and energy across each face, and then one assigns these contributions of the vertices 4 and 5 with positive and negative signs respectively. Since every contribution is transferred from one control volume into another, all quantities are perfectly conserved. Mesh points on the inner and outer boundaries lie on the surface of their own control volumes, and the accumulation of the flux balance in these volumes has to be correspondingly modified. At a solid surface, it is also necessary to enforce the boundary condition that there is no convective flux through the faces contained in the surface.

While the original formulation of this method used a face-based loop to accumulate the fluxes, it is possible to group the 'umbrella' of faces surrounding each edge (Figure 26), thus reducing the accumulation to an edge-based loop. This further reduces the computational cost because the number of edges in the mesh is typically smaller than the number of faces.

5.6 Multidimensional shock capturing schemes

The simplest approach to the treatment of multidimensional problems on structured meshes is to apply the one-dimensional construction separately in each mesh direction. On triangulated meshes in two or three dimensions, shock waves may be captured with the assistance of added artificial dissipation. These shock-capturing schemes are derived from general class of schemes that maintain the positivity of the coefficients, thereby preventing maxima from increasing and minima from decreasing with the consequence that the schemes satisfy LED property (Jameson, 1995a,b).

A simple way to introduce dissipation is to add a term generated from the difference between the value at a given node and its nearest neighbors. That is, at node 0, we add a term

$$D_o = \sum_k \epsilon_{ko}^{(1)}(w_k - w_o) \tag{130}$$

where the sum is over the nearest neighbors. This contribution is balanced by a corresponding contribution at node k, with the result that the scheme remains conservative. The coefficients $\epsilon_{ko}^{(1)}$ may incorporate metric information depending on local cell volumes and face areas, and can also be adapted to gradients of the solution. Equation (130) is only first-order accurate (unless the coefficients are proportional to the mesh spacing); a more accurate scheme can be obtained by recycling the edge differencing procedure. After setting

$$E_o = \sum_k (w_k - w_o) \tag{131}$$

at every mesh point, one then sets

$$D_o = -\sum_k \epsilon_{ok}^{(2)}(E_k - E_o) \tag{132}$$

The JST construction (equation (89)) can be emulated by blending equation (130) and (132) and adapting $\epsilon_{ko}^{(1)}$ to the local pressure gradient. The resulting scheme has proven robust, and has been found to have good shock-capturing properties. The required sums can be efficiently assembled by loops over the edges. Diffusive fluxes corresponding to the CUSP and characteristic-based schemes can readily be substituted for the scalar diffusive fluxes in equation (130). Also, the SLIP and USLIP constructions may be implemented along the mesh edges (Jameson, 1995a).

A substantial body of current research is directed toward the implementation of truly multidimensional upwind schemes in which the upwind biasing is determined by properties of the flow rather than the mesh (Hirsch, Lacol and Deconinck, 1987; Powell and van Leer, 1989; Van Leer, 1993; Deconinck *et al.*, 1993; Sidilkover, 1995). A thorough review is given by Paillère and Deconinck (1995).

Residual distribution schemes are an attractive approach for triangulated meshes. In these, the residual defined by the space derivatives is evaluated for each cell and then distributed to the vertices with weights that depend on the direction of convection. For a scalar conservation law, the weights can be chosen to maintain positivity with minimum cross diffusion in the direction normal to the flow. For the Euler equations, the residual can be linearized by assuming that the parameter vector with components $\sqrt{\rho}$, $\sqrt{(\rho)}u_i$, and $\sqrt{(\rho)}H$ varies linearly over the cell. Then

$$\frac{\partial f_j(w)}{\partial x_j} = A_j \frac{\partial w}{\partial x_j}$$

where the Jacobian matrices $A_j = (\partial f_j/\partial w)$ are evaluated with Roe averaging of the values of w at the vertices. Waves in the direction **n** can then be expressed in terms of the eigenvectors of $n_j A_j$, and a positive distribution scheme is used for waves in preferred directions. The best choice of these directions is the subject of ongoing research, but preliminary results indicate the possibility of achieving high resolution of shocks and contact discontinuities, which are not aligned with mesh lines (Paillère and Deconinck, 1995).

5.7 Discretization of the viscous terms

The discretization of the viscous terms of the Navier–Stokes equations requires an approximation to the velocity derivatives $(\partial u_i/\partial x_j)$ in order to calculate the tensor σ_{ij}, equation (5). Then the viscous terms may be included in the flux balance (120). In order to evaluate the derivatives, one may apply the Gauss formula to a control volume V with the boundary S.

$$\int_V \frac{\partial u_i}{\partial x_j}\,\mathrm{d}v = \int_S u_i n_j\,\mathrm{d}s$$

where n_j is the outward normal. For a polyhedral cell, this gives

$$\overline{\frac{\partial u_i}{\partial x_j}} = \frac{1}{vol}\sum_{\text{faces}} \overline{u}_i n_j s \tag{133}$$

where $\overline{u}_i$ is an estimate of the average of u_i over the face. If u varies linearly over a tetrahedral cell, this is exact. Alternatively, assuming a local transformation to computational coordinates ξ_j, one may apply the chain rule

$$\frac{\partial u}{\partial x} = \left[\frac{\partial u}{\partial \xi}\right]\left[\frac{\partial \xi}{\partial x}\right] = \frac{\partial u}{\partial \xi}\left[\frac{\partial x}{\partial \xi}\right]^{-1} \tag{134}$$

Here the transformation derivatives $(\partial x_i/\partial \xi_j)$ can be evaluated with the same finite difference formulas as the velocity derivatives $(\partial u_i/\partial \xi_j)$ In this case, $(\partial u/\partial \xi)$ is exact if u is a linearly varying function.

For a cell-centered discretization (Figure 27a), $(\partial u/\partial \xi)$ is needed at each face. The simplest procedure is to evaluate $(\partial u/\partial \xi)$ in each cell, and to average $(\partial u/\partial \xi)$ between the two cells on either side of a face (Jayaram and Jameson, 1988). The resulting discretization does not have a compact stencil, and supports undamped oscillatory modes. In a one-dimensional calculation, for example, $(\partial^2 u/\partial x^2)$ would be discretized as $(u_{i+2} - 2u_i + u_{i-2})/4\Delta x^2$. In order to produce a compact stencil, $(\partial u/\partial x)$ may be estimated from a control volume centered on each face, using formulas (133) or (134) (Rieger and Jameson, 1988). This is computationally expensive because the number of faces is much larger than the number of cells. In a hexahedral mesh with a large number of vertices, the number of faces approaches 3 times the number of cells.

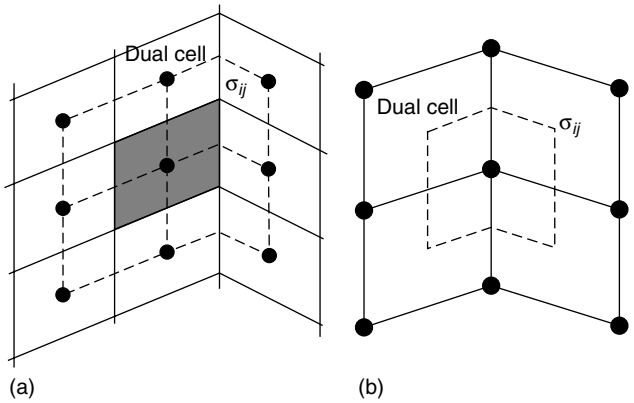

Figure 27. Viscous discretizations for cell-centered and cell-vertex algorithms. (a) Cell-centered scheme. σ_{ij} evaluated at vertices of the primary mesh, (b) cell-vertex scheme. σ_{ij} evaluated at cell centers of the primary mesh.

This motivates the introduction of dual meshes for the evaluation of the velocity derivatives and the flux balance as sketched in Figure 27. The figure shows both cell-centered and cell-vertex schemes. The dual mesh connects cell centers of the primary mesh. If there is a kink in the primary mesh, the dual cells should be formed by assembling contiguous fractions of the neighboring primary cells. On smooth meshes, comparable results are obtained by either of these formulations (Martinelli and Jameson, 1988; Martinelli, Jameson and Malfa, 1993; Liu and Jameson, 1992). If the mesh has a kink, the cell-vertex scheme has the advantage that the derivatives $(\partial u_i/\partial x_j)$ are calculated in the interior of a regular cell, with no loss of accuracy.

A desirable property is that a linearly varying velocity distribution, as in a Couette flow, should produce a constant stress and hence an exact stress balance. This property is not necessarily satisfied in general by finite difference or finite volume schemes on curvilinear meshes. The characterization k-exact has been proposed for schemes that are exact for polynomials of degree k. The cell-vertex finite volume scheme is linearly exact if the derivatives are evaluated by equation (134), since then $(\partial u_i/\partial x_j)$ is exactly evaluated as a constant, leading to constant viscous stresses σ_{ij} and an exact viscous stress balance. This remains true when there is a kink in the mesh, because the summation of constant stresses over the faces of the kinked control volume sketched in Figure 27 still yields a perfect balance. The use of equation (134) to

evaluate $(\partial u_i/\partial x_j)$, however, requires the additional calculation or storage of the nine metric quantities $(\partial u_i/\partial x_j)$ in each cell, whereas equation (133) can be evaluated from the same face areas that are used for the flux balance.

In the case of an unstructured mesh, the weak form (121) leads to a natural discretization with linear elements, in which the piecewise linear approximation yields a constant stress in each cell. This method yields a representation that is globally correct when averaged over the cells, as is proved by energy estimates for elliptic problems (Bauer *et al.*, 1975). It should be noted, however, that it yields formulas that are not necessarily locally consistent with the differential equations if Taylor series expansions are substituted for the solution at the vertices appearing in the local stencil. Figure 28 illustrates the discretization of the Laplacian $u_{xx} + u_{yy}$, which is obtained with linear elements. It shows a particular triangulation such that the approximation is locally consistent with $u_{xx} + 3u_{yy}$. Thus, the use of an irregular triangulation in the boundary layer may significantly degrade the accuracy.

Anisotropic grids are needed in order to resolve the thin boundary layers that appear in viscous flows at high Reynolds numbers. Otherwise an excessively large number of grid cells may be required. The use of flat tetrahedra can have an adverse effect on both the accuracy of the solution and the rate of convergence to a steady state. This has motivated the use of hybrid prismatic-tetrahedral grids in which prismatic cells are used in the wall regions (Parthasarathy, Kallinderis and Nakajima, 1995). A review of many of the key issues in the design of flow solvers for unstructured meshes is given by Venkatakrishnan (1996).

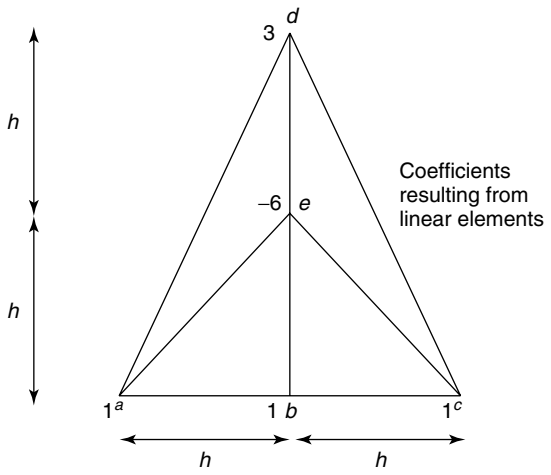

Figure 28. Example of discretization $u_{xx} + u_{yy}$ on a triangular mesh. The discretization is locally equivalent to the approximation $u_{xx} = (u_a - 2u_b + u_c)/h^2$, $3u_{yy} = (3u_d - 6u_e + 3u_b)/h^2$.

6 TIME-STEPPING SCHEMES

6.1 Time-stepping schemes

If the space discretization procedure is implemented separately, it leads to a set of coupled ordinary differential equations, which can be written in the form

$$\frac{\mathrm{d}\mathbf{w}}{\mathrm{d}t} + \mathbf{R}(\mathbf{w}) = 0 \tag{135}$$

where $\mathbf{w}$ is the vector of the flow variables at the mesh points and $\mathbf{R(w)}$ is the vector of the residuals, consisting of the flux balances defined by the space discretization scheme, together with the added dissipative terms. It now becomes necessary to choose a time-stepping scheme to complete the discretization of the problem.

While three-dimensional solutions are generally needed in practice, the two-dimensional conservation law

$$\frac{\partial w}{\partial t} + \frac{\partial}{\partial x} f(w) + \frac{\partial}{\partial y} g(w) = 0 \tag{136}$$

is sufficient to illustrate the essential issues in the formulation of time-stepping schemes. Using D_x and D_y to denote the spatial operators approximating $(\partial/\partial x)$ and $(\partial/\partial y)$, which may be derived by finite difference, finite volume, or finite element methods, the local residual in equation (135) takes the form

$$R(w) = D_x f(w) + D_y g(w) + D(w) \tag{137}$$

where $D(w)$ denotes the numerical diffusive terms introduced by upwind biasing.

In many engineering applications, such as the analysis of flow past a wing, the prime objective is to calculate the solution of steady flow, and details of the transient solution are immaterial. In this situation, the time-stepping scheme may be designed solely to maximize the rate of convergence to a steady state, without regard for the order of accuracy. If on the other hand, the flow to be analyzed is inherently unsteady, though possibly periodic in time as in the case of a helicopter rotor in forward flight, the order of accuracy of the time-stepping scheme may be critically important. Both situations will be considered in the following sections.

The first decision that must be made is whether to use an explicit scheme, in which the space derivatives are calculated from known values of the flow variables at the beginning of the time step, or an implicit scheme, in which the formulas for the space derivatives include as yet unknown values of the flow variables at the end of the time step, leading to the need to solve coupled equations for the new values. The permissible time step for an explicit

scheme is limited by the Courant-Friedrichs-Lewy (CFL) condition, which states that a difference scheme cannot be a convergent and stable approximation unless its domain of dependence contains the domain of dependence of the corresponding differential equation. One can anticipate that implicit schemes will yield convergence in a smaller number of time steps, because the time step is no longer constrained by the CFL condition. Implicit schemes will be efficient, however, only if the decrease in the number of time steps outweighs the increase in the computational effort per time step consequent upon the need to solve coupled equations.

6.2 Explicit time-stepping schemes

The prototype explicit scheme is the simple forward Euler scheme

$$\mathbf{w}_{n+1} = \mathbf{w}_n + \Delta t \mathbf{R}(\mathbf{w}_n)$$

In the scalar case, the general semidiscrete scheme (81) now leads to the fully discrete scheme

$$\begin{aligned} v_j^{n+1} &= v_j^n + \Delta t \sum_{k \neq j} c_{jk}(v_k - v_j) \\ &= \sum a_{jk} v_k^n \end{aligned} \tag{138}$$

where

$$\begin{aligned} a_{jj} &= 1 - \Delta t \sum_{k \neq j} c_{jk} \\ a_{jk} &= \Delta t \;\; c_{jk}, \qquad j \neq k \end{aligned} \tag{139}$$

and

$$\sum_k a_{jk} = 1 \tag{140}$$

If we consider the linear advection equation with a three-point discretization in space, as illustrated in Figure 29, the true region of dependence of v_j^{n+1} is along the characteristic

$$x - at = x_j - at^{n+1}$$

If the absolute value of the CFL number

$$|\lambda| = \left| \frac{a \Delta t}{\Delta x} \right| > 1$$

the numerical domain of dependence defined by the interval (x_{j-1}, x_{j+1}) will not contain the true domain of dependence. Accordingly the CFL condition

$$|\lambda| \leq 1$$

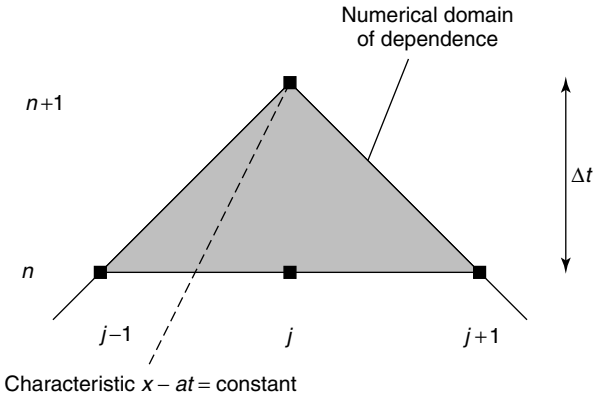

Figure 29. Characteristic line.

is a necessary condition for the stability and convergence of any 3-point forward Euler scheme. The actual condition for a fully discrete LED scheme can be more stringent. According to equation (138)

$$|v_j^{n+1}| \leq \sum_k |a_{jk}||v_k^n| \leq \left(\sum_k |a_{jk}| \right) \|v^n\|_\infty \tag{141}$$

so for an LED scheme we need

$$\sum_k |a_{jk}| \leq 1$$

but according to equation (140) this is only possible if

$$a_{jk} \geq 0$$

Hence by equation (139) there is a restriction on the time step

$$\Delta t \leq \frac{1}{\sum_{k \neq j} c_{jk}}$$

in addition to the requirement $c_{jk} \geq 0$ for the semidiscrete scheme.

6.2.1 Lax–Wendroff schemes

A number of popular explicit schemes are based on the Lax–Wendroff formulation, in which the change $\boldsymbol{\delta}\mathbf{w}$ during a time step is calculated from the first two terms of the Taylor series for $w(t + \Delta t)$

$$\delta w = \Delta t \frac{\partial w}{\partial t} + \frac{\Delta t^2}{2} \frac{\partial^2 w}{\partial t^2} \tag{142}$$

In a two-dimensional case for which the local residual $R(w)$ approximates $(\partial/\partial x) f(w) + (\partial/\partial y) g(w)$, the second

derivative is then estimated by substituting

$$\frac{\partial^2 w}{\partial t^2} = -\frac{\partial}{\partial t} R(w) \tag{143}$$

$$= -\frac{\partial R}{\partial w}\frac{\partial w}{\partial t} \tag{144}$$

$$= \left(\frac{\partial}{\partial x} A + \frac{\partial}{\partial y} B\right) R(w) \tag{145}$$

where A and B are the Jacobian matrices

$$A = \frac{\partial f}{\partial w}, \quad B = \frac{\partial g}{\partial w} \tag{146}$$

and central differences are used to approximate the derivatives $(\partial/\partial x)$ and $(\partial/\partial y)$.

In a variation that has been successfully used to drive multigrid calculations by Ni (1982) and Hall (1985), the flow variables are stored at the cell vertices. The correction at a vertex is then calculated from the average of the residuals in the four neighboring cells, augmented by differences in the x and y directions of the residuals multiplied by the Jacobian matrices. Accordingly

$$\delta w = -\left\{\mu_x \mu_y - \frac{\Delta t}{2}\left(\frac{1}{\Delta x}\mu_y \delta_x A + \frac{1}{\Delta y}\mu_x \delta_y B\right)\right\} \Delta t Q(w) \tag{147}$$

where μ and δ denote averaging and difference operators, and $Q(w)$ is the flux balance in one cell, calculated by trapezoidal integration around the vertices of the cell. Ni views this as a rule for distributing a correction calculated at the center of each cell unequally to its four corners.

There are numerous variations of two step Lax–Wendroff schemes in which $\Delta t(\partial w/\partial t) + (\Delta t^2/2)(\partial^2 w/\partial t^2)$ is replaced by an estimate of $(\partial w/\partial t)$ at the time $t + (\Delta t/2)$ thus avoiding the need to evaluate the Jacobians A and B. In the widely used MacCormack scheme, the predictor and corrector steps are

$$w^* = w^n - \Delta t(D_x^+ f^n + D_y^+ g^n) \tag{148}$$

and

$$w^{n+1} = w^n - \frac{\Delta t}{2}(D_x^+ f^n + D_y^+ g^n) - \frac{\Delta t}{2}(D_x^- f^* + D_y^- g^*) \tag{149}$$

where D_x^+, D_x^-, D_y^+, and D_y^- are forward and backward-difference operators approximating $\partial/\partial x$ and $\partial/\partial y$. Here the use of different approximations for $\partial f/\partial x + \partial g/\partial y$ in the two stages leads to a dependence of the steady state solution on Δt. Moreover, none of the Lax–Wendroff schemes satisfy the conditions for the LED property.

6.2.2 *Multistage schemes*

Other higher-order explicit schemes that might be considered include linear multilevel methods such as the leap-frog and Adams–Bashforth schemes, and two-level multistage methods such as the classical Runge–Kutta schemes. The two-level multistage schemes have the advantages that they require no special start up procedure, and that they can readily be tailored to give a large stability region. They have proved extremely effective in practice as a method of solving the Euler equations (Jameson, Schmidt, and Turkel, 1981; Jameson and Baker, 1983; Jameson, Baker, and Weatherill, 1986b).

Let $\mathbf{w^n}$ be the result after n steps. The general form of an m stage scheme is

$$\mathbf{w}^{(0)} = \mathbf{w}^n \tag{150}$$

$$\mathbf{w}^{(1)} = \mathbf{w}^{(0)} - \alpha_1 \Delta t \mathbf{R}^{(0)}$$

$$\cdots$$

$$\mathbf{w}^{(m-1)} = \mathbf{w}^{(0)} - \alpha_{m-1}\Delta t \mathbf{R}^{(m-2)}$$

$$\mathbf{w}^{(m)} = \mathbf{w}^{(0)} - \Delta t \mathbf{R}^{(m-1)}$$

$$\mathbf{w}^{n+1} = \mathbf{w}^{(m)} \tag{151}$$

The residual in the $(q+1)st$ stage is evaluated as

$$\mathbf{R^{(q)}} = \sum_{r=0}^{q} \beta_{qr} \mathbf{R(w^{(r)})} \tag{152}$$

where

$$\sum_{r=0}^{q} \beta_{qr} = 1 \tag{153}$$

Shu and Osher (1988) have developed higher-order Runge–Kutta schemes that preserve the LED or TVD property, provided that it is satisfied by the semidiscretization. Their third-order scheme is

$$\mathbf{w}^{(1)} = \mathbf{w}^{(0)} - \Delta t \mathbf{R}(\mathbf{w}^{(0)})$$

$$\mathbf{w}^{(2)} = \frac{3}{4}\mathbf{w}^{(0)} + \frac{1}{4}\mathbf{w}^{(1)} - \frac{1}{4}\Delta t \mathbf{R}(\mathbf{w}^{(1)})$$

$$\mathbf{w}^{(3)} = \frac{1}{3}\mathbf{w}^{(0)} + \frac{2}{3}\mathbf{w}^{(2)} - \frac{2}{3}\Delta t \mathbf{R}(\mathbf{w}^{(2)}) \tag{154}$$

which is LED if the CFL number has an absolute value ≤ 1. This scheme has demonstrated to give good results for shock tube problems (Jiang and Shu, 1996).

The classical fourth-order Runge–Kutta scheme

$$\begin{aligned}
\mathbf{w}^{(1)} &= \mathbf{w}^{(0)} - \frac{1}{2}\Delta t \mathbf{R}(\mathbf{w}^{(0)}) \\
\mathbf{w}^{(2)} &= \mathbf{w}^{(0)} - \frac{1}{2}\Delta t \mathbf{R}(\mathbf{w}^{(1)}) \\
\mathbf{w}^{(3)} &= \mathbf{w}^{(0)} - \Delta t \mathbf{R}(\mathbf{w}^{(2)}) \\
\mathbf{w}^{(4)} &= \mathbf{w}^{(0)} - \frac{1}{6}\Delta t \left(\mathbf{R}(\mathbf{w}^{(0)}) + 2\mathbf{R}(\mathbf{w}^{(1)}) \right. \\
&\quad \left. + 2\mathbf{R}(\mathbf{w}^{(2)}) + \mathbf{R}(\mathbf{w}^{(3)})\right)
\end{aligned} \tag{155}$$

although not LED, is also very useful in problems where oscillation control is not critical. For steady state calculations, the complexity can be reduced by simply evaluating the residual at each stage with the latest available values

$$\mathbf{R}^{(q)} = \mathbf{R}(\mathbf{w}^{(q)})$$

If one reduces the linear model problem corresponding to (135) to an ordinary differential equation by substituting a Fourier mode $w_j = \hat{w}e^{ipx_j}$, the resulting Fourier symbol has an imaginary part proportional to the wave speed, and a negative real part proportional to the diffusion. It is then known how to choose the coefficients α_q to maximize the stability interval along the imaginary axis (Kinnmark, 1984).

With a diffusive or upwind-biased scheme, the time-stepping scheme should also have a stability region that contains a substantial interval of the negative real axis. To achieve this, it pays to treat the convective and dissipative terms in a distinct fashion. Accordingly, the residual is split as

$$\mathbf{R}(\mathbf{w}) = \mathbf{Q}(w) + \mathbf{D}(w)$$

where $Q(w)$ is the convective part and $D(w)$ the dissipative part. Denote the time level $n\Delta t$ by a superscript n. Then, the multistage time stepping scheme is formulated as

$$\begin{aligned}
\mathbf{w}^{(0)} &= \mathbf{w}^n \\
&\cdots \\
\mathbf{w}^{(k)} &= \mathbf{w}^n - \alpha_k \Delta t \left(\mathbf{Q}^{(k-1)} + \mathbf{D}^{(k-1)}\right) \\
&\cdots \\
\mathbf{w}^{n+1} &= \mathbf{w}^{(m)}
\end{aligned} \tag{156}$$

where the superscript k denotes the k-th stage, $\alpha_m = 1$, and

$$\begin{aligned}
&\mathbf{Q}^{(0)} = \mathbf{Q}(\mathbf{w}^n), \quad \mathbf{D}^{(0)} = \mathbf{D}(\mathbf{w}^n) \\
&\cdots \\
&\mathbf{Q}^{(k)} = \mathbf{Q}(\mathbf{w}^{(k)}) \\
&\mathbf{D}^{(k)} = \beta_k \mathbf{D}(\mathbf{w}^{(k)}) + (1-\beta_k)\mathbf{D}^{(k-1)}
\end{aligned}$$

The coefficients α_k are chosen to maximize the stability interval along the imaginary axis, and the coefficients β_k are chosen to increase the stability interval along the negative real axis.

These schemes do not fall within the standard framework of Runge–Kutta schemes, and they have much larger stability regions (Jameson, 1985b). Two schemes that have been found to be particularly effective are tabulated below. The first is a four-stage scheme with two evaluations of dissipation. Its coefficients are

$$\begin{aligned}
\alpha_1 &= \frac{1}{3},\ \beta_1 = 1 \\
\alpha_2 &= \frac{4}{15}, \beta_2 = \frac{1}{2} \\
\alpha_3 &= \frac{5}{9},\ \beta_3 = 0 \\
\alpha_4 &= 1,\ \beta_4 = 0
\end{aligned} \tag{157}$$

The second is a five-stage scheme with three evaluations of dissipation. Its coefficients are

$$\begin{aligned}
\alpha_1 &= \frac{1}{4}, \beta_1 = 1 \\
\alpha_2 &= \frac{1}{6}, \beta_2 = 0 \\
\alpha_3 &= \frac{3}{8}, \beta_3 = 0.56 \\
\alpha_4 &= \frac{1}{2}, \beta_4 = 0 \\
\alpha_5 &= 1, \beta_5 = 0.44
\end{aligned} \tag{158}$$

Figures 30, 31, and 32 display the stability regions for the standard fourth-order RK4 scheme (155) and the 4-2 and 5-3 schemes defined by equations (157 and 158). The expansion of the stability region is apparent. They also show the locus of the Fourier symbol using the linear advection equation as a representative model problem (Jameson, 1985b), with third-order artificial diffusion in an amount chosen to damp high-frequency modes.

6.3 Implicit schemes

The prototype implicit scheme can be formulated by estimating $(\partial \mathbf{w}/\partial t)$ at $t + \mu\Delta t$ as a linear combination of $\mathbf{R}(\mathbf{w}^n)$ and $\mathbf{R}(\mathbf{w}^{n+1})$. The resulting equation

$$\mathbf{w}^{n+1} = \mathbf{w}^n - \Delta t\{(1-\mu)\mathbf{R}(\mathbf{w}^n) + \mu\mathbf{R}(\mathbf{w}^{n+1})\} \tag{159}$$

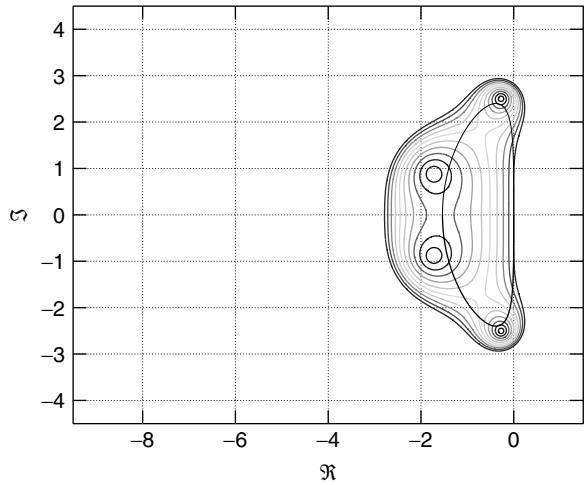

Figure 30. Stability region for the standard 4 stage RK scheme (equation (155)). Black line – locus of Fourier symbol for linear advection with CFL number 2.4. A color version of this image is available at http://www.mrw.interscience.wiley.com/ecm

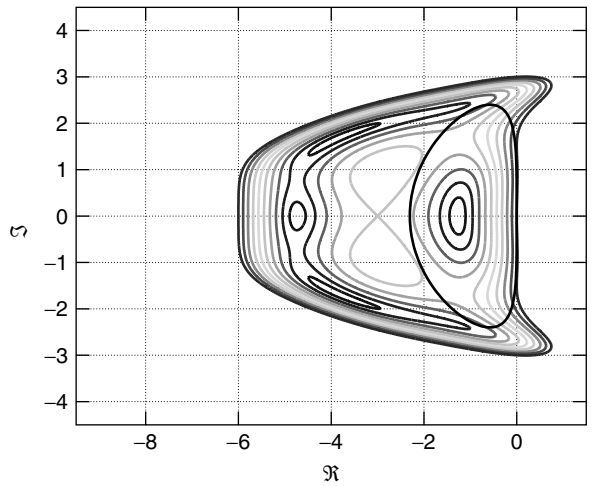

Figure 31. Stability region for the 4-2 scheme (equation (157)). Black line – locus of Fourier symbol for linear advection with CFL number 2.4. A color version of this image is available at http://www.mrw.interscience.wiley.com/ecm

represents the first-order accurate backward Euler scheme if $\mu = 1$, and the second-order accurate trapezoidal rule if $\mu = (1/2)$. This equation calls for the solution of a large number of coupled nonlinear equations for the unknown state vector $\mathbf{w}^{n+1}$. The complexity is actually comparable to that of the steady state problem

$$\mathbf{R(w)} = 0 \tag{160}$$

The implicit equation (159) can most readily be solved via linearization or by resorting to an iterative method.

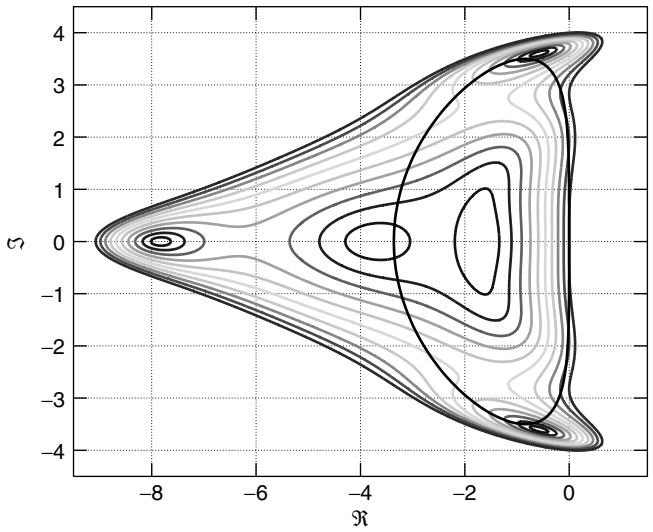

Figure 32. Stability region for the 5-3 scheme (equation (158)). Black line – locus of Fourier symbol for linear advection with CFL number 3.5. A color version of this image is available at http://www.mrw.interscience.wiley.com/ecm

Defining the correction vector

$$\delta w = w^{n+1} - w^n$$

equation (159) can be linearized by approximating the local fluxes as

$$f(w^{n+1}) \sim f(w^n) + A\delta w, \quad g(w^{n+1}) \sim g(w^n) + B\delta w$$

where A and B are the Jacobian matrices (146), and the neglected terms are $O(\| \boldsymbol{\delta}\mathbf{w} \|^2)$. This leads to a linearized implicit scheme that has the local form

$$\{I + \mu\Delta t(D_x A + D_y B)\}\delta w + \Delta t R(w) = 0 \tag{161}$$

Here we can recognize $D_x A + D_y B$ as $(\partial R/\partial w)$.

If one sets $\mu = 1$ and lets $\Delta t \to \infty$, this reduces to the Newton iteration for the steady state problem (160), which has been successfully used in two-dimensional calculations (Venkatakrishnan, 1988; Giles, Drela and Thompkins, 1985). In the three-dimensional case with, say, an $N \times N \times N$ mesh, the bandwidth of the matrix that must be inverted is of order N^2. Direct inversion requires a number of operations proportional to the number of unknowns multiplied by the square of the bandwidth, resulting in a complexity of the order of N^7. This is prohibitive, and forces recourse to either an approximate factorization method or an iterative solution method.

The main possibilities for approximate factorization are the alternating direction and LU decomposition methods. The alternating direction method, which may be traced back

to the work of Gourlay and Mitchell (1966), was given an elegant formulation for nonlinear problems by Beam and Warming (1976). In a two-dimensional case equation, (161) is replaced by

$$(I + \mu \Delta t D_x A)(I + \mu \Delta t D_y B)\delta w + \Delta t R(w) = 0 \quad (162)$$

where D_x and D_y are difference operators approximating $\partial/\partial x$ and $\partial/\partial y$, and A and B are the Jacobian matrices. This may be solved in two steps:

$$(I + \mu \Delta t D_x A)\delta w^* = -\Delta t R(w)$$
$$(I + \mu \Delta t D_y B)\delta w = \delta w^*$$

Each step requires block tridiagonal matrix inversions and may be performed in $O(N^2)$ operations on an $N \times N$ mesh. The algorithm is amenable to vectorization by simultaneous solution of the tridiagonal system of equations along parallel coordinate lines. The method has been refined to a high level of efficiency by Pulliam and Steger (1985), and Yee has extended it to incorporate a TVD scheme (Yee, 1985b). Its main disadvantage is that its extension to three dimensions is inherently unstable according to a Von Neumann analysis.

The idea of the LU decomposition method (Jameson and Turkel, 1981) is to replace the operator in equation (150) by the product of lower and upper block-triangular factors L and U,

$$LU\delta w + \Delta t R(w) = 0 \quad (163)$$

Two factors are used independent of the number of dimensions, and the inversion of each can be accomplished by inversion of its diagonal blocks. The method can be conveniently illustrated by considering a one-dimensional example. Let the Jacobian matrix $A = \partial \mathbf{f}/\partial \mathbf{w}$ be split as

$$A = A^+ + A^- \quad (164)$$

where the eigenvalues of A^+ and A^- are positive and negative respectively. Then we can take

$$L = I + \mu \Delta t D_x^- A^+, \quad U = I + \mu \Delta t D_x^+ A^- \quad (165)$$

where D_x^+ and D_x^- denote forward and backward-difference operators approximating $\partial/\partial x$. The reason for splitting A is to ensure the diagonal dominance of L and U, independent of Δt. Otherwise stable inversion of both factors will only be possible for a limited range of Δt. A crude choice is

$$A^{\pm} = \tfrac{1}{2}(A \pm \epsilon I) \quad (166)$$

where ϵ is at least equal to the spectral radius of A. If flux splitting is used in the calculation of the residual, it is natural to use the corresponding splitting for L and U. An interesting variation is to combine an alternating direction scheme with LU decomposition in the different coordinate directions (Obayashi and Kuwakara, 1984; Obayashi *et al.*, 1986).

If one chooses to adopt the iterative solution technique, the principal alternatives are variants of the Jacobi and Gauss–Seidel methods. These may be applied to either the nonlinear equation (159) or the linearized equation (161). A Jacobi method of solving (159) can be formulated by regarding it as an equation

$$\mathbf{w} - \mathbf{w}^{(0)} + \mu \Delta t \mathbf{R}(\mathbf{w}) + (1 - \mu)\Delta t \mathbf{R}(\mathbf{w}^{(0)}) = 0 \quad (167)$$

to be solved for $\mathbf{w}$. Here $\mathbf{w}^{(0)}$ is a fixed value obtained as the result of the previous time step. Now, using bracketed superscripts to denote the iterations, we have

$$\mathbf{w}^{(0)} = \mathbf{w}^n \quad (168)$$
$$\mathbf{w}^{(1)} = \mathbf{w}^{(0)} + \Delta t \mathbf{R}(\mathbf{w}^{(0)}) \quad (169)$$

and for $k > 1$

$$\mathbf{w}^{(k+1)} = \mathbf{w}^{(k)} + \sigma_{k+1}\left\{\left(\mathbf{w}^{(k)} - \mathbf{w}^{(0)} + \mu \Delta t \mathbf{R}(\mathbf{w}^{(k)}) + (1 - \mu)\Delta t \mathbf{R}(\mathbf{w}^{(0)})\right)\right\} \quad (170)$$

where the parameters σ_{k+l} can be chosen to optimize convergence. Finally, if we stop after m iterations,

$$\mathbf{w}^{n+1} = \mathbf{w}^{(m)} \quad (171)$$

We can express as $\mathbf{w}^{(k+1)}$

$$\mathbf{w}^{(k+1)} = \mathbf{w}^{(0)} + (1 + \sigma_{k+1})(\mathbf{w}^{(k)} - \mathbf{w}^{(0)}) + \sigma_{k+1}\left\{\left(\mu \Delta t \mathbf{R}(\mathbf{w}^{(k)}) + (1 - \mu)\Delta t \mathbf{R}(\mathbf{w}^{(0)})\right)\right\} \quad (172)$$

Since

$$\mathbf{w}^{(1)} - \mathbf{w}^{(0)} = \sigma_1 \Delta t \mathbf{R}(\mathbf{w}^{(0)}) \quad (173)$$

it follows that for all k we can express $(\mathbf{w}^{(k)} - \mathbf{w}^{(0)})$ as a linear combination of $\mathbf{R}(\mathbf{w}^{(j)})$, $j < k$. Thus, this scheme is a variant of the multistage time-stepping scheme described by equations (150) and (152). It has the advantage that it permits simultaneous or overlapped calculation of the corrections at every mesh point, and is readily amenable to parallel and vector processing.

Symmetric Gauss–Seidel schemes have proved to be particularly effective (MacCormack, 1985; Hemker and Spekreijse, 1984b; Chakravarthy, 1984; Yoon and Jameson, 1987; Rieger and Jameson, 1988). Following the analysis of

Jameson (1986a), consider the case of a flux-split scheme in one dimension, for which

$$R(w) = D_x^+ f^-(w) + D_x^- f^+(w) \tag{174}$$

where the flux is split so that the Jacobian matrices

$$A^+ = \frac{\partial f^+}{\partial w} \quad \text{and} \quad A^- = \frac{\partial f^-}{\partial w} \tag{175}$$

have positive and negative eigenvalues respectively. Now equation (159) becomes

$$\left\{I + \mu\Delta t\left(D_x^+ A^- + D_x^- A^+\right)\right\}\delta w + \Delta t R(w) = 0 \tag{176}$$

At the jth mesh point, this is

$$\begin{aligned}\{I + \alpha(A_j^+ - A_j^-)\}\delta w_j + \alpha A_{j+1}^- \delta w_{j+1} \\ - \alpha A_{j-1}^+ \delta w_{j-1} + \Delta t R_j = 0\end{aligned} \tag{177}$$

where

$$\alpha = \mu\frac{\Delta t}{\Delta x} \tag{178}$$

Set $\delta w_j^{(0)} = 0$. A two sweep symmetric Gauss–Seidel scheme is then

$$\{I + \alpha(A_j^+ - A_j^-)\}\delta w_j^{(1)} - \alpha A_{j-1}^+ \delta w_{j-1}^{(1)} + \Delta t R_j = 0$$

$$\begin{aligned}\{I + \alpha(A_j^+ - A_j^-)\}\delta w_j^{(2)} + \alpha A_{j+1}^- \delta w_{j+1}^{(2)} - \alpha A_{j-1}^+ \delta w_{j-1}^{(1)} \\ + \Delta t R_j = 0\end{aligned}$$

Subtracting (1) from (2) we find that

$$\begin{aligned}\{I + \alpha(A_j^+ - A_j^-)\}\delta w_j^{(2)} + \alpha A_{j+1}^- \delta w_{j+1}^{(2)} \\ = \{I + \alpha(A_j^+ - A_j^-)\}\delta w_j^{(1)}\end{aligned} \tag{179}$$

Define the lower-triangular, upper-triangular, and diagonal operators L, U, and D as

$$\begin{aligned}L &= I - \alpha A^- + \mu t D_x^- A^+ \\ U &= I + \alpha A^+ + \mu t D_x^+ A^- \\ D &= I + \alpha(A^+ - A^-)\end{aligned}$$

It follows that the scheme can be written as

$$LD^{-1}U\delta w = -\Delta t R(w) \tag{180}$$

Commonly the iteration is terminated after one double sweep. The scheme is then a variation of an LU implicit scheme.

If we use the simple choice (166) for $A^{\pm}$, D reduces to a scalar factor and the scheme requires no inversion. This is a significant advantage for the treatment of flows with chemical reaction with large numbers of species, and a correspondingly large numbers of equations.

The terms $\Delta t R_i - \alpha A_{i-1}^+ \delta\tilde{v}_{i-1}$ of equation (177) are a linearization of $\Delta t R_i$ evaluated with $\tilde{v}_{i-1} = v_{i-1} + \delta\tilde{v}_{i-1}$. Following this line of reasoning, the *LU-SGS* scheme can be recast (Jameson and Caughey, 2001) as

$$\{I + \alpha(A_i^+ - A_i^-)\}\delta\widetilde{w}_i + \Delta t\widetilde{R}_i = 0 \tag{181}$$

$$\{I + \alpha(A_i^+ - A_i^-)\}\delta\widetilde{\widetilde{w}}_i + \Delta t\widetilde{\widetilde{R}}_i = 0 \tag{182}$$

where

$$\widetilde{w}_i = w_i + \delta\widetilde{w}_i; \quad \tilde{f}_i^{\pm} = f^{\pm}(\widetilde{w}_i) \tag{183}$$

$$w_i^{n+1} = \widetilde{\widetilde{w}}_i = \widetilde{w}_i + \delta\widetilde{\widetilde{w}}_i; \quad \tilde{\tilde{f}}_i^{\pm} = f^{\pm}(\widetilde{\widetilde{w}}_i) \tag{184}$$

and

$$\widetilde{R}_i = \frac{1}{\Delta x}\left(f_{i+1}^- - f_i^- + f_i^+ - \tilde{f}_{i-1}^+\right) \tag{185}$$

$$\widetilde{\widetilde{R}}_i = \frac{1}{\Delta x}\left(\tilde{\tilde{f}}_{i+1} - - \tilde{f}_i^- + \tilde{f}_i^+ - \tilde{f}_{i-1}^+\right) \tag{186}$$

With the definitions of equation (175), equations (181) and (182) can be written as

$$\delta\widetilde{w}_i = -\frac{\Delta t}{1+\mathcal{C}}\widetilde{R}_i \tag{187}$$

$$\delta\widetilde{\widetilde{w}}_i = -\frac{\Delta t}{1+\mathcal{C}}\widetilde{\widetilde{R}}_i \tag{188}$$

where $\mathcal{C} = \rho\Delta t/\Delta x$ is the Courant number.

Alternatively, one may use the Jacobian splitting defined as

$$A^+ = \tfrac{1}{2}(A + |A|), \quad A^- = \tfrac{1}{2}(A - |A|) \tag{189}$$

where $|A| = M|\Lambda|M^{-1}$, and $|\Lambda|$ is the diagonal matrix whose entries are the absolute values of the eigenvalues of the Jacobian matrix A, while M and M^{-1} are the modal matrix of A and its inverse as defined in equations (14–25). Then equations (181) and (182) can be written

$$\{I + \alpha|A|\}\,\delta\widetilde{w}_i = -\Delta t\widetilde{R}_i \tag{190}$$

$$\{I + \alpha|A|\}\,\delta\widetilde{\widetilde{w}}_i = -\Delta t\widetilde{\widetilde{R}}_i \tag{191}$$

and, in the limit as the time step Δt goes to infinity, these equations represent the *SGS* Newton iteration

$$|A|\delta\widetilde{w}_i = -\Delta x \widetilde{R}_i \tag{192}$$

$$|A|\delta\widetilde{\widetilde{w}}_i = -\Delta x \widetilde{\widetilde{R}}_i \tag{193}$$

The introduction of the splitting defined by equations (189) is motivated, in part, by the success of the similar preconditioner introduced by Allmaras (1993) and used by Pierce and Giles (1997) to accelerate the convergence of codes based on explicit Runge–Kutta time stepping. This preconditioner seems to have its roots in the Diagonally Dominant *ADI* scheme (Bardina and Lombard, 1987; MacCormack, 1997).

When the scheme corresponding to equations (192) and (193) is implemented for the finite volume form (Jameson, Schmidt, and Turkel, 1981) of the equations, it can be represented (in two dimensions) as

$$\{|A| + |B|\}\,\delta\widetilde{w}_{i,j} = -\sigma\widetilde{R}_{i,j} \tag{194}$$

$$\{|A| + |B|\}\,\delta\widetilde{\widetilde{w}}_{i,j} = -\sigma\widetilde{\widetilde{R}}_{i,j} \tag{195}$$

where

$$\widetilde{R}_{i,j} = F^-_{i+1,j} - F^-_{i,j} + F^+_{i,j} - \widetilde{F}^+_{i-1,j} + G^-_{i,j+1} - G^-_{i,j} + G^+_{i,j} - \widetilde{G}^+_{i,j-1} \tag{196}$$

$$\widetilde{\widetilde{R}}_{i,j} = \widetilde{\widetilde{F}}^-_{i+1,j} - \widetilde{F}^-_{i,j} + \widetilde{F}^+_{i,j} - \widetilde{F}^+_{i-1,j} + \widetilde{\widetilde{G}}^-_{i,j+1} - \widetilde{G}^-_{i,j} + \widetilde{G}^+_{i,j} - \widetilde{G}^+_{i,j-1} \tag{197}$$

and σ is a relaxation factor that can be used to optimize convergence rates. In these equations, F^+, F^-, G^+, and G^- represent the split approximations to the cell area h times the contravariant components of the flux vectors in the corresponding mesh coordinate directions. The residual fluxes are approximated using either the scalar or CUSP versions of the SLIP approximations developed by Jameson, (1995a,b).

The implementation of this procedure is made computationally very efficient by locally transforming the residuals to those corresponding to the equations written in symmetrizing variables (see e.g. Warming, Beam and Hyett, 1975), then transforming the corrections back to the conserved variables. Numerical experiments indicate that it can be beneficial to perform additional corrections in supersonic zones, when they are present in the solution. The CPU time required for these multiple sweeps is reduced by "freezing" the matrix coefficients $|A|$ and $|B|$ that appear in equations (192) and (193). The additional memory required to store these coefficient matrices is minimized by storing only the symmetrized form of the Jacobians (which requires only 7 additional quantities to be stored for each mesh cell).

Some of these interconnections between two different schemes are illustrated in Figure 33. Schemes in three main classes appear to be the most appealing.

1. Variations of multistage time stepping, including the application of a Jacobi iterative method to the implicit scheme, (indicated by a single asterisk).
2. Variations of *LU* decomposition, including the application of a Gauss–Seidel iterative method to the implicit scheme (indicated by a double asterisk).
3. Alternating direction schemes, including schemes in which an *LU* decomposition is separately used in each coordinate direction (indicated by a triple asterisk).

6.4 Multigrid methods

Radical improvements in the rate of convergence to a steady state can be realized by the multigrid time-stepping technique. The concept of acceleration by the introduction of multiple grids was first proposed by Fedorenko (1964). There is by now a fairly well-developed theory of multigrid methods for elliptic equations based on the concept that the updating scheme acts as a smoothing operator on each grid (Brandt, 1977; Hackbusch, 1978). This theory does not hold for hyperbolic systems. Nevertheless, it seems that it ought to be possible to accelerate the evolution of a hyperbolic system to a steady state by using large time steps on coarse grids so that disturbances will be

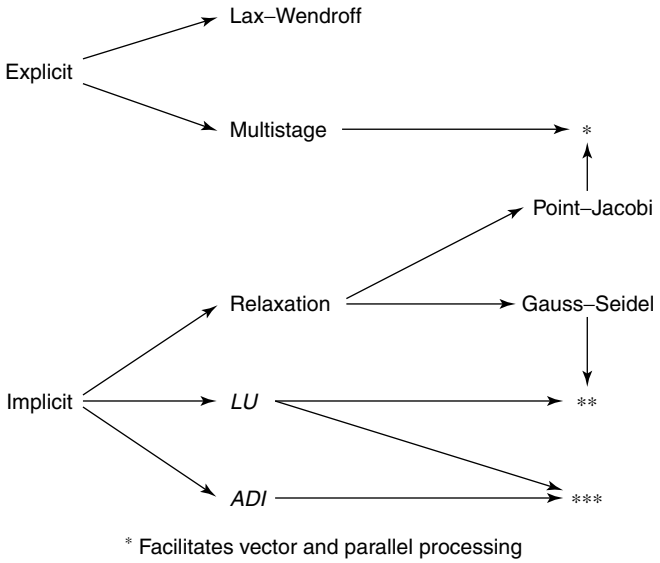

Figure 33. Time-stepping schemes.

more rapidly expelled through the outer boundary. Various multigrid time-stepping schemes designed to take advantage of this effect have been proposed (Ni, 1982; Jameson, 1983; Hall, 1985; Jameson, 1986a; Jameson, 1986b; Caughey, 1987; Anderson, Thomas and Whitfield, 1986; Hemker and Spekreijse, 1984a).

One can devise a multigrid scheme using a sequence of independently generated coarser meshes by eliminating alternate points in each coordinate direction. In order to give a precise description of the multigrid scheme, subscripts may be used to indicate the grid. Several transfer operations need to be defined. First, the solution vector on grid k must be initialized as

$$w_k^{(0)} = T_{k,k-1} w_{k-1}$$

where w_{k-1} is the current value on grid $k-1$ and $T_{k,k-1}$ is a transfer operator. Next, it is necessary to transfer a residual forcing function such that the solution on grid k is driven by the residuals calculated on grid $k-1$. This can be accomplished by setting

$$P_k = Q_{k,k-1} R_{k-1}\left(w_{k-1}\right) - R_k\left[w_k^{(0)}\right]$$

where $Q_{k,k-1}$ is another transfer operator. Then $R_k(w_k)$ is replaced by $R_k(w_k) + P_k$ in the time-stepping scheme. Thus, the multistage scheme is reformulated as

$$w_k^{(1)} = w_k^{(0)} - \alpha_1 \Delta t_k \left[R_k^{(0)} + P_k\right]$$

$$\cdots \quad \cdots \tag{198}$$

$$w_k^{(q+1)} = w_k^{(0)} - \alpha_{q+1} \Delta t_k \left[R_k^{(q)} + P_k\right] \tag{199}$$

The result $w_k^{(m)}$ then provides the initial data for grid $k+1$. Finally, the accumulated correction on grid k has to be transferred back to grid $k-1$ with the aid of an interpolation operator $I_{k-1,k}$. With properly optimized coefficients multistage time-stepping schemes can be very efficient drivers of the multigrid process. A W-cycle of the type illustrated in Figure 34 proves to be a particularly effective strategy for managing the work split between the meshes.

In a three-dimensional case, the number of cells is reduced by a factor of eight on each coarser grid. On examination of the figure, it can therefore be seen that the work measured in units corresponding to a step on the fine grid is of the order of

$$1 + \frac{2}{8} + \frac{4}{64} + \cdots < \frac{4}{3}$$

and consequently the very large effective time step of the complete cycle costs only slightly more than a single time step in the fine grid.

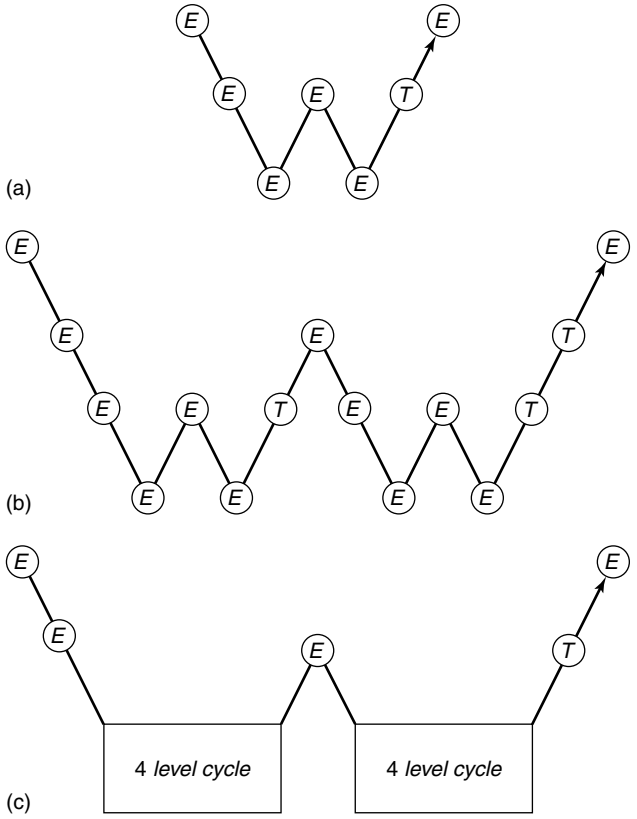

Figure 34. Multigrid W-cycle for managing the grid calculation. E, evaluate the change in the flow for one step; T, transfer the data without updating the solution. (a) 3 levels, (b) 4 levels, (c) 5 levels.

Table 2. Force coefficients for the fast, preconditioned multigrid solutions using CUSP spatial discretization.

Case	Figure	MG cycles	C_L	C_D
RAE 2822; $M_\infty = 0.75$;	—	100	1.1417	0.04851
$\alpha = 3.00$	36c	5	1.1429	0.04851
	36a	3	1.1451	0.04886
NACA 0012; $M_\infty = 0.80$;	—	100	0.3725	0.02377
$\alpha = 1.25$	36d	5	0.3746	0.02391
	36b	3	0.3770	0.02387

This procedure has proved extremely successful for the solution of the Euler equations for inviscid flow. The most dramatic results to date have been achieved by using the nonlinear SGS scheme to drive a multigrid procedure using W cycles (Jameson and Caughey, 2001). Figures 35, 36 and Table 2 illustrate the results for two-dimensional transonic flow calculations. In Figure 36, the fully converged solution is shown by the solid lines, and it can be seen that the results are essentially fully converged after five cycles. This is an example of 'text book' multigrid efficiency.

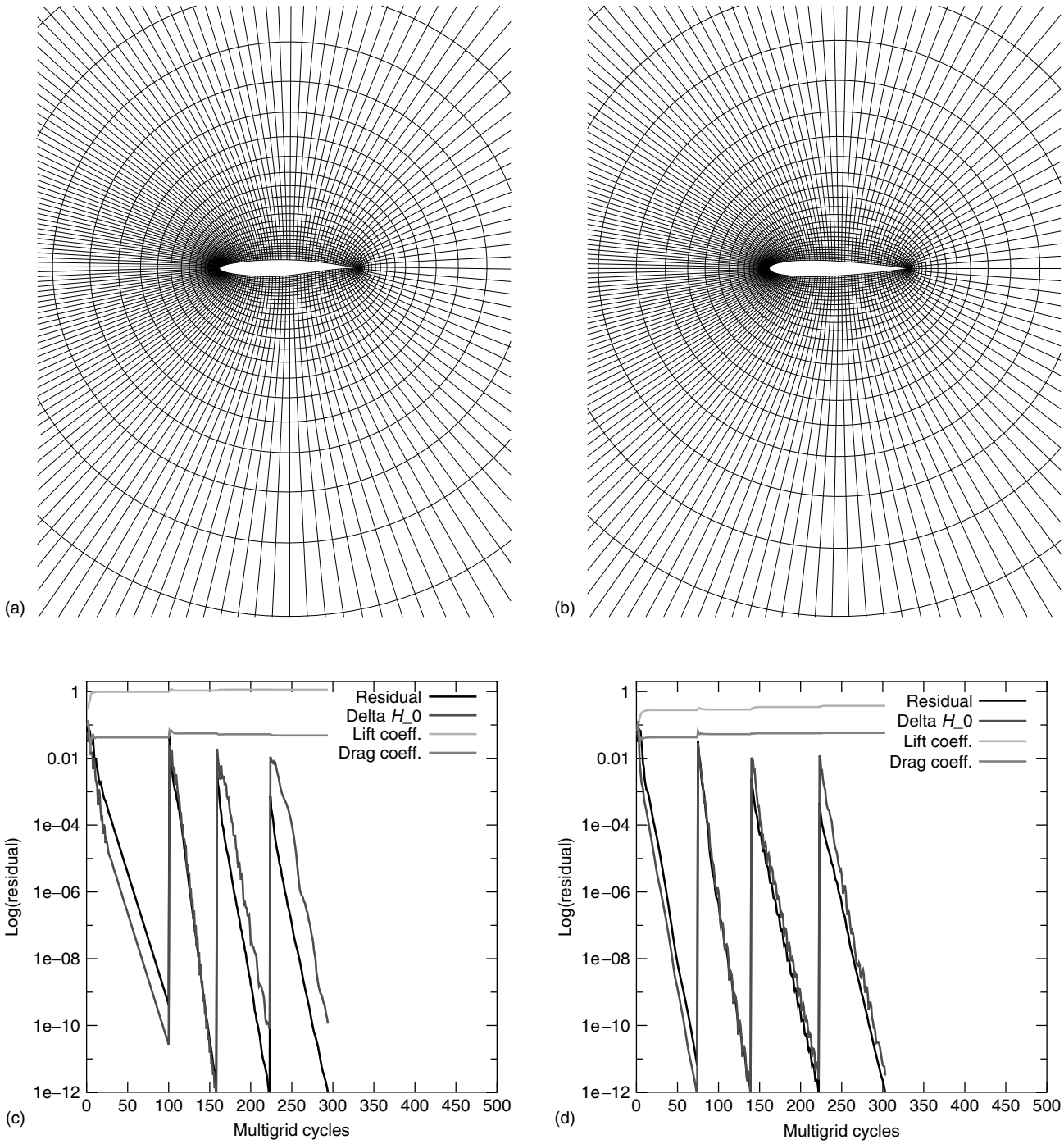

Figure 35. Grid and convergence history of flow past the RAE 2822 at $M_\infty = 0.75$, $\alpha = 3$ degrees, and NACA 0012 airfoil at $M_\infty = 0.8$, $\alpha = 1.25$ degrees. A color version of this image is available at http://www.mrw.interscience.wiley.com/ecm

Multigrid methods have so far proved less effective in calculations of turbulent viscous flows using the Reynolds-averaged Navier–Stokes equations. These require highly anisotropic grids with very fine mesh intervals normal to the wall to resolve the boundary layers. While simple multigrid methods still yield fast initial convergence, they tend to slow down as the calculation proceeds to a low asymptotic rate. This has motivated the introduction of semicoarsening and directional coarsening methods (Mulder, 1989, 1992; Allmaras, 1993, 1995, 1997; Pierce and Giles, 1996; Pierce *et al.*, 1997).

The multigrid method can be applied on unstructured meshes by interpolating between a sequence of separately generated meshes with progressively increasing cell sizes

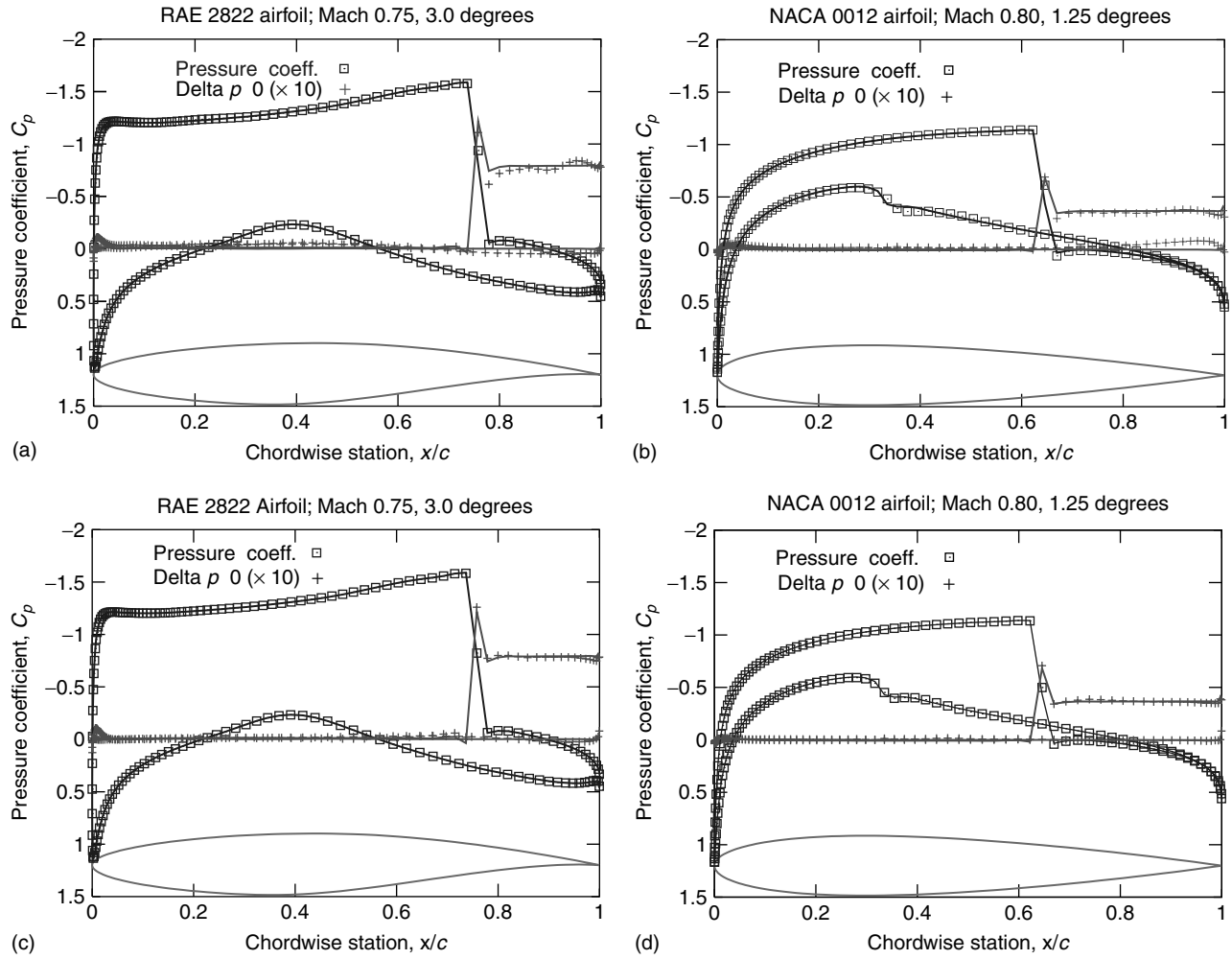

Figure 36. Pressure distribution for flow past the RAE 2822 and NACA 0012 airfoil. Solid lines represent fully converged solution. (a) RAE 2822 after 3 cycles, (b) NACA 0012 after 3 cycles, (c) RAE 2822 after 5 cycles, (d) NACA 0012 after 5 cycles. A color version of this image is available at http://www.mrw.interscience.wiley.com/ecm

(Jameson and Mavriplis, 1987; Mavriplis and Jameson, 1990; Mavriplis and Martinelli, 1991; Peraire, Peirö and Morgan, 1992). It is not easy to generate very coarse meshes for complex configurations. An alternative approach, which removes this difficulty, is to automatically generate successively coarser meshes by agglomerating control volumes or by collapsing edges. This approach yields comparable rates of convergence and has proved to be quite robust (Lallemand and Dervieux, 1987; Lallemand, Steve and Dervieux, 1992; Mavriplis and Venkatakrishnan, 1996; Crumpton and Giles, 1995).

6.5 Preconditioning

Another way to improve the rate of convergence to a steady state is to multiply the space derivatives in equation (135) by a preconditioning matrix P, which is designed to equalize the eigenvalues, so that all the waves can be advanced with optimal time steps. Van Leer, Lee, and Roe have proposed a symmetric preconditioner that minimizes the ratio between the largest and smallest eigenvalues (Van Leer, Lee and Roe, 1991). When the equations are written in stream-aligned coordinates with the symmetrizing variables (15), it has the form

$$P = \begin{bmatrix} \frac{\tau}{\beta^2}M^2 & -\frac{\tau}{\beta}M & 0 & 0 & 0 \\ -\frac{\tau}{\beta}M & \frac{\tau}{\beta^2}+1 & 0 & 0 & 0 \\ 0 & 0 & \tau & 0 & 0 \\ 0 & 0 & 0 & \tau & 0 \\ 0 & 0 & 0 & 0 & 1 \end{bmatrix}$$

where

$$\beta = \tau = \sqrt{1 - M^2}, \quad \text{if} \quad M < 1 \tag{200}$$

$$\beta = \sqrt{M^2 - 1}, \tau = \sqrt{1 - \frac{1}{M^2}}, \quad \text{if} \quad M \geq 1 \tag{201}$$

Turkel has proposed an asymmetric preconditioner designed to treat flow at low Mach numbers (Turkel, 1987). A special case of the Turkel preconditioner advocated by Weiss and Smith (1995) has the simple diagonal form

$$P = \begin{bmatrix} \epsilon^2 & 0 & 0 & 0 & 0 \\ 0 & 1 & 0 & 0 & 0 \\ 0 & 0 & 1 & 0 & 0 \\ 0 & 0 & 0 & 1 & 0 \\ 0 & 0 & 0 & 0 & 1 \end{bmatrix}$$

when written in the symmetrizing variables. If ϵ^2 varies as M^2 as $M \to 0$, all the eigenvalues of PA depend only on the speed q. In order to improve the accuracy the absolute Jacobian matrix, $|A|$ appearing in the artificial diffusion should be replaced by $P^{-1}|PA|$. In effect, this makes the diffusion depend on the modified wave speeds. The use of preconditioners of this type can lead to instability at stagnation points where there is a zero eigenvalue, which cannot be equalized with the eigenvalues $\pm c$. With a judiciously chosen limit on ϵ^2 as $M \to 0$, they have been proved effective in treating low speed flows.

The preconditioners of Van Leer and Turkel do not take account of the effect of differences in the mesh intervals in the different coordinate directions. The need to resolve the boundary layer generally compels the introduction of mesh cells with very high aspect ratios near the boundary, and these can lead to a severe reduction in the rate of convergence to a steady state. Allmaras has analyzed explicit and implicit Jacobi-based preconditioners that include the influence of the mesh intervals (Allmaras, 1993, 1995, 1997). Using a block-Jacobi preconditioner with coarsening only in the direction normal to the wall, Pierce has obtained impressive results on viscous flows with high aspect ratio grids (Pierce and Giles, 1996; Pierce *et al.*, 1997). Mavriplis has successfully combined block preconditioners with line solvers to accelerate the convergence of viscous flow solutions on highly stretched unstructured grids (Mavriplis, 1997). A low Mach preconditioner may also be combined with a block-Jacobi preconditioner. Successful results of such a combination, sometimes called preconditioning squared (Turkel, 1997), have been demonstrated by Darmofal and Siu (1999) and Hosseini and Alonso (2004).

An alternative approach has been proposed by Ta'asan (1993), in which the equations are written in a canonical form that separates the equations describing acoustic waves from those describing convection. In terms of the velocity components u, v, and the vorticity ω, temperature T, entropy s and total enthalpy H, the equations describing steady two-dimensional flow can be written as

$$\begin{bmatrix} D_1 & D_2 & 0 & 0 & 0 \\ -\dfrac{\partial}{\partial y} & \dfrac{\partial}{\partial x} & -1 & 0 & 0 \\ 0 & 0 & -q & -\dfrac{c^2}{\gamma(\gamma-1)} D_3 & \dfrac{1}{q} D_3 \\ 0 & 0 & 0 & T\rho Q & 0 \\ 0 & 0 & 0 & 0 & \rho Q \end{bmatrix} \begin{bmatrix} u \\ v \\ \omega \\ s \\ H \end{bmatrix} = 0$$

where

$$D_1 = \frac{\rho}{c^2}\left((c^2 - u^2)\frac{\partial}{\partial x} - uv\frac{\partial}{\partial y}\right) \tag{202}$$

$$D_2 = \frac{\rho}{c^2}\left((c^2 - u^2)\frac{\partial}{\partial y} - uv\frac{\partial}{\partial x}\right) \tag{203}$$

$$D_3 = v\frac{\partial}{\partial x} - u\frac{\partial}{\partial y} \tag{204}$$

$$Q = u\frac{\partial}{\partial x} + v\frac{\partial}{\partial y} \tag{205}$$

and

$$q^2 = u^2 + v^2$$

Here the first three equations describe an elliptic system if the flow is subsonic, while the remaining equations are convective. Now separately optimized multigrid procedures are used to solve the two sets of equations, which are essentially decoupled. An alternative approach to the optimal splitting of the flow equations into convective and acoustic parts has been developed by Sidilkover (Sidilkover, 1997; Roberts and Swanson, 1997).

6.6 Dual time-stepping schemes

Time-dependent calculations are needed for a number of important applications, such as flutter analysis or the analysis of the flow past a helicopter rotor, in which the stability limit of an explicit scheme forces the use of much smaller time steps than would be needed for an accurate simulation. This motivates the 'dual time-stepping' scheme, in which a multigrid explicit scheme can be used in an inner iteration to solve the equations of a fully implicit time-stepping scheme (Jameson, 1991).

Suppose that (135) is approximated as

$$D_t w^{n+1} + R(w^{n+1}) = 0$$

Here D_t is the kth-order accurate backward-difference formula (BDF) form

$$D_t = \frac{1}{\Delta t}\sum_{q=1}^{k}\frac{1}{q}(\Delta^-)^q$$

where

$$\Delta^- w^{n+1} = w^{n+1} - w^n$$

Applied to the linear differential equation

$$\frac{\mathrm{d}w}{\mathrm{d}t} = \alpha w$$

the schemes with $k = 1, 2$ are stable for all $\alpha\Delta t$ in the left half plane (A-stable). Dahlquist has shown that A-stable linear multistep schemes are at best second-order accurate (Dahlquist, 1963). Gear, however, has shown that the schemes with $k \leq 6$ are stiffly stable (Gear, 1967), and one of the higher-order schemes may offer a better compromise between accuracy and stability, depending on the application.

Equation (135) is now treated as a modified steady state problem to be solved by a multigrid scheme using variable local time steps in a fictitious time t^*. For example, in the case of the second-order BDF one solves

$$\frac{\partial w}{\partial t^*} + R^*(w) = 0$$

where

$$R^*(w) = \frac{3}{2\Delta t}w + R(w) - \frac{2}{\Delta t}w^n + \frac{1}{2\Delta t}w^{n-1}$$

and the last two terms are treated as fixed source terms. In the RK–BDF method, the modified Runge–Kutta scheme (156) is used in the inner iterations. The first term shifts the Fourier symbol of the equivalent model problem to the left in the complex plane. While this promotes stability, it may also require a limit to be imposed on the magnitude of the local time step Δt^*, relative to that of the implicit time step Δt. This may be relieved by a point-implicit modification of the multistage scheme (Melson, Sanetrik and Atkins, 1993). In the case of problems with moving boundaries, the equations must be modified to allow for movement and deformation of the mesh.

This method has proved effective for the calculation of unsteady flows that might be associated with wing flutter (Alonso and Jameson, 1994; Alonso, Martinelli and Jameson, 1995) and also in the calculation of unsteady incompressible flows (Belov, Martinelli and Jameson, 1995). It has the advantage that it can be added as an option to a computer program that uses an explicit multigrid scheme, allowing it to be used for the efficient calculation of both steady and unsteady flows. A similar approach has been successfully adopted for unsteady flow simulations on unstructured grids by Venkatakrishnan and Mavriplis (1996).

Alternatively, in the SGS–BDF method, the nonlinear SGS scheme (equation (194)–(197)) is used in the inner iterations. The unsteady flow past a pitching airfoil provides a useful test case for time-integration methods. A case for which experimental data is also available is a NACA 64A010 at Mach 0.796, pitching about zero angle of attack with an amplitude ± 1.01 degrees, at a reduced frequency

$$\omega_r = \frac{\omega_{\text{chord}}}{2u_\infty} = 0.202$$

This is test case CT6 in Advisory Group for Aerospace Research and Development (AGARD) report. A snap shot of the resulting shock motion is shown in Figure 37, while Figure 38 shows the oval curve traced by the lift coefficient due to its phase lag as the angle of attack varies sinusoidally. These results were obtained using the nonlinear SGS scheme with the third-order accurate BDF. It can be seen that the results overplot when 24 or 36 time steps are used in each pitching cycle. In the case of 24 steps, the maximum CFL number is 4153 in the vicinity of the trailing edge. It can also be seen that the results using three multigrid cycles in each time step are almost identical to those using nine multigrid cycles in each time step.

6.7 Time-spectral methods

There are many unsteady flows in engineering devices such as turbomachinery or helicopter rotors in which the flow is periodic. In this situation, there is the opportunity to gain spectral accuracy by using a Fourier representation in time (Hall, 1985; McMullen, Jameson and Alonso, 2002). Suppose the period T is divided into N time steps, $\Delta t = T/N$. Let $\hat{w}_k$ be the discrete Fourier transform of w^n,

$$\hat{w}_k = -\sum_{n=0}^{N-1} w^n \mathrm{e}^{-ikn\Delta t}$$

Then the semidiscretization (135) is discretized as the pseudospectral scheme

$$D_t w^n + R(w^n) = 0 \tag{206}$$

where

$$D_t w^n = \sum_{k=-(N/2)}^{(N/2)-1} ik\hat{w}_k \mathrm{e}^{ikn\Delta t}$$

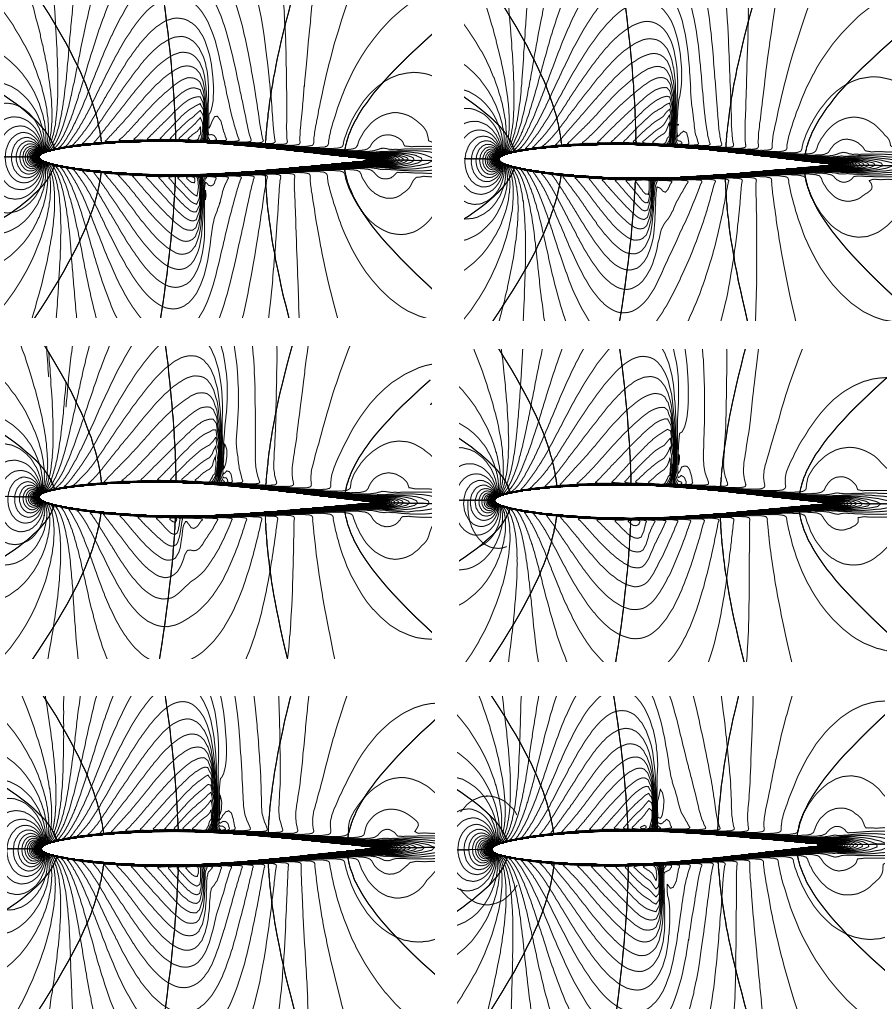

Figure 37. Pressure contours at various time instances AGARD case CT6 showing the oscillating shock waves.

Here D_t is a central-difference formula connecting all the time levels so equation (206) is an integrated space-time formulation that requires the simultaneous solution of the equations for all the time levels. Provided, however, that the solution is sufficiently smooth, equation (206) should yield spectral accuracy (exponential convergence with increasing N).

The time-spectral equation (206) may be solved by dual time-stepping as

$$\frac{\mathrm{d}w^n}{\mathrm{d}t^*} + D_t w^n + R(w^n) = 0 \tag{207}$$

in pseudotime t^*, as in the case of the BDF. Alternatively, it may be solved in the frequency domain. In this case, we represent equation (206) as

$$\hat{R}_k^* = ik\hat{w}_k + \hat{R}_k = 0 \tag{208}$$

where $\hat{R}_k$ is the Fourier transform of $R(w(t))$. Because $R(w)$ is nonlinear, $\hat{R}_k$ depends on all the modes $\hat{w}_k$. We now solve equation (208) by time evolution in pseudotime.

$$\frac{\mathrm{d}w_k}{\mathrm{d}t^*} + \hat{R}_k^* = 0 \tag{209}$$

At each iteration in pseudotime, $\hat{R}_k$ is evaluated indirectly. First $w(t)$ is obtained as the reverse transform of $\hat{w}_k$. Then we calculate the corresponding time history of the residual

$$R(t) = R(w(t))$$

and obtain $\hat{R}_k$ as the Fourier transform of $R(t)$, as shown in Figure 39. McMullen (2003) has shown that the modified RK method with multigrid acceleration achieves essentially the same rate of convergence for the solution of the frequency-domain equation (208) as it does for the BDF.

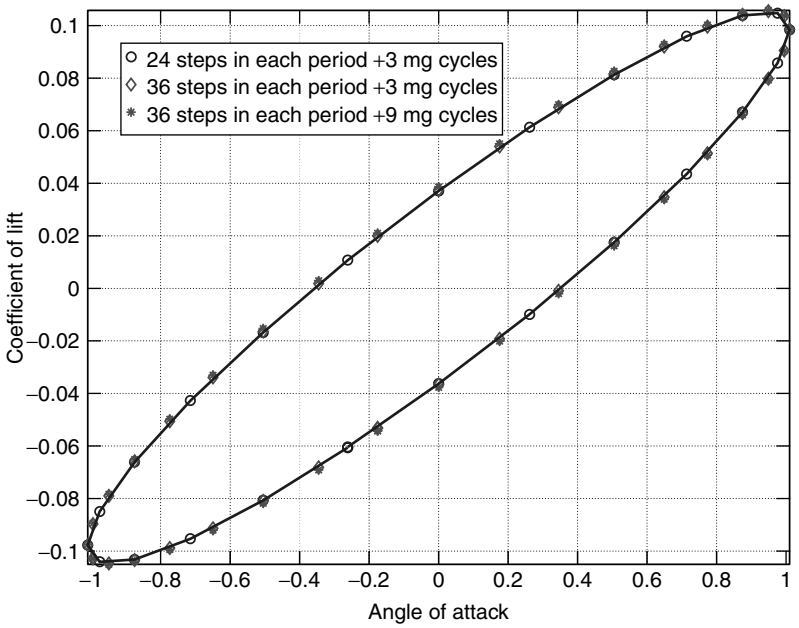

Figure 38. Results of the SGS−BDF method for AGARD case CT6. A color version of this image is available at http://www.mrw.interscience.wiley.com/ecm

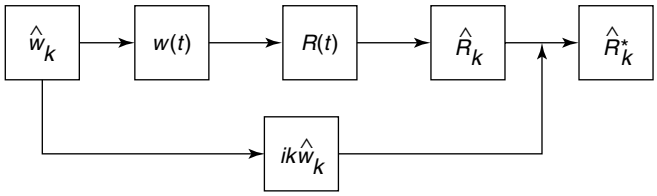

Figure 39. Solution of the time-spectral method in the frequency domain.

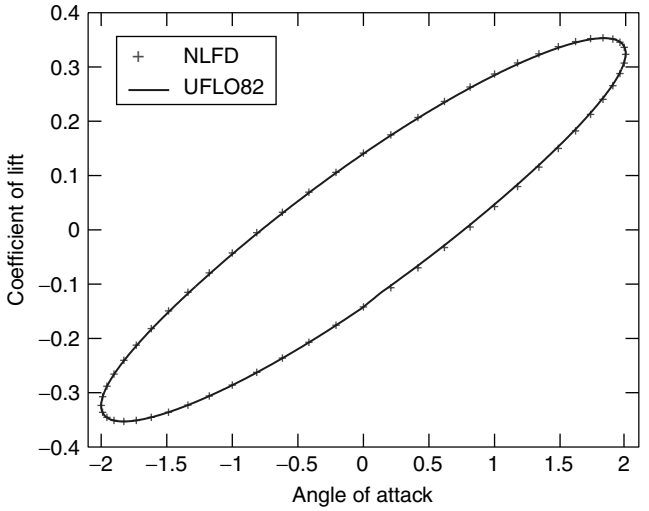

Figure 40. Comparison of the time-spectral and dual time-stepping schemes. A color version of this image is available at http://www.mrw.interscience.wiley.com/ecm

While the time-spectral method should make it possible to achieve spectral accuracy, numerical tests have shown that it can give the accuracy required for practical applications ('engineering accuracy') with very small numbers of modes. Figure 40 shows perfect agreement between the dual time-stepping and time-spectral method for the pitching airfoil considered in Section 7.1. Figure 41 shows comparisons of inviscid and viscous simulations with the experimental data. It can be seen that simulations using one, two, and three harmonics essentially overplot each other. There remain some discrepancies between the viscous simulations and the experimental data, which may be due to the failure of the turbulence model (in this case a Baldwin−Lomax model) to resolve the complex physics of shock wave boundary layer interactions.

7 AERODYNAMIC SHAPE OPTIMIZATION

7.1 The design problem

In considering the objectives of computational aerodynamics, three levels of desirable performance can be identified: (i) capability to predict the flow past an airplane or its important components in different flight regimes such as take-off or cruise, and off-design conditions such as flutter; (ii) interactive calculations to allow rapid improvement of the design; and (iii) integration of the predictive capability

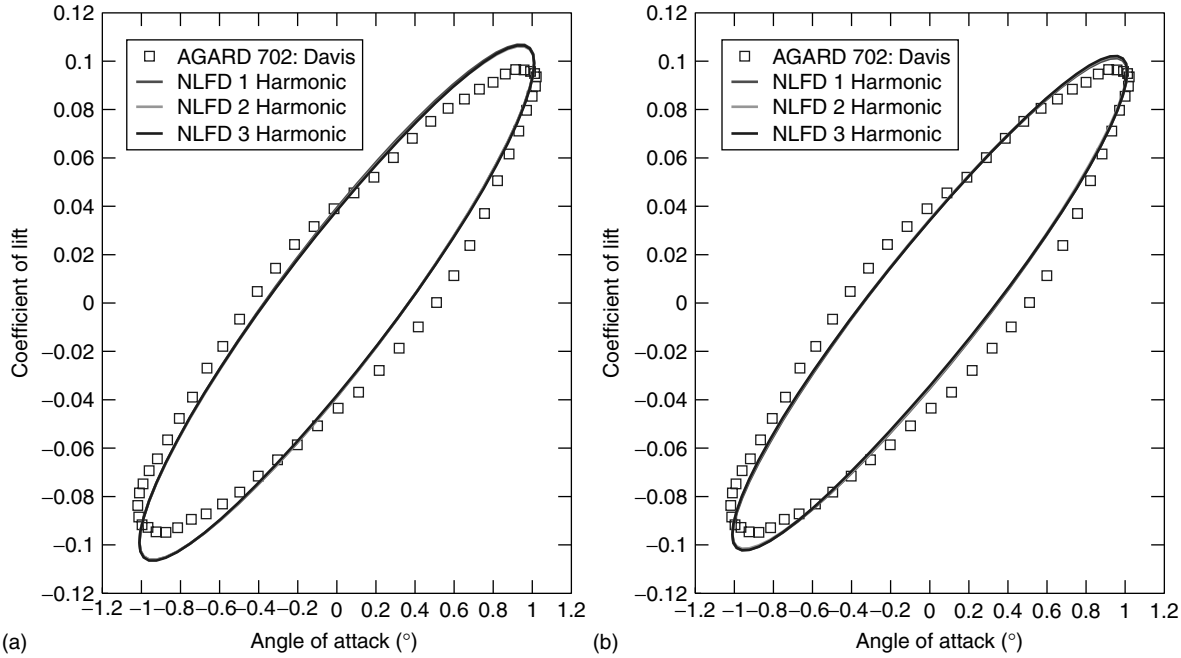

Figure 41. C_l over the pitching cycle. (a) Inviscid, (b) viscous. A color version of this image is available at http://www.mrw.interscience.wiley.com/ecm

into an automatic design method that incorporates computer optimization.

Although the results presented in this article demonstrate that substantial progress has been made toward the first objective, various problems of viscous separated flows still remain beyond our reach. Also in relatively simple cases, such as an airfoil or wing in inviscid flow, calculation can be performed fast enough that the second objective is attainable. The third objective must eventually prevail. What the designer really needs is a method of determining shapes that will have the desired aerodynamic properties. The ability to predict the flow over a given shape is not good enough for this purpose, as it does not provide any guidance on how to change the shape if it is unsatisfactory.

Traditionally the process of selecting design variations has been carried out by trial and error, relying on the intuition and experience of the designer. With currently available equipment, the turn around for numerical simulations is becoming so rapid that it is feasible to examine an extremely large number of variations. It is not at all likely that repeated trials in an interactive design and analysis procedure can lead to a truly optimum design. In order to take full advantage of the possibility of examining a large design space, the numerical simulations need to be combined with automatic search and optimization procedures. This can lead to automatic design methods that will fully realize the potential improvements in aerodynamic efficiency.

The need to find optimum aerodynamic designs was already well recognized by the pioneers of classical aerodynamic theory. A notable example is the determination that the optimum span–load distribution that minimizes the induced drag of a monoplane wing is elliptic (Glauert, 1926; Prandtl and Tietjens, 1934). There are also a number of famous results for linearized supersonic flow. The body of revolution of minimum drag was determined by Sears (1947), while conditions for minimum drag of thin wings due to thickness and sweep were derived by Jones (1981, 1982). The use of numerical optimization techniques to find aerodynamic shapes that meet a desired objective dates back to the work of Hicks and Henne (1979).

It has also been recognized that an experienced designer generally has an idea of the kind of pressure distribution that will lead to favorable characteristics. For example, he can avoid adverse pressure gradients that will induce premature separation of the boundary layer. Thus, in addition to the direct problem of calculation of the pressure distribution over a given shape, the inverse problem of finding the shape that will yield a specified pressure distribution can also play an important role. The problem of designing a two-dimensional profile to attain a desired pressure distribution was solved by Lighthill for the case of incompressible flow by means of conformal mapping (Lighthill, 1945). It was implemented in the author's program syn1, written in 1970.

Subsequently, there has been continuing interest in the problem, and a variety of methods have been proposed for the solution of the inverse problem in compressible

flow (Henne, 1980; McFadden, 1979; Volpe and Melnik, 1986; Giles, Drela and Thompkins, 1985). One source of difficulty is that the desired pressure distribution is not necessarily attainable, unless it satisfies certain constraints, with the result that the problem needs to be very carefully formulated; otherwise it may be ill posed.

The difficulty that the target pressure may be unattainable may be circumvented by treating the inverse problem as a special case of the optimization problem, with a cost function that measures the error in the solution of the inverse problem. For example, if p_d is the desired surface pressure, one may take the cost function to be an integral over the body surface of the square of the pressure error,

$$I = \frac{1}{2}\int_{\mathcal{B}} (p - p_d)^2 \, \mathrm{d}\mathcal{B}$$

or possibly a more general Sobolev norm of the pressure error. This has the advantage of converting a possibly ill-posed problem into a well posed one. It has the disadvantage that it incurs the computational costs associated with optimization procedures.

The hodograph transformation offers an alternative approach to the design of airfoils to produce shock-free transonic flows. Garabedian and Korn achieved a striking success by using the method of complex characteristics to solve the equations in the hodograph plane (Garabedian and Korn, 1971).

7.2 Optimization and design

The simplest approach to optimization is to define the geometry through a set of design parameters, which may, for example, be the weights α_i applied to a set of shape functions $b_i(x)$ so that the shape is represented as

$$f(x) = \sum \alpha_i b_i(x)$$

Then a cost function I is selected which might, for example, be the drag coefficient at a final lift coefficient, and I is regarded as a function of the parameters α_i. The sensitivities $\partial I/\partial \alpha_i$ may now be estimated by making a small variation $\delta\alpha_i$ in each design parameter in turn and recalculating the flow to obtain the change in I. Then

$$\frac{\partial I}{\partial \alpha_i} \approx \frac{I(\alpha_i + \delta\alpha_i) - I(\alpha_i)}{\delta\alpha_i}$$

The gradient vector $\partial I/\partial \alpha$ may now be used to determine a direction of improvement. The simplest procedure is to make a step in the negative gradient direction by setting

$$\alpha^{n+1} = \alpha^n - \lambda \frac{\partial I}{\partial \alpha}$$

so that to first order

$$I + \delta I = I - \frac{\partial I^T}{\partial \alpha}\delta\alpha = I - \lambda \frac{\partial I^T}{\partial \alpha}\frac{\partial I}{\partial \alpha}$$

More sophisticated search procedures may be used such as quasi-Newton methods, which attempt to estimate the second derivative $\partial^2 I/\partial\alpha_i\partial\alpha_j$ of the cost function from changes in the gradient $\partial I/\partial\alpha$ in successive optimization steps. These methods also generally introduce line searches to find the minimum in the search direction that is defined at each step. The main disadvantage of this approach is the need for a number of flow calculations proportional to the number of design variables to estimate the gradient. The computational costs can thus become prohibitive as the number of design variables is increased.

7.3 Application of control theory

In order to reduce the computational costs, it turns out that there are advantages in formulating both the inverse problem and more general aerodynamic problems within the framework of the mathematical theory for the control of systems governed by partial differential equations (Lions, 1971). A wing, for example, is a device to produce lift by controlling the flow, and its design can be regarded as a problem in the optimal control of the flow equations by variation of the shape of the boundary. If the boundary shape is regarded as arbitrary within some requirements of smoothness, then the full generality of shapes cannot be defined with a finite number of parameters, and one must use the concept of the Frechet derivative of the cost with respect to a function. Clearly, such a derivative cannot be determined directly by finite differences of the design parameters because there are now an infinite number of these. Using techniques of control theory, however, the gradient can be determined indirectly by solving an adjoint equation that has coefficients defined by the solution of the flow equations. The cost of solving the adjoint equation is comparable to that of solving the flow equations. Thus the gradient can be determined with roughly the computational costs of two flow solutions, independently of the number of design variables, which may be infinite if the boundary is regarded as a free surface.

The underlying concepts are clarified by the following abstract description of the adjoint method. For flow about an airfoil or wing, the aerodynamic properties that define the cost function are functions of the flow-field variables (w) and the physical location of the boundary, which may be represented by the function $\mathcal{F}$, say. Then

$$I = I(w, \mathcal{F})$$

and a change in $\mathcal{F}$ results in a change

$$\delta I = \left[\frac{\partial I^T}{\partial w}\right]_I \delta w + \left[\frac{\partial I^T}{\partial \mathcal{F}}\right]_{II} \delta \mathcal{F} \tag{210}$$

in the cost function. Here, the subscripts I and II are used to distinguish the contributions due to the variation δw in the flow solution from the change associated directly with the modification $\delta \mathcal{F}$ in the shape. This notation assists in grouping the numerous terms that arise during the derivation of the full Navier–Stokes adjoint operator, outlined in the next section, so that the basic structure of the approach as it is sketched in the present section can easily be recognized.

Suppose that the governing equation R, which expresses the dependence of w and $\mathcal{F}$ within the flow-field domain D can be written as

$$R(w, \mathcal{F}) = 0 \tag{211}$$

Then δw is determined from the equation

$$\delta R = \left[\frac{\partial R}{\partial w}\right]_I \delta w + \left[\frac{\partial R}{\partial \mathcal{F}}\right]_{II} \delta \mathcal{F} = 0 \tag{212}$$

Since the variation δR is zero, it can be multiplied by a Lagrange Multiplier ψ and subtracted from the variation δI without changing the result. Thus equation (210) can be replaced by

$$\begin{aligned}\delta I &= \frac{\partial I^T}{\partial w}\delta w + \frac{\partial I^T}{\partial \mathcal{F}}\delta \mathcal{F} - \psi^T \left(\left[\frac{\partial R}{\partial w}\right]\delta w + \left[\frac{\partial R}{\partial \mathcal{F}}\right]\delta \mathcal{F}\right) \\ &= \left\{\frac{\partial I^T}{\partial w} - \psi^T \left[\frac{\partial R}{\partial w}\right]\right\}_I \delta w + \left\{\frac{\partial I^T}{\partial \mathcal{F}} - \psi^T \left[\frac{\partial R}{\partial \mathcal{F}}\right]\right\}_{II} \delta \mathcal{F}\end{aligned} \tag{213}$$

Choosing ψ to satisfy the adjoint equation,

$$\left[\frac{\partial R}{\partial w}\right]^T \psi = \frac{\partial I}{\partial w} \tag{214}$$

the first term is eliminated, and we find that

$$\delta I = \mathcal{G} \delta \mathcal{F} \tag{215}$$

where

$$\mathcal{G} = \frac{\partial I^T}{\partial \mathcal{F}} - \psi^T \left[\frac{\partial R}{\partial \mathcal{F}}\right]$$

The advantage is that (215) is independent of δw, with the result that the gradient of I with respect to an arbitrary number of design variables can be determined without the need for additional flow-field evaluations. In the case that (211) is a partial differential equation, the adjoint equation (214) is also a partial differential equation and determination of the appropriate boundary conditions requires careful mathematical treatment.

The adjoint equations for transonic flows modeled by both the potential flow equation and the Euler equations were first derived by the author (Jameson, 1988). One motivation for developing the theory for the partial differential equations of the flow is to provide an indication in principle of how such a solution could be approached if sufficient computational resources were available. Another motivation is that it highlights the possibility of generating ill posed formulations of the problem. For example, if one attempts to calculate the sensitivity of the pressure at a particular location to changes in the boundary shape, there is the possibility that a shape modification could cause a shock wave to pass over that location. Then the sensitivity could become unbounded. The movement of the shock, however, is continuous as the shape changes. Therefore a quantity such as the drag coefficient, which is determined by integrating the pressure over the surface, also depends continuously on the shape. The adjoint equation allows the sensitivity of the drag coefficient to be determined without the explicit evaluation of pressure sensitivities, which would be ill posed.

In order to obtain numerical solutions, both the flow and the adjoint equations must be discretized. The control theory might be applied directly to the discrete flow equations that result from the numerical approximation of the flow equations by finite element, finite volume, or finite difference procedures. This leads directly to a set of discrete adjoint equations with a matrix that is the transpose of the Jacobian matrix of the full set of discrete nonlinear flow equations. On a three-dimensional mesh with indices i, j, k, the individual adjoint equations may be derived by collecting together all the terms multiplied by the variation $\delta w_{i,j,k}$ of the discrete flow variable $w_{i,j,k}$. The resulting discrete adjoint equations represent a possible discretization of the adjoint partial differential equation. If these equations are solved exactly they can provide an exact gradient of the inexact cost function that results from the discretization of the flow equations. The discrete adjoint equations derived directly from the discrete flow equations become very complicated when the flow equations are discretized with higher-order upwind-biased schemes using flux limiters. On the other hand, any consistent discretization of the adjoint partial differential equation will yield the exact gradient in the limit as the mesh is refined. The trade-off between the complexity of the adjoint discretization, the accuracy of the resulting estimate of the gradient, and its impact on the computational

cost to approach an optimum solution is a subject of ongoing research.

The discrete adjoint equations, whether they are derived directly or by discretization of the adjoint partial differential equation, are linear. Therefore, they could be solved by direct numerical inversion. In three-dimensional problems on a mesh with, say, n intervals in each coordinate direction, the number of unknowns is proportional to n^3 and the bandwidth to n^2. The complexity of direct inversion is proportional to the number of unknowns multiplied by the square of the bandwidth, resulting in a complexity proportional to n^7. The cost of direct inversion can thus become prohibitive as the mesh is refined, and it becomes more efficient to use iterative solution methods. Moreover, because of the similarity of the adjoint equations to the flow equations, the same iterative methods that have been proved to be efficient for the solution of the flow equations are efficient for the solution of the adjoint equations.

The control theory formulation for optimal aerodynamic design has proved effective in a variety of applications (Jameson, 1989, 1994; Reuther and Jameson, 1995). Pironneau has studied the use of control theory for optimal shape design of systems governed by elliptic equations (Pironneau, 1984), and more recently the Navier–Stokes equations, and also wave reflection problems (Pironneau, 1994). The adjoint equations have also been used by Baysal and Eleshaky (1991), and by Ta'asan, Kuruvila and Salas (1992), who have implemented a one shot approach in which the constraint represented by the flow equations is only required to be satisfied by the final converged solution. In their work, computational costs are also reduced by applying multigrid techniques to the geometry modifications as well as the solution of the flow and adjoint equations. Adjoint methods have been applied to incompressible viscous flow problems by Cabuk, Shung and Modi (1991), Huan and Modi (1994), and Desai and Ito (1994). Recent applications of adjoint methods on unstructured meshes include the work of Anderson and Venkatakrishnan (1997), and Elliot and Peraire (1996).

7.4 Three-dimensional design using the compressible Euler and Navier–Stokes equations

In order to illustrate the application of control theory to aerodynamic design problems, this section treats three-dimensional wing design using the compressible Euler and Navier–Stokes equations to model the flow. In comparison with incompressible viscous flow, the adjoint equations contain numerous extra terms that arise from the variation of the energy equation. In order to simplify the calculation of the effect of shape changes, it is convenient to introduce a body-fitted coordinate system, so that the flow and adjoint equations are solved in a fixed computational domain.

The transformed Navier–Stokes equations (27–35) can then be written in the computational domain as

$$\frac{\partial (Jw)}{\partial t} + R(w) = 0 \quad \text{in } \mathcal{D} \tag{216}$$

where

$$R(w) = \frac{\partial}{\partial \xi_i} \left(F_i - F_{v_i} \right) \tag{217}$$

where the inviscid and viscous flux contributions are now defined with respect to the computational cell faces by $F_i = S_{ij} f_j$ and $F_{vi} = S_{ij} f_{vj}$. In the subsequent analysis of the effect of a shape variation, it is useful to note that

$$\begin{aligned} S_{1j} &= \epsilon_{jpq} \frac{\partial x_p}{\partial \xi_2} \frac{\partial x_q}{\partial \xi_3} \\ S_{2j} &= \epsilon_{jpq} \frac{\partial x_p}{\partial \xi_3} \frac{\partial x_q}{\partial \xi_1} \\ S_{3j} &= \epsilon_{jpq} \frac{\partial x_p}{\partial \xi_1} \frac{\partial x_q}{\partial \xi_2} \end{aligned} \tag{218}$$

For convenience, the coordinates ξ_i describing the fixed computational domain are chosen so that each boundary conforms to a constant value of one of these coordinates. Variations in the shape then result in corresponding variations in the mapping derivatives defined by K_{ij}.

Suppose that the performance is measured by a cost function

$$I = \int_{\mathcal{B}} \mathcal{M}(w, S) \, \mathrm{d}B_\xi + \int_{\mathcal{D}} \mathcal{P}(w, S) \, \mathrm{d}D_\xi$$

containing both boundary and field contributions where $\mathrm{d}B_\xi$ and $\mathrm{d}D_\xi$ are the surface and volume elements in the computational domain. In general, $\mathcal{M}$ and $\mathcal{P}$ will depend on both the flow variables w and the metrics S defining the computational space. The design problem is now treated as a control problem where the boundary shape represents the control function, which is chosen to minimize I subject to the constraints defined by the flow equations (216). A shape change produces a variation in the flow solution δw and the metrics δS, which in turn produce a variation in the cost function

$$\delta I = \int_{\mathcal{B}} \delta \mathcal{M}(w, S) \, \mathrm{d}B_\xi + \int_{\mathcal{D}} \delta \mathcal{P}(w, S) \, \mathrm{d}D_\xi \tag{219}$$

This can be split as

$$\delta I = \delta I_I + \delta I_{II} \tag{220}$$

with

$$\begin{aligned}\delta\mathcal{M} &= [\mathcal{M}_w]_I \delta w + \delta\mathcal{M}_{II} \\ \delta\mathcal{P} &= [\mathcal{P}_w]_I \delta w + \delta\mathcal{P}_{II}\end{aligned} \tag{221}$$

where we continue to use the subscripts I and II to distinguish between the contributions associated with the variation of the flow solution δw and those associated with the metric variations δS. Thus $\left[\mathcal{M}_w\right]_I$ and $\left[\mathcal{P}_w\right]_I$ represent $\partial\mathcal{M}/\partial w$ and $\partial\mathcal{P}/\partial w$ with the metrics fixed, while $\delta\mathcal{M}_{II}$ and $\delta\mathcal{P}_{II}$ represent the contribution of the metric variations δS to $\delta\mathcal{M}$ and $\delta\mathcal{P}$.

In the steady state, the constraint equation (53) specifies the variation of the state vector δw by

$$\delta R = \frac{\partial}{\partial \xi_i} \delta \left(F_i - F_{vi}\right) = 0 \tag{222}$$

Here, also, δR, δF_i, and δF_{vi} can be split into contributions associated with δw and δS using the notation

$$\begin{aligned}\delta R &= \delta R_I + \delta R_{II} \\ \delta F_i &= \left[F_{i\,w}\right]_I \delta w + \delta F_{i\,II} \\ \delta F_{vi} &= \left[F_{vi\,w}\right]_I \delta w + \delta F_{vi\,II}\end{aligned} \tag{223}$$

The inviscid contributions are easily evaluated as

$$\left[F_{i\,w}\right]_I = S_{ij} \frac{\partial f_i}{\partial w}, \quad \delta F_{vi\,II} = \delta S_{ij} f_j$$

The details of the viscous contributions are complicated by the additional level of derivatives in the stress and heat flux terms.

Multiplying by a costate vector ψ, which will play an analogous role to the Lagrange multiplier introduced in equation (213), and integrating over the domain produces

$$\int_{\mathcal{D}} \psi^T \frac{\partial}{\partial \xi_i} \delta \left(F_i - F_{vi}\right) \, \mathrm{d}\mathcal{D}_\xi = 0 \tag{224}$$

Assuming that ψ is differentiable, the terms with subscript I may be integrated by parts to give

$$\begin{aligned}&\int_{\mathcal{B}} n_i \psi^T \delta \left(F_i - F_{vi}\right)_I \, \mathrm{d}\mathcal{B}_\xi - \int_{\mathcal{D}} \frac{\partial \psi^T}{\partial \xi_i} \delta \left(F_i - F_{vi}\right)_I \, \mathrm{d}\mathcal{D}_\xi \\ &\quad + \int_{\mathcal{D}} \psi^T \delta R_{II} \, \mathrm{d}\mathcal{D}_\xi = 0\end{aligned} \tag{225}$$

This equation results directly from taking the variation of the weak form of the flow equations, where ψ is taken to be an arbitrary differentiable test function. Since the left-hand expression equals zero, it may be subtracted from the variation in the cost function (219) to give

$$\begin{aligned}\delta I = \delta I_{II} &- \int_{\mathcal{D}} \psi^T \delta R_{II} \, \mathrm{d}\mathcal{D}_\xi \\ &- \int_{\mathcal{B}} \left[\delta\mathcal{M}_I - n_i \psi^T \delta \left(F_i - F_{vi}\right)_I\right] \mathrm{d}\mathcal{B}_\xi \\ &+ \int_{\mathcal{D}} \left[\delta\mathcal{P}_I + \frac{\partial \psi^T}{\partial \xi_i} \delta \left(F_i - F_{vi}\right)_I\right] \mathrm{d}\mathcal{D}_\xi\end{aligned} \tag{226}$$

Now, since ψ is an arbitrary differentiable function, it may be chosen in such a way that δI no longer depends explicitly on the variation of the state vector δw. The gradient of the cost function can then be evaluated directly from the metric variations without having to recompute the variation δw resulting from the perturbation of each design variable.

Comparing equations (221) and (223), the variation δw may be eliminated from (226) by equating all field terms with subscript 'I' to produce a differential adjoint system governing ψ

$$\frac{\partial \psi^T}{\partial \xi_i} \left[F_{i\,w} - F_{vi\,w}\right]_I + [\mathcal{P}_w]_I = 0 \quad \text{in } \mathcal{D} \tag{227}$$

The corresponding adjoint boundary condition is produced by equating the subscript 'I' boundary terms in equation (226) to produce

$$n_i \psi^T \left[F_{i\,w} - F_{vi\,w}\right]_I = [\mathcal{M}_w]_I \quad \text{on } \mathcal{B} \tag{228}$$

The remaining terms from equation (226) then yield a simplified expression for the variation of the cost function, which defines the gradient

$$\delta I = \delta I_{II} + \int_{\mathcal{D}} \psi^T \delta R_{II} \, \mathrm{d}\mathcal{D}_\xi \tag{229}$$

which consists purely of the terms containing variations in the metrics with the flow solution fixed. Hence an explicit formula for the gradient can be derived once the relationship between mesh perturbations and shape variations is defined.

The details of the derivation of the adjoint equation are quite complicated and have been presented in Jameson (1988), Jameson, Martinelli and Pierce (1998b), Jameson *et al.* (1998a), and Jameson and Martinelli (2000). Taking the transpose of equation (227), the inviscid adjoint equation may be written as

$$C_i^T \frac{\partial \psi}{\partial \xi_i} = 0 \quad \text{in } \mathcal{D} \tag{230}$$

where the inviscid Jacobian matrices in the transformed space are given by

$$C_i = S_{ij}\frac{\partial f_j}{\partial w}$$

The derivation of the viscous adjoint terms is simplified by transforming to the primitive variables

$$\widetilde{w}^T = (\rho, u_1, u_2, u_3, p)^T$$

because the viscous stresses depend on the velocity derivatives $(\partial u_i/\partial x_j)$, while the heat fluxes can be expressed as

$$\kappa\frac{\partial}{\partial x_i}\left(\frac{p}{\rho}\right)$$

Here

$$\kappa = \frac{k}{R} = \frac{\gamma}{\gamma - 1}\frac{\mu}{Pr}$$

where k is the conductivity, R is the gas constant, and Pr is the Prandtl number. The relationship between the conservative and primitive variations are defined by the expressions

$$\delta w = M\delta\widetilde{w}, \quad \delta\widetilde{w} = M^{-1}\delta w$$

which make use of the transformation matrices $M = (\partial w/\partial\widetilde{w})$ and $M^{-1} = (\partial\widetilde{w}/\partial w)$. The conservative and primitive adjoint operators L and $\tilde{L}$ corresponding to the variations δw and $\delta\widetilde{w}$ are then related by

$$\int_{\mathcal{D}} \delta w^T L\psi \; \mathrm{d}\mathcal{D}_\xi = \int_{\mathcal{D}} \delta\widetilde{w}^T \tilde{L}\psi \; \mathrm{d}\mathcal{D}_\xi$$

with

$$\tilde{L} = M^T L$$

where

$$M^T = \begin{bmatrix} 1 & u_1 & u_2 & u_3 & \dfrac{u_i u_i}{2} \\ 0 & \rho & 0 & 0 & \rho u_1 \\ 0 & 0 & \rho & 0 & \rho u_2 \\ 0 & 0 & 0 & \rho & \rho u_3 \\ 0 & 0 & 0 & 0 & \dfrac{1}{\gamma - 1} \end{bmatrix}$$

The derivation of the viscous adjoint operator is provided in Jameson, Martinelli and Pierce (1998b) with the simplification that variations in the transport coefficients are ignored. It is convenient to introduce the notation

$$\phi_i = \psi_{i+1}, \;\; i = 1, 2, 3, \;\; \theta = \psi_5$$

in order to allow the use of the summation convention for repeated indices over the range 1 to 3. Then, collecting together the contributions from the momentum and energy equations, the viscous adjoint operator in primitive variables can finally be expressed as

$$(\tilde{L}\psi)_1 = -\frac{p}{(\gamma - 1)\rho^2}\frac{\partial}{\partial\xi_l}\left(S_{lj}k\frac{\partial\theta}{\partial x_j}\right)$$

$$\begin{aligned}(\tilde{L}\psi)_{i+1} = {} & \frac{\partial}{\partial\xi_l}\left\{S_{lj}\left[\mu\left(\frac{\partial\phi_i}{\partial x_j} + \frac{\partial\phi_j}{\partial x_i}\right) + \lambda\delta_{ij}\frac{\partial\phi_k}{\partial x_k}\right]\right\} \\ & + \frac{\partial}{\partial\xi_l}\left\{S_{lj}\left[\mu\left(u_i\frac{\partial\theta}{\partial x_j} + u_j\frac{\partial\theta}{\partial x_i}\right) + \lambda\delta_{ij}u_k\frac{\partial\theta}{\partial x_k}\right]\right\} \\ & - \sigma_{ij}S_{lj}\frac{\partial\theta}{\partial x_l} \quad \text{for } i = 1, 2, 3,\end{aligned}$$

$$(\tilde{L}\psi)_5 = \frac{\rho}{(\gamma - 1)}\frac{\partial}{\partial\xi_l}\left(S_{lj}k\frac{\partial\theta}{\partial x_j}\right)$$

The conservative viscous adjoint operator may then be obtained by the transformation

$$L = M^{-1^T}\tilde{L}$$

The final formula for the gradient depends on the way in which the boundary shape is parameterized as a function of the design variables, and the way in which the mesh is deformed as the boundary is modified. Using the relationship between the mesh deformation and the surface modification, the field integral is reduced to a surface integral by integrating along the coordinate lines emanating from the surface. Thus the expression (226) for δI is finally reduced to the form of equation (215)

$$\delta I = \int_{\mathcal{B}} \mathcal{G}\delta\mathcal{F} \; \mathrm{d}\mathcal{B}_\xi$$

where $\mathcal{F}$ represents the design variables, and $\mathcal{G}$ is the gradient, which is a function defined over the boundary surface.

The boundary conditions satisfied by the flow equations restrict the form of the left-hand side of the adjoint boundary condition (228). Consequently, the boundary contribution to the cost function $\mathcal{M}$ cannot be specified arbitrarily. Instead, it must be chosen from the class of functions that allow cancellation of all terms containing δw in the boundary integral of equation (226). On the other hand, there is no such restriction on the specification of the field contribution to the cost function $\mathcal{P}$, since these terms may always be absorbed into the adjoint field equation (227) as source terms. The adjoint boundary conditions have been presented

in detail by Jameson and Martinelli (2000). Their derivation is illustrated in the following paragraphs for the case of inviscid flow.

For simplicity, it will be assumed that the portion of the boundary that undergoes shape modifications is restricted to the coordinate surface $\xi_2 = 0$. Then equations (226) and (228) may be simplified by incorporating the conditions

$$n_1 = n_3 = 0, \quad n_2 = 1, \quad \mathrm{d}\mathcal{B}_\xi = \mathrm{d}\xi_1\,\mathrm{d}\xi_3$$

so that only the variation δF_2 needs to be considered at the wall boundary. The condition that there is no flow through the wall boundary at $\xi_2 = 0$ is equivalent to

$$U_2 = 0$$

so that

$$\delta U_2 = 0$$

when the boundary shape is modified. Consequently, the variation of the inviscid flux at the boundary reduces to

$$\delta F_2 = \delta p \begin{Bmatrix} 0 \\ S_{21} \\ S_{22} \\ S_{23} \\ 0 \end{Bmatrix} + p \begin{Bmatrix} 0 \\ \delta S_{21} \\ \delta S_{22} \\ \delta S_{23} \\ 0 \end{Bmatrix} \tag{231}$$

Since δF_2 depends only on the pressure, it is now clear that the performance measure on the boundary $\mathcal{M}(w, S)$ may only be a function of the pressure and metric terms. Otherwise, complete cancellation of the terms containing δw in the boundary integral would be impossible. One may, for example, include arbitrary measures of the forces and moments in the cost function, since these are functions of the surface pressure.

In order to design a shape that will lead to a desired pressure distribution, a natural choice is to set

$$I = \frac{1}{2}\int_{\mathcal{B}} (p - p_d)^2\,\mathrm{d}S$$

where p_d is the desired surface pressure, and the integral is evaluated over the actual surface area. In the computational domain, this is transformed to

$$I = \frac{1}{2}\iint_{\mathcal{B}_w} (p - p_d)^2\,|S_2|\,\mathrm{d}\xi_1\,\mathrm{d}\xi_3$$

where the quantity

$$|S_2| = \sqrt{S_{2j}S_{2j}}$$

denotes the face area corresponding to a unit element of face area in the computational domain. Now, to cancel the dependence of the boundary integral on δp, the adjoint boundary condition reduces to

$$\psi_j n_j = p - p_d \tag{232}$$

where n_j are the components of the surface normal

$$n_j = \frac{S_{2j}}{|S_2|}$$

This amounts to a transpiration boundary condition on the costate variables corresponding to the momentum components. Note that it imposes no restriction on the tangential component of ψ at the boundary.

We find finally that

$$\delta I = -\int_{\mathcal{D}} \frac{\partial \psi^T}{\partial \xi_i}\delta S_{ij} f_j\,\mathrm{d}\mathcal{D} - \iint_{B_W} \left(\delta S_{21}\psi_2 + \delta S_{22}\psi_3 + \delta S_{23}\psi_4\right) p\,\mathrm{d}\xi_1\,\mathrm{d}\xi_3 \tag{233}$$

Here the expression for the cost variation depends on the mesh variations throughout the domain, which appear in the field integral. However, the true gradient for a shape variation should not depend on the way in which the mesh is deformed, but only on the true flow solution. In the next section, we show how the field integral can be eliminated to produce a reduced gradient formula that depends only on the boundary movement.

7.5 The reduced gradient formulation

Consider the case of a mesh variation with a fixed boundary. Then,

$$\delta I = 0$$

but there is a variation in the transformed flux,

$$\delta F_i = C_i \delta w + \delta S_{ij} f_j$$

Here the true solution is unchanged. Thus, the variation δw is due to the mesh movement δx at each mesh point. Therefore

$$\delta w = \nabla w \cdot \delta x = \frac{\partial w}{\partial x_j}\delta x_j \left(= \delta w^*\right)$$

and since

$$\frac{\partial}{\partial \xi_i}\delta F_i = 0$$

it follows that

$$\frac{\partial}{\partial \xi_i}\left(\delta S_{ij} f_j\right) = -\frac{\partial}{\partial \xi_i}\left(C_i \delta w^*\right) \tag{234}$$

It is verified in the following paragraph that this relation holds in the general case with boundary movement. Now

$$\begin{aligned}\int_{\mathcal{D}} \phi^T \delta R \, \mathrm{d}\mathcal{D} &= \int_{\mathcal{D}} \phi^T \frac{\partial}{\partial \xi_i} C_i \left(\delta w - \delta w^*\right) \mathrm{d}\mathcal{D} \\ &= \int_{\mathcal{B}} \phi^T C_i \left(\delta w - \delta w^*\right) \mathrm{d}\mathcal{B} \\ &\quad - \int_{\mathcal{D}} \frac{\partial \phi^T}{\partial \xi_i} C_i \left(\delta w - \delta w^*\right) \mathrm{d}\mathcal{D}\end{aligned} \tag{235}$$

Here on the wall boundary

$$C_2 \delta w = \delta F_2 - \delta S_{2j} f_j \tag{236}$$

Thus, by choosing ϕ to satisfy the adjoint equation (230) and the adjoint boundary condition (228), we reduce the cost variation to a boundary integral that depends only on the surface displacement:

$$\begin{aligned}\delta I = &\int_{\mathcal{B}_W} \psi^T \left(\delta S_{2j} f_j + C_2 \delta w^*\right) \mathrm{d}\xi_1 \, \mathrm{d}\xi_3 \\ &- \iint_{B_W} \left(\delta S_{21} \psi_2 + \delta S_{22} \psi_3 + \delta S_{23} \psi_4\right) p \, \mathrm{d}\xi_1 \, \mathrm{d}\xi_3\end{aligned} \tag{237}$$

For completeness, the general derivation of equation (234) is presented here. Using the formula (31) and the property (32)

$$\begin{aligned}&\frac{\partial}{\partial \xi_i}\left(\delta S_{ij} f_j\right) \\ &\quad = \frac{1}{2}\frac{\partial}{\partial \xi_i}\left\{\epsilon_{jpq}\epsilon_{irs}\left(\frac{\partial \delta x_p}{\partial \xi_r}\frac{\partial x_q}{\partial \xi_s} + \frac{\partial x_p}{\partial \xi_r}\frac{\partial \delta x_q}{\partial \xi_s}\right) f_j\right\} \\ &\quad = \frac{1}{2}\epsilon_{jpq}\epsilon_{irs}\left(\frac{\partial \delta x_p}{\partial \xi_r}\frac{\partial x_q}{\partial \xi_s} + \frac{\partial x_p}{\partial \xi_r}\frac{\partial \delta x_q}{\partial \xi_s}\right)\frac{\partial f_j}{\partial \xi_i} \\ &\quad = \frac{1}{2}\epsilon_{jpq}\epsilon_{irs}\left\{\frac{\partial}{\partial \xi_r}\left(\delta x_p \frac{\partial x_q}{\partial \xi_s}\frac{\partial f_j}{\partial \xi_i}\right)\right\} \\ &\qquad + \frac{1}{2}\epsilon_{jpq}\epsilon_{irs}\left\{\frac{\partial}{\partial \xi_s}\left(\delta x_q \frac{\partial x_p}{\partial \xi_r}\frac{\partial f_j}{\partial \xi_i}\right)\right\} \\ &\quad = \frac{\partial}{\partial \xi_r}\left(\delta x_p \epsilon_{pqj}\epsilon_{rsi}\frac{\partial x_q}{\partial \xi_s}\frac{\partial f_j}{\partial \xi_i}\right)\end{aligned} \tag{238}$$

Now express δx_p in terms of a shift in the original computational coordinates

$$\delta x_p = \frac{\partial x_p}{\partial \xi_k}\delta \xi_k$$

Then we obtain

$$\frac{\partial}{\partial \xi_i}\left(\delta S_{ij} f_j\right) = \frac{\partial}{\partial \xi_r}\left(\epsilon_{pqj}\epsilon_{rsi}\frac{\partial x_p}{\partial \xi_k}\frac{\partial x_q}{\partial \xi_s}\frac{\partial f_j}{\partial \xi_i}\delta \xi_k\right) \tag{239}$$

The term in $\partial/\partial\xi_1$ is

$$\epsilon_{123}\epsilon_{pqj}\frac{\partial x_p}{\partial \xi_k}\left(\frac{\partial x_q}{\partial \xi_2}\frac{\partial f_j}{\partial \xi_3} - \frac{\partial x_q}{\partial \xi_3}\frac{\partial f_j}{\partial \xi_2}\right)\delta \xi_k$$

Here the term multiplying $\delta\xi_1$ is

$$\epsilon_{jpq}\left(\frac{\partial x_p}{\partial \xi_1}\frac{\partial x_q}{\partial \xi_2}\frac{\partial f_j}{\partial \xi_3} - \frac{\partial x_p}{\partial \xi_1}\frac{\partial x_q}{\partial \xi_3}\frac{\partial f_j}{\partial \xi_2}\right)$$

According to the formulas (218) this may be recognized as

$$S_{2j}\frac{\partial f_1}{\partial \xi_2} + S_{3j}\frac{\partial f_1}{\partial \xi_3}$$

or, using the quasilinear form (217) of the equation for steady flow, as

$$-S_{1j}\frac{\partial f_1}{\partial \xi_1}$$

The terms multiplying $\delta\xi_2$ and $\delta\xi_3$ are

$$\epsilon_{jpq}\left(\frac{\partial x_p}{\partial \xi_2}\frac{\partial x_q}{\partial \xi_2}\frac{\partial f_j}{\partial \xi_3} - \frac{\partial x_p}{\partial \xi_2}\frac{\partial x_q}{\partial \xi_3}\frac{\partial f_j}{\partial \xi_2}\right) = -S_{1j}\frac{\partial f_1}{\partial \xi_2}$$

and

$$\epsilon_{jpq}\left(\frac{\partial x_p}{\partial \xi_3}\frac{\partial x_q}{\partial \xi_2}\frac{\partial f_j}{\partial \xi_3} - \frac{\partial x_p}{\partial \xi_3}\frac{\partial x_q}{\partial \xi_3}\frac{\partial f_j}{\partial \xi_2}\right) = -S_{1j}\frac{\partial f_1}{\partial \xi_3}$$

Thus the term in $\partial/\partial\xi_1$ is reduced to

$$-\frac{\partial}{\partial \xi_1}\left(S_{1j}\frac{\partial f_1}{\partial \xi_k}\delta \xi_k\right)$$

Finally, with similar reductions of the terms in $\partial/\partial\xi_2$ and $\partial/\partial\xi_3$, we obtain

$$\frac{\partial}{\partial \xi_i}\left(\delta S_{ij} f_j\right) = -\frac{\partial}{\partial \xi_i}\left(S_{ij}\frac{\partial f_j}{\partial \xi_k}\delta \xi_k\right) = -\frac{\partial}{\partial \xi_i}\left(C_i \delta w^*\right)$$

as was to be proved.

7.6 Optimization procedure

7.6.1 The need for a Sobolev inner product in the definition of the gradient

Another key issue for successful implementation of the continuous adjoint method is the choice of an appropriate inner product for the definition of the gradient. It turns out that there is an enormous benefit from the use of a modified Sobolev gradient, which enables the generation of a sequence of smooth shapes. This can be illustrated by considering the simplest case of a problem in the calculus of variations.

Suppose that we wish to find the path $y(x)$ that minimizes

$$I = \int_a^b F(y, y')\,\mathrm{d}x$$

with fixed end points $y(a)$ and $y(b)$. Under a variation $\delta y(x)$, the variation in the cost is

$$\begin{aligned}\delta I &= \int_a^b \left(\frac{\partial F}{\partial y}\delta y + \frac{\partial F}{\partial y'}\delta y'\right)\mathrm{d}x \\ &= \int_a^b \left(\frac{\partial F}{\partial y} - \frac{\mathrm{d}}{\mathrm{d}x}\frac{\partial F}{\partial y'}\right)\delta y\,\mathrm{d}x\end{aligned}$$

Thus defining the gradient as

$$g = \frac{\partial F}{\partial y} - \frac{\mathrm{d}}{\mathrm{d}x}\frac{\partial F}{\partial y'}$$

and the inner product as

$$(u, v) = \int_a^b uv\,\mathrm{d}x$$

we find that

$$\delta I = (g, \delta y)$$

If we now set

$$\delta y = -\lambda g, \quad \lambda > 0$$

we obtain an improvement

$$\delta I = -\lambda(g, g) \le 0$$

unless $g = 0$, the necessary condition for a minimum.

Note that g is a function of y, y', y'',

$$g = g(y, y', y'')$$

In the well-known case of the Brachistrone problem, for example, which calls for the determination of the path of quickest descent between two laterally separated points when a particle falls under gravity,

$$F(y, y') = \sqrt{\frac{1 + y'^2}{y}}$$

and

$$g = -\frac{1 + y'^2 + 2yy''}{2\left(y(1 + y'^2)\right)^{3/2}}$$

It can be seen that each step

$$y^{n+1} = y^n - \lambda^n g^n$$

reduces the smoothness of y by two classes. Thus the computed trajectory becomes less and less smooth, leading to instability.

In order to prevent this, we can introduce a weighted Sobolev inner product (Jameson, Martinelli and Vassberg, 2003a),

$$\langle u, v\rangle = \int (uv + \epsilon u'v')\,\mathrm{d}x$$

where ϵ is a parameter that controls the weight of the derivatives. We now define a gradient $\overline{g}$ such that

$$\delta I = \langle \overline{g}, \delta y\rangle$$

Then we have

$$\begin{aligned}\delta I &= \int (\overline{g}\delta y + \epsilon \overline{g}'\delta y')\,\mathrm{d}x \\ &= \int (\overline{g} - \frac{\partial}{\partial x}\epsilon\frac{\partial \overline{g}}{\partial x})\delta y\,\mathrm{d}x \\ &= (g, \delta y)\end{aligned}$$

where

$$\overline{g} - \frac{\partial}{\partial x}\epsilon\frac{\partial \overline{g}}{\partial x} = g$$

and $\overline{g} = 0$ at the end points. Thus $\overline{g}$ can be obtained from g by a smoothing equation. Now the step

$$y^{n+1} = y^n - \lambda^n \overline{g}^n$$

gives an improvement

$$\delta I = -\lambda^n \langle \overline{g}^n, \overline{g}^n\rangle$$

but y^{n+1} has the same smoothness as y^n, resulting in a stable process.

7.6.2 Sobolev gradient for shape optimization

In applying control theory to aerodynamic shape optimization, the use of a Sobolev gradient is equally important for the preservation of the smoothness class of the redesigned surface. Accordingly, using the weighted Sobolev inner product defined above, we define a modified gradient $\bar{\mathcal{G}}$ such that

$$\delta I = \langle \bar{\mathcal{G}}, \delta \mathcal{F} \rangle$$

In the one-dimensional case, $\bar{\mathcal{G}}$ is obtained by solving the smoothing equation

$$\bar{\mathcal{G}} - \frac{\partial}{\partial \xi_1} \epsilon \frac{\partial}{\partial \xi_1} \bar{\mathcal{G}} = \mathcal{G} \tag{240}$$

In the multidimensional case, the smoothing is applied in product form. Finally we set

$$\delta \mathcal{F} = -\lambda \bar{\mathcal{G}} \tag{241}$$

with the result that

$$\delta I = -\lambda \langle \bar{\mathcal{G}}, \bar{\mathcal{G}} \rangle \quad < 0$$

unless $\bar{\mathcal{G}} = 0$, and correspondingly $\mathcal{G} = 0$.

When second-order central differencing is applied to (240), the equation at a given node, i, can be expressed as

$$\bar{\mathcal{G}}_i - \epsilon \left(\bar{\mathcal{G}}_{i+1} - 2\bar{\mathcal{G}}_i + \bar{\mathcal{G}}_{i-1} \right) = \mathcal{G}_i, \qquad 1 \le i \le n$$

where $\mathcal{G}_i$ and $\bar{\mathcal{G}}_i$ are the point gradients at node i before and after the smoothing respectively, and n is the number of design variables equal to the number of mesh points in this case. Then,

$$\bar{\mathcal{G}} = A\mathcal{G}$$

where A is the $n \times n$ tridiagonal matrix such that

$$A^{-1} = \begin{bmatrix} 1+2\epsilon & -\epsilon & 0 & . & 0 \\ \epsilon & . & . & & \\ 0 & . & . & . & \\ . & & . & . & -\epsilon \\ 0 & & & \epsilon & 1+2\epsilon \end{bmatrix}$$

Using the steepest descent method in each design iteration, a step, $\delta \mathcal{F}$, is taken such that

$$\delta \mathcal{F} = -\lambda A \mathcal{G} \tag{242}$$

As can be seen from the form of this expression, implicit smoothing may be regarded as a preconditioner that allows the use of much larger steps for the search procedure and leads to a large reduction in the number of design iterations needed for convergence.

7.6.3 Outline of the design procedure

The design procedure can finally be summarized as follows:

1. Solve the flow equations for ρ, u_1, u_2, u_3, p.
2. Solve the adjoint equations for ψ subject to appropriate boundary conditions.
3. Evaluate $\mathcal{G}$ and calculate the corresponding Sobolev gradient $\bar{\mathcal{G}}$.
4. Project $\bar{\mathcal{G}}$ into an allowable subspace that satisfies any geometric constraints.
5. Update the shape based on the direction of steepest descent.
6. Return to 1 until convergence is reached.

Practical implementation of the design method relies heavily upon fast and accurate solvers for both the state (w) and costate (ψ) systems. The result obtained in Section 7.8 have been obtained using well-validated software for the solution of the Euler and Navier–Stokes equations developed over the course of many years (Jameson, Schmidt, and Turkel, 1981; Martinelli and Jameson, 1988; Tatsumi, Martinelli and Jameson, 1995). For inverse design, the lift is fixed by the target pressure. In drag minimization, it is also appropriate to fix the lift coefficient, because the induced drag is a major fraction of the total drag, and this could be reduced simply by reducing the lift. Therefore the angle of attack is adjusted during each flow solution to force a specified lift coefficient to be attained, and the influence of variations of the angle of attack is included in the calculation of the gradient. The vortex drag also depends on the span loading, which may be constrained by other considerations such as structural loading or buffet onset. Consequently, the option to force the span loading by adjusting the twist distribution as well as the angle of attack during the flow solution is provided.

7.7 Computational costs

In order to address the issues of the search costs, Jameson and Vassberg investigated a variety of techniques using a trajectory optimization problem (the Brachistochrone) as a representative model (Jameson and Vassberg, 1999). The study verified that the search cost (i.e. number of steps) of a simple steepest descent method applied to this problem scales as N^2, where N is the number of design variables, while the cost of quasi-Newton methods scaled linearly with N as expected. On the other hand, with an

appropriate amount of smoothing, the smoothed descent method converged in a fixed number of steps, independent of N. Considering that the evaluation of the gradient by a finite difference method requires $N+1$ flow calculations, while the cost of its evaluation by the adjoint method is roughly that of two flow calculations, one arrives at the estimates of total computational cost given in Tables 3–4.

Table 3. Cost of search algorithm.

Steepest Descent	$\mathcal{O}(N^2)$ steps
Quasi-Newton	$\mathcal{O}(N)$ steps
Smoothed Gradient	$\mathcal{O}(K)$ steps
(Note: K is independent of N)	

Table 4. Total computational cost of design.

Finite Difference Gradients + Steepest Descent	$\mathcal{O}(N^3)$
Finite Difference Gradients + Quasi-Newton Search	$\mathcal{O}(N^2)$
Adjoint Gradients + Quasi-Newton Search	$\mathcal{O}(N)$
Adjoint Gradients + Smoothed Gradient Search (Note: K is independent of N)	$\mathcal{O}(K)$

7.8 Case studies

Over the last decade, the adjoint method has been successfully used to refine a variety of designs for flight at both transonic and supersonic cruising speeds. In the case of transonic flight, it is often possible to produce a shock-free flow that eliminates the shock drag by making very small changes, typically no larger than the boundary layer displacement thickness. Consequently, viscous effects need to be considered in order to realize the full benefits of the optimization. Several design efforts that have utilized these methods include: Raytheon's and Gulfstream business jets, NASA's High-Speed Civil Transport, regional jet designs, as well as several Boeing projects such as the MDXX and the Blended-Wing-Body (Liebeck, 2002; Roman, Allen and Liebeck, 2000). Some representative examples of design calculations are presented in this section.

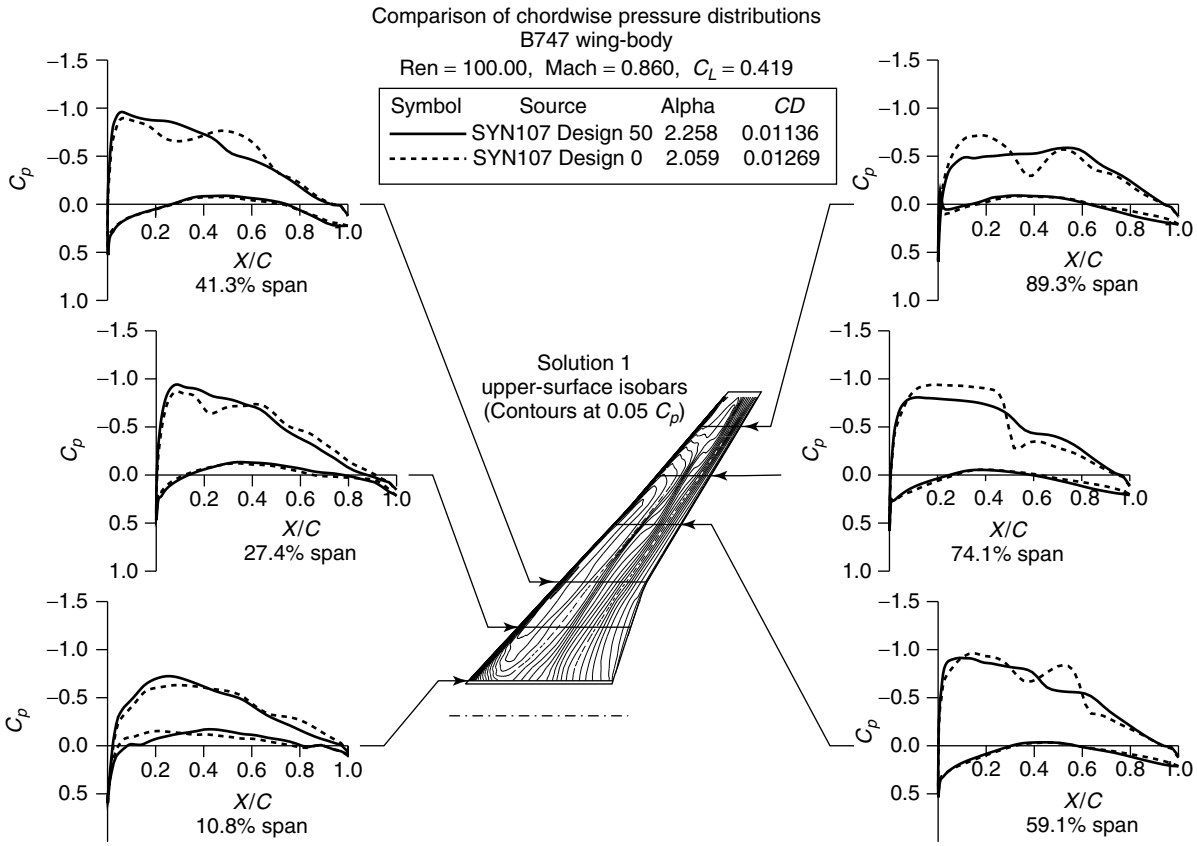

Figure 42. Redesigned Boeing 747 wing at Mach 0.86, C_p distributions.

7.8.1 Redesign of the Boeing 747 wing

Here the optimization of the wing of the Boeing 747-200 is presented to illustrate the kind of benefits that can be obtained. In these calculations, the flow was modeled by the RANS equations. A Baldwin–Lomax turbulence model was considered sufficient, since the optimization is for the cruise condition with attached flow. The calculations were performed to minimize the drag coefficient at a fixed lift coefficient, subject to the additional constraints that the span loading should not be altered and the thickness should not be reduced. It might be possible to reduce the induced drag by modifying the span loading to an elliptic distribution, but this would increase the root bending moment, and consequently require an increase in the skin thickness and structure weight. A reduction in wing thickness would not only reduce the fuel volume, but it would also require an increase in skin thickness to support the bending moment. Thus these constraints assure that there will be no penalty in either structure weight or fuel volume.

Figure 42 displays the result of an optimization at a Mach number of 0.86, which is roughly the maximum cruising Mach number attainable by the existing design before the onset of significant drag rise. The lift coefficient of 0.42 is the contribution of the exposed wing. Allowing for the fuselage to total lift coefficient is about 0.47. It can be seen that the redesigned wing is essentially shock free, and the drag coefficient is reduced from 0.01269 (127 counts) to 0.01136 (114 counts). The total drag coefficient of the aircraft at this lift coefficient is around 270 counts, so this would represent a drag reduction of the order of 5 percent.

Figure 43 displays the result of an optimization at Mach 0.90. In this case the shock waves are not eliminated, but their strength is significantly weakened, while the drag coefficient is reduced from 0.01819 (182 counts) to 0.01293 (129 counts). Thus the redesigned wing has essentially the same drag at Mach 0.9 as the original wing at Mach 0.86. The Boeing 747 wing could apparently be modified to allow such an increase in the cruising Mach number because it has a higher sweepback than later designs, and a rather thin wing section with a thickness to chord ratio of 8 percent. Figures 44a and 44b verify that the span loading and thickness were not changed by the redesign, while Figures 44c and 44d indicate the required section changes at 42 and 69.

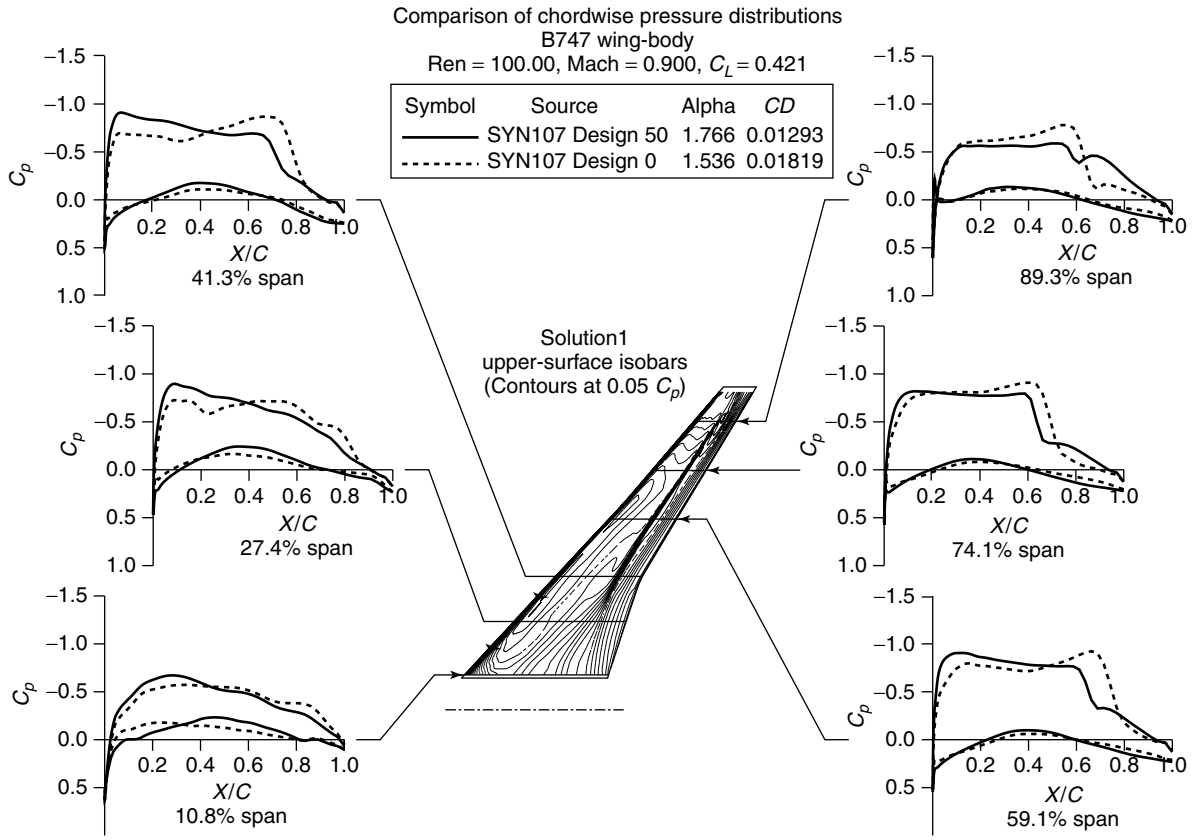

Figure 43. Redesigned Boeing 747 wing at Mach 0.90, C_p distributions.

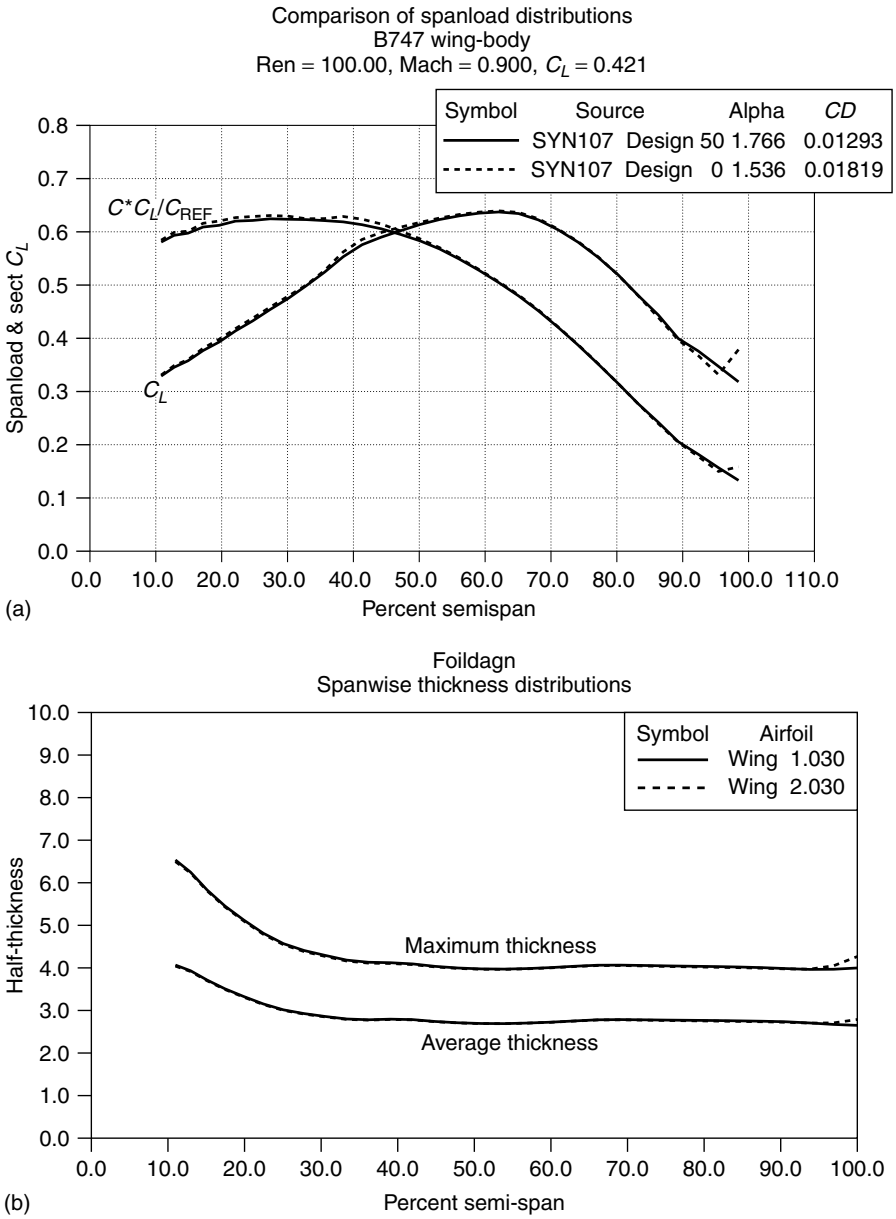

Figure 44. Redesigned Boeing 747 wing at Mach 0.90. (a) Span loading, (b) Spanwise thickness distribution, (c) Section geometry at $\eta = 0.42$, (d) Section geometry at $\eta = 0.69$.

7.8.2 Planform and aero-structural optimization

The shape changes in the section needed to improve the transonic wing design are quite small. However, in order to obtain a true optimum design, larger-scale changes such as changes in the wing planform (sweepback, span, chord, section thickness, and taper) should be considered. Because these directly affect the structure weight, a meaningful result can only be obtained by considering a cost function that accounts for both the aerodynamic characteristics and the weight.

In references Leoviriyakit and Jameson (2003, 2004) and Leoviriyakit, Kim and Jameson (2003), the cost function is defined as

$$I = \alpha_1 C_D + \alpha_2 \frac{1}{2} \int_{\mathcal{B}} (p - p_d)^2 \, \mathrm{d}S + \alpha_3 C_W$$

where $C_W \equiv (W/q_\infty S_{\text{ref}})$ is a dimensionless measure of the wing weight, which can be estimated either from statistical formulas, or from a simple analysis of a representative structure, allowing for failure modes such as

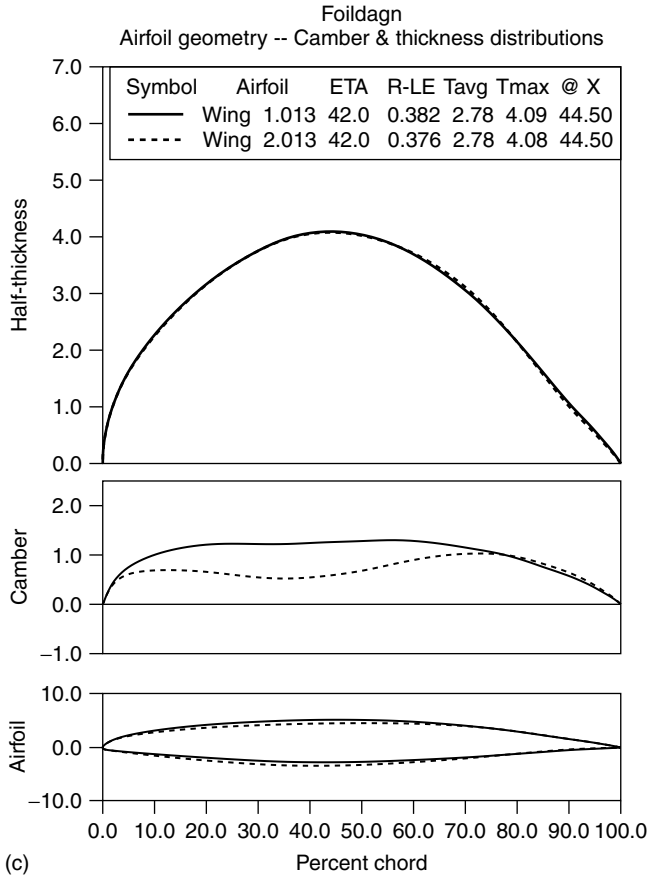

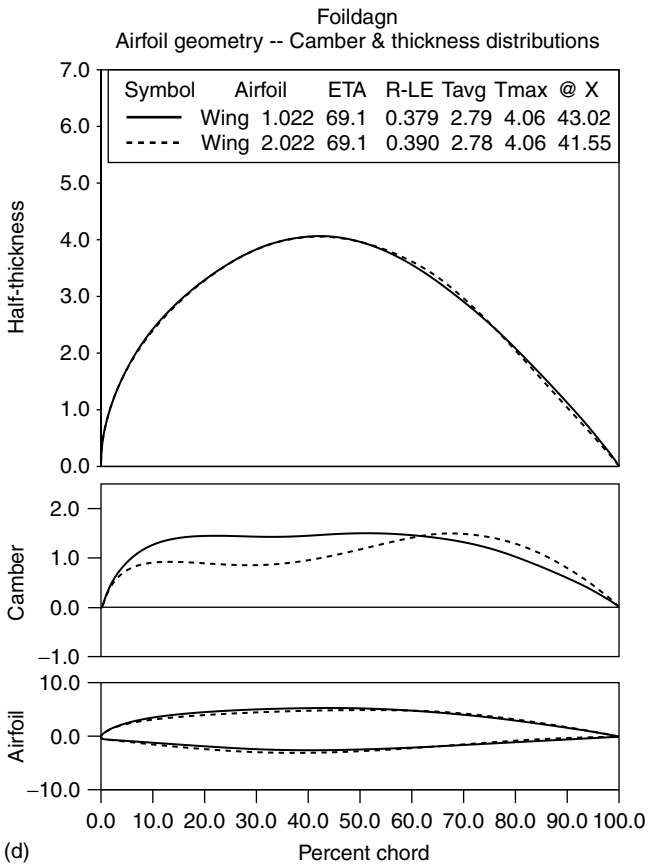

Figure 44. (*Continued*).

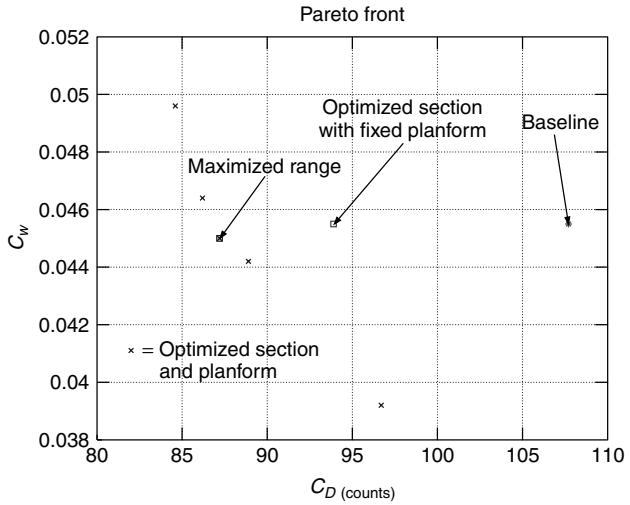

Figure 45. Pareto front of section-and-planform modifications. (Reproduced by permission of Kasidit Leoviriyakit.) A color version of this image is available at http://www.mrw.interscience.wiley.com/ecm

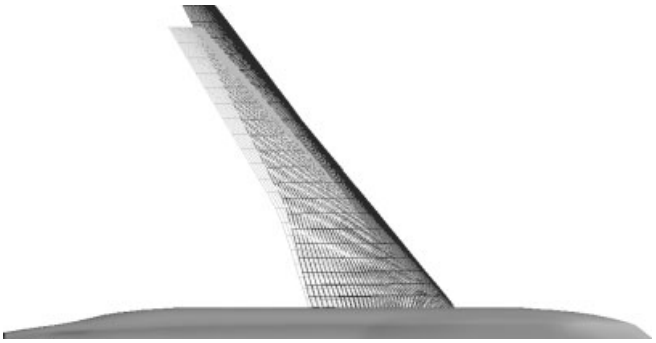

Figure 46. Superposition of the baseline (green) and the optimized section-and-planform (blue) geometries of Boeing 747. The redesigned geometry has a longer span, a lower sweep angle, and thicker wing sections, improving both aerodynamic and structural performances. The optimization is performed at Mach 0.87 and fixed C_L 0.42, where (α_3/α_1) is chosen to maximize the range of the aircraft. A color version of this image is available at http://www.mrw.interscience.wiley.com/ecm

panel buckling. The coefficient α_2 is introduced to provide the designer some control over the pressure distribution, while the relative importance of drag and weight are represented by the coefficients α_1 and α_3. By varying these it is possible to calculate the Pareto front of designs that have the least weight for a given drag coefficient, or the least drag coefficient for a given weight. The relative

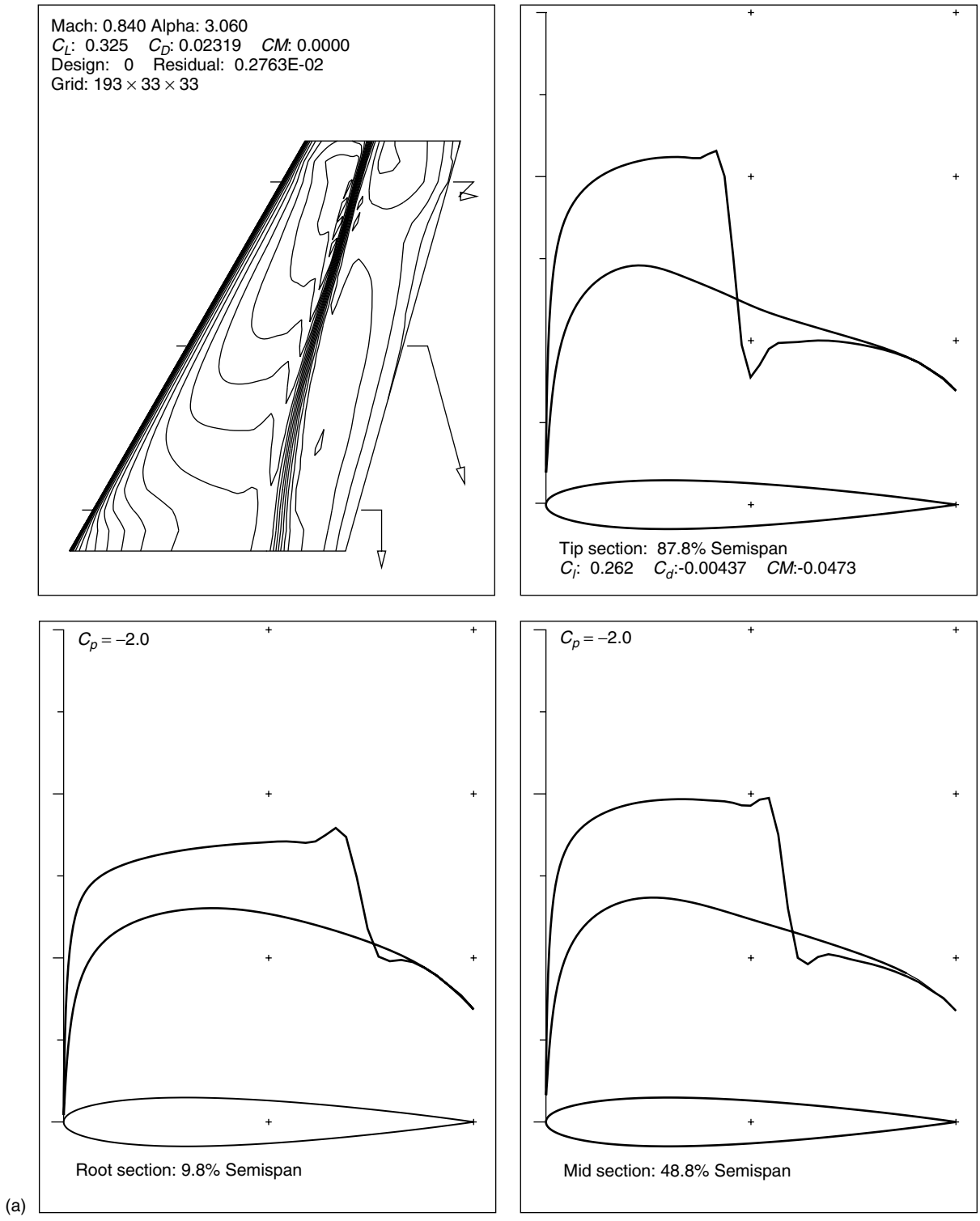

Figure 47. Inverse design of NACA0012; initial (- - - -) and final (——) geometry, attained (+, ×) and target (○) pressure distributions. (a) Baseline geometry, (b) Redesigned geometry, (c) 0% of the wing span (d) 20% of the wing span.

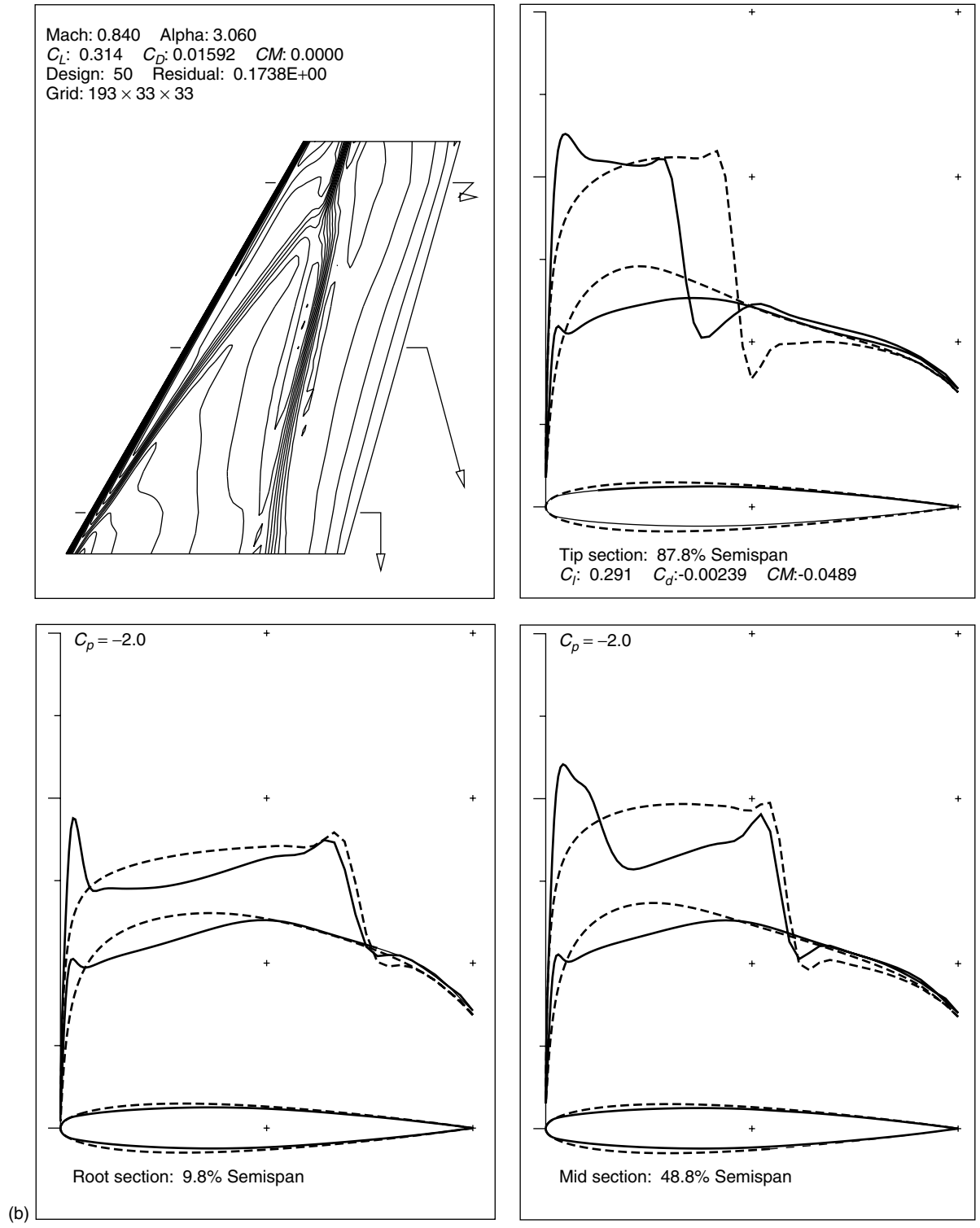

(b)

Figure 47. (*Continued*).

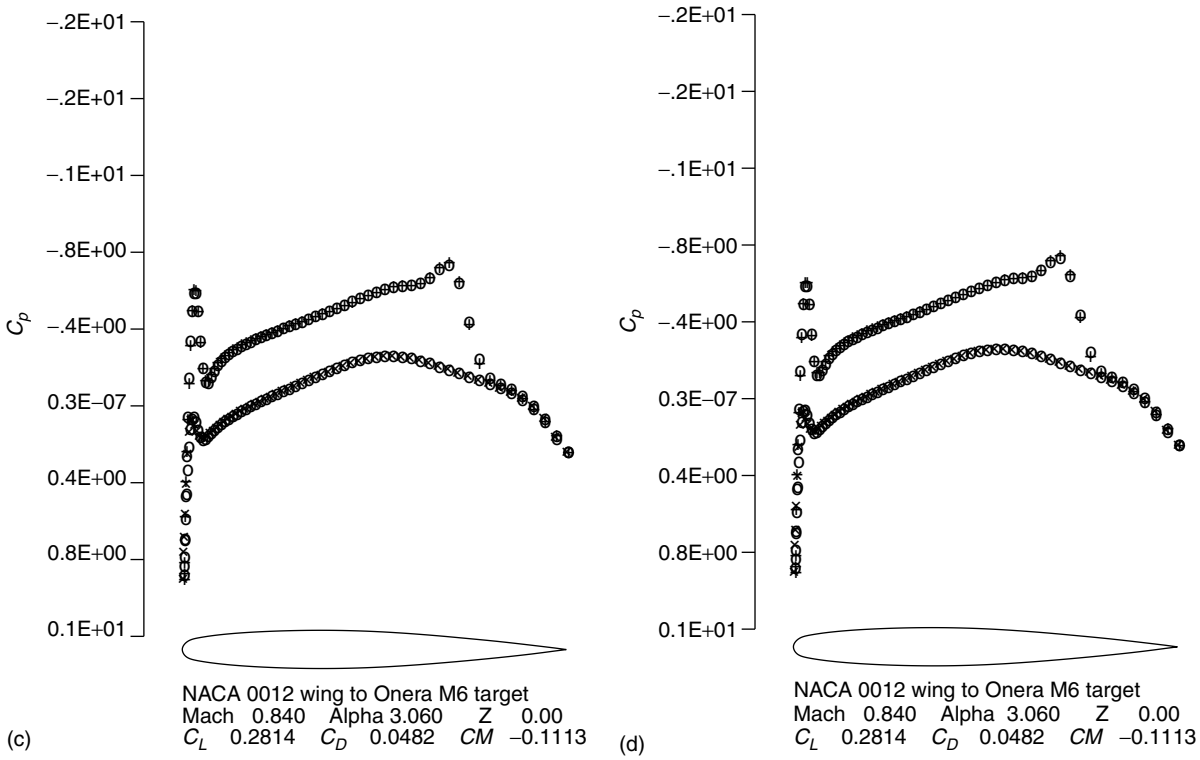

Figure 47. (*Continued*).

importance of these can be estimated from the Breguet range equation (1);

$$\frac{\delta R}{R} = -\left(\frac{\delta C_D}{C_D} + \frac{1}{\log \dfrac{W_1}{W_2}} \frac{\delta W_2}{W_2}\right)$$

$$= -\left(\frac{\delta C_D}{C_D} + \frac{1}{\log \dfrac{W_1}{W_2}} \frac{\delta C_W}{\dfrac{W_2}{q_\infty S_{\text{ref}}}}\right)$$

Figure 45 shows the Pareto front obtained from a study of the Boeing 747 wing (Leoviriyakit and Jameson, 2004), in which the flow was modeled by the Euler equations. The wing planform and section were varied simultaneously, with the planform defined by six parameters; sweepback, span, the chord at three span stations, and wing thickness. It also shows the point on the Pareto front when α_3/α_1 is chosen such that the range of the aircraft is maximized. The optimum wing, as illustrated in Figure 46, has a larger span, a lower sweep angle, and a thicker wing section in the inboard part of the wing. The increase in span leads to a reduction in the induced drag, while the section shape changes keep the shock drag low. At the same time, the lower sweep angle and thicker wing section reduce the structural weight. Overall, the optimum wing improves both aerodynamic performance and structural weight. The drag coefficient is reduced from 108 to 87 counts (19%), while the weight factor C_W is reduced from 455 to 450 counts (1%).

7.8.3 Design using an unstructured mesh

A major obstacle to the treatment of arbitrarily complex configurations is the difficulty and cost of mesh generation. This can be mitigated by the use of unstructured meshes. Thus it appears that the extension of the adjoint method to unstructured meshes may provide the most promising route to the optimum shape design of key elements of complex configurations, such as wing-pylon-nacelle combinations. Some results are presented in the following paragraphs. These have been obtained with new software to implement the adjoint method for unstructured meshes. This is currently under development (Jameson, Sriram and Martinelli, 2003b).

7.8.4 Wing inverse design

Figures 47a and 47b show the result of an inverse design calculation, where the initial geometry was a wing made up of NACA 0012 sections, and the target pressure distribution was the pressure distribution over the Onera M6

wing. Figures 47c, 47d, 48a, 48b, 48c, and 48d show the target and computed pressure distribution at six spanwise sections. It can be seen from these plots that the target pressure distribution is almost perfectly reproduced in 50 design cycles, verifying that the design process is capable of recovering pressure distributions that are significantly different from the initial distribution. This is a particularly challenging test because it calls for the recovery of a smooth symmetric profile from an asymmetric pressure distribution containing a triangular pattern of shock waves.

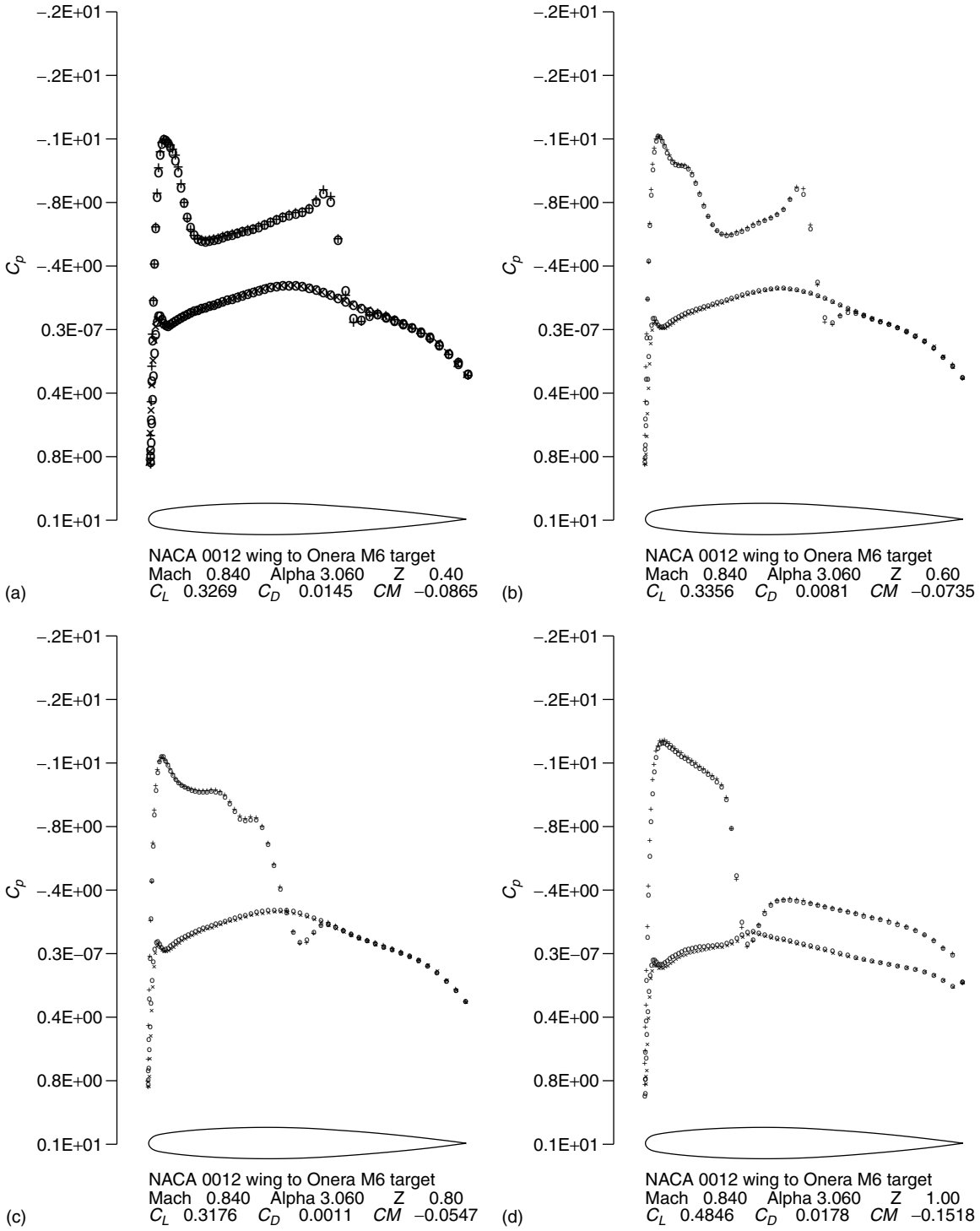

Figure 48. Inverse design of NACA0012; initial (- - - -) and final (——) geometry, attained (+, ×) and target (○) pressure distributions. (a) 40% of the wing span, (b) 60% of the wing span, (c) 80% of the wing span, (d) 100% of the wing span.

7.8.5 Shape optimization for a transonic business jet

The unstructured design method has also been applied to complete aircraft configurations. The results for a business jet are presented in Figures 49 and 50. Figure 49 shows the baseline design while flying at cruise conditions ($M_\infty = 0.80$, $\alpha = 2^\circ$). It can be seen that there is a strong shock on the outboard wing. Figure 50 shows the results of a drag

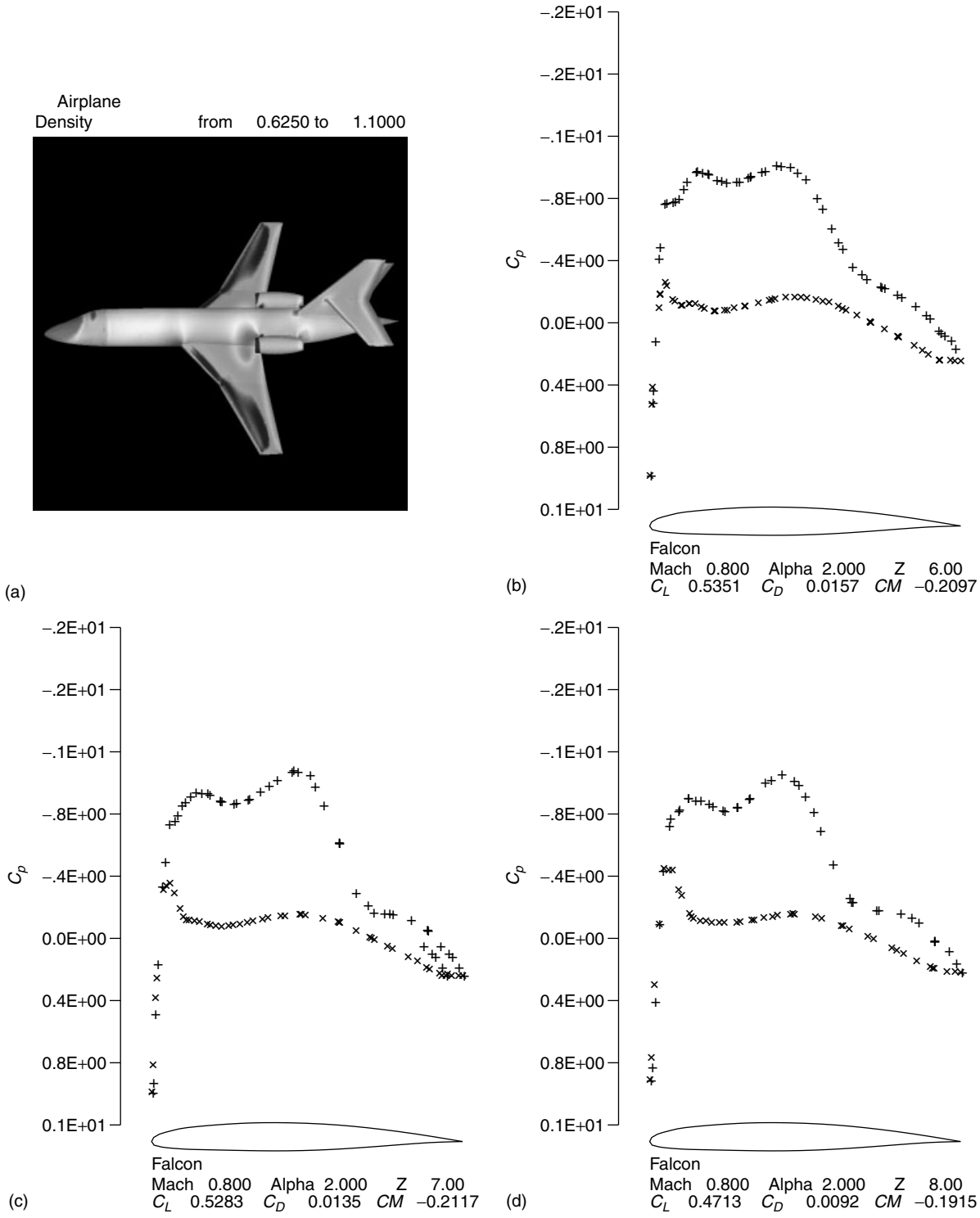

Figure 49. A business jet at $M = 0.8$, $\alpha = 2$. (a) Density contours, (b) 66% wing span, (c) 77% wing span, (d) 88% wing span. A color version of this image is available at http://www.mrw.interscience.wiley.com/ecm

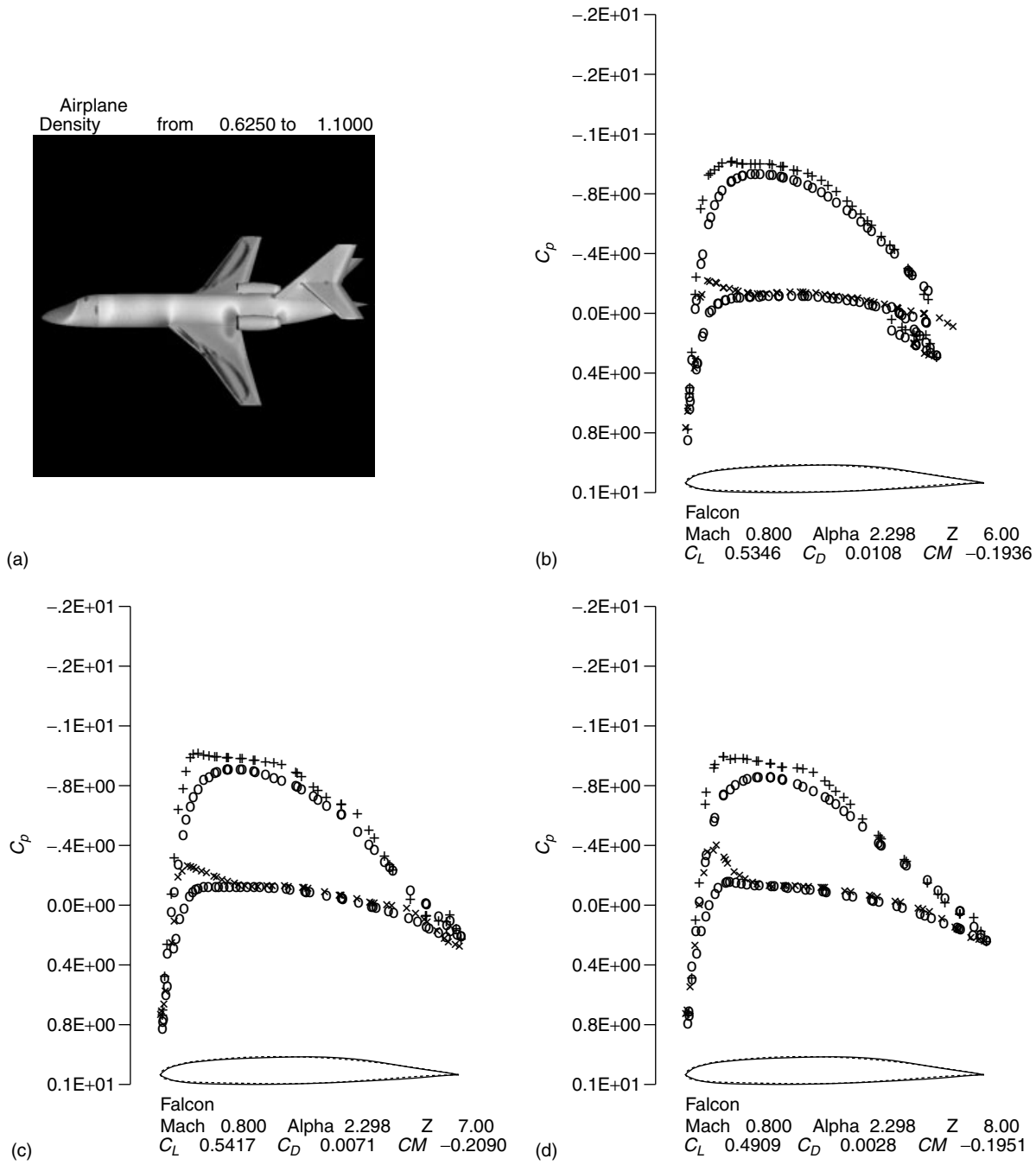

Figure 50. A redesign of a business jet at $M = 0.8$, $\alpha = 2.3$; dashed line: original geometry, solid line: redesigned geometry. A color version of this image is available at http://www.mrw.interscience.wiley.com/ecm

minimization: the drag has been reduced from 235 to 215 counts in about 8 design cycles, while the shocks have been eliminated. The lift was constrained at 0.4 by perturbing the angle of attack. Furthermore, the original thickness of the wing was maintained during the design process in order to ensure that both fuel volume and structural integrity will be maintained by the redesigned shape. Thickness constraints on the wing were imposed on cutting planes along the span of the wing, and the constrained shape movement was transferred back to the nodes of the surface triangulation. The volume mesh was deformed to conform to the shape changes induced using the spring method. The entire design process typically takes about 4 hours on a 1.7 GHz Athlon processor with 1 GB of memory. Parallel implementation of the design procedure further reduces the computational cost.

7.9 Conclusion

The accumulated experience of the last decade suggests that most existing aircraft that cruise at transonic speeds are amenable to a drag reduction of the order of 3 to 5 percent, or an increase in the drag rise Mach number of at least 0.02. These improvements can be achieved by very small shape modifications, which are too subtle to allow their determination by trial and error methods. The potential economic benefits are substantial, considering the fuel costs of the entire airline fleet. Moreover, if one were to take full advantage of the increase in the lift to drag ratio during the design process, a smaller aircraft could be designed to perform the same task, with consequent further cost reductions. It seems inevitable that some method of this type will provide a basis for aerodynamic designs of the future.

8 RELATED CHAPTERS

(*See also* **Chapter 12** and **Chapter 13 of this Volume**)

ACKNOWLEDGMENT

Much of the author's earlier research at the Courant Institute and Princeton University was made possible by grants from NASA, the Office of Naval Research, and the International Business Machines Corporation. During the last decade, the research on aerodynamic shape optimization has benefited greatly from the continuing support of the Air Force Office of Scientific Research.

REFERENCES

Aftosmis MJ, Melton JE and Berger MJ. *Adaptation and surface modeling for Cartesian mesh methods*. AIAA Paper, Collection of Technical Papers. Pt. 2 (A95-36501 09-34) 95-1725. In 12th AIAA Computational Fluid Dynamics Conference and Open forum, San Diego, 1995.

Aiso H. Admissibility of difference approximations for scalar conservation laws. *Hiroshima Math. J.* 1993; **23**:15–61.

Allmaras S. *Analysis of a local matrix preconditioner for the 2-D Navier–Stokes equations*. AIAA Paper 93-3330. In AIAA 11th Computational Fluid Dynamics Conference, Orlando, 1993.

Allmaras S. *Analysis of semi-implicit preconditioners for multigrid solution of the 2-D Navier–Stokes equations*. AIAA Paper 95-1651. In AIAA 12th Computational Fluid Dynamics Conference, San Diego, 1995.

Allmaras S. *Algebraic smoothing analysis of multigrid methods for the 2-D compressible Navier–Stokes equations*. AIAA Paper 97-1954. In AIAA 13th Computational Fluid Dynamics Conference, Snowmass, 1997.

Alonso JJ and Jameson A. *Fully-implicit time-marching aeroelastic solutions*. AIAA Paper 94-0056. In AIAA 32nd Aerospace Sciences Meeting, Reno, 1994.

Alonso JJ, Martinelli L and Jameson A. *Multigrid unsteady Navier–Stokes calculations with aeroelastic applications*. AIAA Paper 95-0048. In AIAA 33rd Aerospace Sciences Meeting, Reno, 1995.

Anderson WK, Thomas JL and Whitfield DL. *Multigrid acceleration of the flux split Euler equations*. AIAA Paper 86-0274. In AIAA 24th Aerospace Sciences Meeting, Reno, 1986.

Anderson WK and Venkatakrishnan V. *Aerodynamic design and optimization on unstructured grids with a continuous adjoint formulation*. AIAA Paper 97-0643. In AIAA 35th Aerospace Sciences Meeting, Reno, 1997.

Anderson BK, Thomas JL and Van Leer B. *A comparison of flux vector splittings for the Euler equations*. AIAA Paper 85-0122. In AIAA 23rd Aerospace Sciences Meeting, Reno, 1985.

Ashley H and Landahl M. *Aerodynamics of Wings and Bodies*. Dover, 1965 Reprinted by Dover, 1985.

Baker TJ. Mesh generation by a sequence of transformations. *Appl. Numer. Math.* 1986; **2**:515–528.

Balakrishnan N and Deshpande SM. *New Upwind Schemes with Wave-Particle Splitting for Inviscid Compressible Flows*. Report 91 FM 12, Indian Institute of Science, 1991.

Bardina J and Lombard CK. Three-dimensional hypersonic flow simulations with the CSCM implicit upwind Navier–Stokes method. AIAA Paper 87-1114. In *AIAA 8th Computational Fluid Dynamics Conference*, Honolulu, June, 1987.

Barth TJ. Aspects of Unstructured Grids and Finite Volume Solvers for the Euler and Navier Stokes Equations. In von Karman Institute for Fluid Dynamics Lecture Series Notes 1994-05, Brussels, 1994.

Barth TJ and Frederickson PO. Higher order solution of the Euler equations on unstructured grids using quadratic reconstruction. AIAA Paper 90-0013. In *AIAA 28th Aerospace Sciences Meeting*, Reno, January, 1990.

Barth TJ and Jespersen DC. *The design and application of upwind schemes on unstructured meshes*. AIAA Paper 89-0366. In AIAA 27th Aerospace Sciences Meeting, Reno, 1989.

Bauer F, Garabedian P and Korn D. A theory of supercritical wing sections, with computer programs and examples. *Lecture Notes in Economics and Mathematical Systems 66*, vol. 1. Springer-Verlag; New York, 1972; 81–83.

Bauer F, Garabedian P, Korn D and Jameson A. *Supercritical Wing Sections II*. Springer-Verlag: New York, 1975.

Baysal O and Eleshaky ME. *Aerodynamic design optimization using sensitivity analysis and computational fluid dynamics*. AIAA Paper 91-0471. In 29th Aerospace Sciences Meeting, Reno, 1991.

Beam RW and Warming RF. An implicit finite difference algorithm for hyperbolic systems in conservation form. *J. Comput. Phys.* 1976; **23**:87–110.

Belov A, Martinelli L and Jameson A. *A new implicit algorithm with multigrid for unsteady incompressible flow calculations*.

AIAA Paper 95-0049. In AIAA 33rd Aerospace Sciences Meeting, Reno, 1995.

Benek JA, Buning PG and Steger JL. *A 3-D chimera grid embedding technique*. AIAA Paper 85-1523. In AIAA 7th Computational Fluid Dynamics Conference, Cincinnati, 1985.

Benek JA, Donegan TL and Suhs NE. *Extended chimera grid embedding scheme with applications to viscous flows*. AIAA Paper 87-1126. In AIAA 8th Computational Fluid Dynamics Conference, Honolulu, 1987.

Berger M and LeVeque RJ. An adaptive Cartesian mesh algorithm for the Euler equations in arbitrary geometries. AIAA Paper 89-1930. In *AIAA 9th Computational Fluid Dynamics Conference*, Buffalo, June, 1989.

Boris JP ans Book DL. Flux corrected transport, 1 SHASTA, a fluid transport algorithm that works. *J. Comput. Phys.* 1973; **11**:38–69.

Brandt A. Multi-level adaptive solutions to boundary value problems. *Math. Comp.* 1977; **31**:333–390.

Bristeau MO, Pironneau O, Glowinski R, Periaux J, Perrier P and Poirier G. Application of optimal control and finite element methods to the calculation of transonic flows and incompressible viscous flows. In *Proceedings of IMA Conference on Numerical Methods in Applied Fluid Dynamics*, Hunt B (ed.). Academic Press: Reading 1978, 1980a; 203–312.

Bristeau MO, Pironneau O, Glowinski R, Periaux J, Perrier P and Poirier G. Transonic flow simulations by finite elements and least square methods. In *Proceedings of the 3rd International Conference on Finite Elements in Flow Problems*, Norrie DH (ed.). John Wiley & Son: Banff, 1980b; 11–29.

Bristeau MO, Pironneau O, Glowinski R, Periaux J, Perrier P and Poirier G. On the numerical solution of nonlinear problems in fluid dynamics by least squares and finite element methods (II). Application to transonic flow simulations. In *Proceedings of the 3rd International Conference on Finite Element Methods in Nonlinear Mechanics, FENOMECH 84*, Stuttgart, 1984, St. Doltsinis J (ed.). North Holland: Amsterdam, 1985; 363–394.

Cabuk H, Shung CH and Modi V. Adjoint operator approach to shape design for internal incompressible flow. In *Proceedings of the Third International Conference on Inverse Design and Optimization in Engineering Sciences*, Dulikravich GS (ed.). NASA Contractor Report NASA-CR-202363: 1991; 391–404.

Caughey DA. *A diagonal implicit multigrid algorithm for the Euler equations*. AIAA Paper 87-453. In AIAA 25th Aerospace Sciences Meeting, Reno, 1987.

Chakravarthy SR. *Relaxation methods for unfactored implicit upwind schemes*. AIAA Paper 84-0165. In AIAA 23rd Aerospace Sciences Meeting, Reno, 1984.

Crumpton PI and Giles MB. *Implicit time accurate solutions on unstructured dynamic grids*. AIAA Paper 95-1671. In AIAA 12th Computational Fluid Dynamics Conference, San Diego, 1995.

Dahlquist G. A special stability problem for linear multistep methods. *BIT* 1963; **3**:27–43.

Darmofal DL and Siu K. A robust multigrid algorithm for the Euler equations with local preconditioning and semicoarsening. *J. Comput. Phys.* 1999; **151**:728–756.

Deconinck H, Paillère H, Struijs R and Roe PL. Multi-dimensional upwind schemes based on fluctuation-splitting of conservation laws. *Comput. Mech.* 1993; **11**:323–340.

Delaunay B. Sur la Sphere vide. *Bull. Acad. Sci. USSR VII: Class Scil, Math. Nat.* 1934; 793–800.

Desai M and Ito K. Optimal controls of Navier–Stokes equations. *SIAM J. Control Optim.* 1994; **32**(5):1428–1446.

Eiseman PR. A multi-surface method of coordinate generation. *J. Comput. Phys.* 1979; **33**:118–150.

Elliot J and Peraire J. *Practical 3D aerodynamic design and optimization using unstructured meshes*. AIAA Paper 96-4710. In 6th AIAA/NASA/USAF Multidisciplinary and Optimization Symposium, Seattle, 1996.

Engquist B and Osher S. One sided difference approximations for non-linear conservation laws. *Math. Comp.* 1981; **36**:321–352.

Eriksson LE. Generation of boundary-conforming grids around wing-body configurations using transfinite interpolation. *AIAA J.* 1982; **20**:1313–1320.

Fedorenko RP. The speed of convergence of one iterative process. *USSR Comput. Math. Math. Phys.* 1964; **4**:227–235.

Garabedian PR. Estimation of the relaxation factor for small mesh size. *Math. Tables Aids Comput.* 1956; **10**:183–185.

Garabedian PR and Korn DG. Numerical design of transonic airfoils. In *Proceedings of SYNSPADE 1970*, Hubbard B (ed.). Academic Press: New York, 1971; 253–271.

Gear CW. *The Numerical Integration of Stiff Ordinary Differential Equations*. Report 221, University of Illinois Department of Computer Science, 1967.

Giles M, Drela M and Thompkins WT. Newton solution of direct and inverse transonic Euler equations. AIAA Paper 85-1530. In *AIAA 7th Computational Fluid Dynamics Conference*, Cincinnati, July, 1985; 394–402.

Glauert H. *The Elements of Aerofoil and Airscrew Theory*. Cambridge University Press: Cambridge, 1926.

Godunov SK. A difference method for the numerical calculation of discontinuous solutions of hydrodynamic equations. *Math. Sbornik* 1959; **47**:271–306. Translated as JPRS 7225 by U.S. Dept. of Commerce, 1960.

Gourlay AR and Mitchell AR. A stable implicit difference scheme for hyperbolic systems in two space variables. *Numer. Math.* 1966; **8**:367–375.

Haase W, Cahput E, Elsholz E, Leschziner MA and Mueller UR. Validation of CFD codes and assessment of turbulence models ECARD. *Notes on Numerical Fluid Mechanics 58*. Vieweg: Braunschweig, 1997.

Hackbusch W. On the multi-grid method applied to difference equations. *Computing* 1978; **20**:291–306.

Hall MG. Cell vertex multigrid schemes for solution of the Euler equations. In *Conference on Numerical Methods for Fluid Dynamics, University Reading*, Morton KW and Baines MJ (eds). Oxford University Press: Oxford, 1985; 303–345.

Harten A. High resolution schemes for hyperbolic conservation laws. *J. Comput. Phys.* 1983; **49**:357–393.

Harten A, Engquist B, Osher S and Chakravarthy S. Uniformly high order accurate essentially non-oscillatory schemes. *J. Comput. Phys.* 1987; **71**:231–303.

Hayes WD. *Linearized Supersonic Flow*. North American Aviation Report (AL-222), Thesis, California Institute of Technology, American Mathematical Society Report 852, 1947.

Hemker PW and Spekreijse SP. *Multigrid solution of the steady Euler equations*. In Proceedings of Oberwolfach Meeting on Multigrid Methods, 1984a.

Hemker, Henne PW and Spekreijse, SP. *Multigrid solution of the steady Euler equations*. Proceedings of Oberwolfach Meeting on Multigrid Methods, 1984b.

Henne PA. An inverse transonic wing design method. AIAA Paper 80-0330. In *AIAA 18th Aerospace Sciences Meeting*, Pasadena, 1980.

Hess JL and Smith AMO. *Calculation of Non-Lifting Potential Flow About Arbitrary Three Dimensional Bodies*. Douglas Aircraft Report (ES 40622), 1962.

Hicks RM and Henne PA. Wing design by numerical optimization. AIAA Paper 79-0080. In *AIAA 17th Aerospace Sciences Meeting*, New Orleans, 1979.

Hirsch C, Lacol C and Deconinck H. *Convection algorithms based on a diagonalization procedure for the multi-dimensional Euler equations*. AIAA Paper 87-1163, In AIAA 8th Computational Fluid Dynamics Conference, Hawaii, 1987.

Hosseini K and Alonso JJ. *Practical implementation and improvement of preconditioning methods for explicit multistage flow solvers*. AIAA Paper 2004-0763. In AIAA 42nd Aerospace Sciences Meeting, Reno, 2004.

Huan JC and Modi V. Optimum design for drag minimizing bodies in incompressible flow. *Inverse Problems Eng.* 1994; **1**:1–25.

Hughes TJR, Franca LP and Mallet M. A new finite element formulation for computational fluid dynamics, I, Symmetric forms of the compressible Euler and Navier–Stokes equations and the second law of thermodynamics. *Comput. Methods Appl. Mech. Eng.* 1986; **59**:223–231.

Hunt B. The mathematical basis and numerical principles of the boundary integral method for Incompressible potential flow over 3-d aerodynamic configurations. *Numerical Methods in Applied Fluid Dynamics*. Academic Press, 1978; 49–135.

Iserles A. Order stars and a saturation theorem for first order hyperbolics. *IMA J. Numer. Anal.* 1981; **2**:49–61.

Jameson A. Iterative solution of transonic flows over airfoils and wings, including flows at Mach 1. *Commun. Pure Appl. Math.* 1974; **27**:283–309.

Jameson A. Remarks on the calculation of transonic potential flow by a finite volume method. *Proceedings of the Conference on Computational Methods in Fluid Dynamics*. Institute of Mathematical and Applications, 1978.

Jameson A. Solution of the Euler equations by a multigrid method. *Appl. Math. Comput.* 1983; **13**:327–356.

Jameson A. Non-oscillatory shock capturing scheme using flux limited dissipation. In *Large Scale Computations in Fluid Mechanics*, Lectures in Applied Mathematics, vol. 22, Part 1, Engquist BE, Osher S and Sommerville RCJ (eds). AMS, 1985a; 345–370.

Jameson A. Transonic flow calculations for aircraft. In *Numerical Methods in Fluid Dynamics*, Lecture Notes in Mathematics, Brezzi F (ed.). Springer-Verlag, 1985b; 156–242.

Jameson A. Multigrid algorithms for compressible flow calculations. In *Lecture Notes in Mathematics*, vol. 1228, Hackbusch W and Trottenberg U (eds). Springer-Verlag, 1986a; 166–201.

Jameson A. A vertex based multigrid algorithm for three-dimensional compressible flow calculations. In *Numerical Methods for Compressible Flow – Finite Difference, Element and Volume Techniques*. Tezduar TE and Hughes TJR (eds). ASME Publication AMD 78, 1986b; 45–73.

Jameson A. Aerodynamic design via control theory. *J. Sci. Comput.* 1988; **3**:233–260.

Jameson A. Computational aerodynamics for aircraft design. *Science* 1989; **245**:361–371.

Jameson A. *Time dependent calculations using multigrid, with applications to unsteady flows past airfoils and wings*. AIAA Paper 91-1596. In AIAA 10th Computational Fluid Dynamics Conference, Honolulu, 1991.

Jameson A. *Artificial diffusion, upwind biasing, limiters and their effect on accuracy and multigrid convergence in transonic and hypersonic flows*. AIAA Paper 93-3359. In AIAA 11th Computational Fluid Dynamics Conference, Orlando, 1993.

Jameson A. *Optimum Aerodynamic Design via Boundary Control*. AGARD FDP/Von Karman Institute Lecture Notes on Optimum Design Methods in Aerodynamics. AGARD Report 803, 1994; 3-1–3-33.

Jameson A. Analysis and design of numerical schemes for gas dynamics 1, artificial diffusion, upwind biasing, limiters and their effect on multigrid convergence. *Int. J. Comput. Fluid Dyn.* 1995a; **4**:171–218.

Jameson A. Analysis and design of numerical schemes for gas dynamics 2, artificial diffusion and discrete shock structure. *Int. J. Comput. Fluid Dyn.* 1995b; **5**:1–38.

Jameson A. and Baker TJ. *Solution of the Euler equations for complex configurations*. In Proceedings of AlAA 6th Computational Fluid Dynamics Conference, Danvers, 1983; 293–302.

Jameson A and Caughey DA. *A finite volume method for transonic potential flow calculations*. In Proceedings of AIAA 3rd Computational Fluid Dynamics Conference, Albuquerque, 1977; 35–54.

Jameson A and Caughey DA. *How many steps are required to solve the Euler equations of steady compressible flow*. AIAA Paper 2001-2673. In 15th AIAA Computational Fluid Dynamics Conference, Anaheim, 2001.

Jameson A and Martinelli L. Aerodynamic shape optimization techniques based on control theory. In *Computational Mathematics Driven by Industrial Problems*, Lecture Notes in Mathematics, vol. 1739, Capasso V, Engl E and Periux J (eds). Springer, 2000 Lectures given at the 1st Session of the Centro Internazionale Matematico Estivo (C.I.M.E.) held in Martina Franca, Italy.

Jameson A and Mavriplis DJ. Multigrid solution of the Euler equations on unstructured and adaptive grids. In *Multigrid Methods, Theory, Applications and Supercomputing*, Lecture Notes in Pure and Applied Mathematics, vol. 110, McCormick S (ed.). Marcel Dekker: 1987; 413–430.

Jameson A and Turkel E. Implicit Schemes and LU Decompositions. *Math. Comp.* 1981; **37**:385–397.

Jameson A and Vassberg JC. *Studies of alternative numerical optimization methods applied to the brachistochrone problem*. In Proceedings of OptiCON '99, Newport Beach, 1999.

Jameson A, Baker TJ and Weatherill NP. *Calculation of inviscid transonic flow over a complete aircraft*. AIAA Paper 86-0103. In AIAA 24th Aerospace Sciences Meeting, Reno, 1986a.

Jameson, A, Baker, TJ and Weatherill, NP. *Calculation of inviscid transonic flow over a complete aircraft*. AlAA Paper 86-0103. In AlAA 24th Aerospace Sciences Meeting, Reno, 1986b.

Jameson A, Martinelli L and Vassberg J. *Reduction of the adjoint gradient formula in the continuous limit*. AIAA Paper. In 41st AIAA Aerospace Sciences Meeting, Reno, 2003a.

Jameson A, Sriram and Martinelli L. *An unstructured adjoint method for transonic flows*. AIAA Paper. In 16th AIAA CFD Conference, Orlando, 2003b.

Jameson, A, Schmidt, W, and Turkel, E. Numerical solution of the Euler equations by finite volume methods using Runge-Kutta time stepping schemes. AIAA Paper 81-1259. In *AIAA 14th Fluid Dynamics and Plasma Dynamics Conference*, Palo Alto, 1981.

Jameson A, Alonso JJ, Reuther J, Martinelli L and Vassberg JC. *Aerodynamic shape optimization techniques based on control theory*. AIAA Paper 98-2538. In AIAA 29th Fluid Dynamics Conference, Albuquerque, 1998a.

Jameson A, Martinelli L and Pierce NA. Optimum aerodynamic design using the Navier–Stokes equations. *Theor. Comput. Fluid Dyn.* 1998b; **10**:213–237.

Jayaram M and Jameson A. *Multigrid solution of the Navier–Stokes equations for flow over wings*. AIAA Paper 88-0705. In AIAA 26th Aerospace Sciences Meeting, Reno, 1988.

Jiang GS and Shu CW. Efficient implementation of weighted ENO schemes. *J. Comput. Phys.* 1996; **126**:202–228.

Jones RT. The minimum drag of thin wings in frictionless flow. *J. Aerosol Sci.* 1981; **18**:75–81.

Jones RT. Theoretical Determination of the minimum drag of airfoils at supersonic speeds. *J. Aerosol Sci.* 1982; **19**:813–822.

Kinnmark IPE. One step integration methods with large stability limits for hyperbolic partial differential equations. In *Advance In Computer Methods For Partial Differential Equations*, vol. V. Vichnevetsky R and Stepleman RS (eds). Publ. IMACS, 1984.

Kolmogorov NN. The local structure of turbulence in incompressible viscous fluid for very large Reynolds number. *Dokl. Akad. Nauk SSSR* 1941; **30**:9–13. Reprinted in *Proc. R. Soc. London A* 1991; **434**:9–13.

Lallemand MH and Dervieux A. A multigrid finite-element method for solving the two-dimensional Euler equations. In *Proceedings of the Third Copper Mountain Conference on Multigrid Methods*, Lecture Notes in Pure and Applied Mathematics, McCormick SF (ed.). Marcel Dekker: Copper Mountain, New York, 1987; 337–363.

Lallemand MH, Steve H and Dervieux A. Unstructured multigridding by volume aggregation: current status. *Comput. Fluids* 1992; **21**:397–433.

Landsberg AM, Boris JP, Sandberg W and Young TR. Naval Ship Superstructure design: complex three-dimensional flows using an efficient, parallel method. High Performance Computing 1993: Grand Challenges in Computer Simulation, 1993.

Lax PD. Hyperbolic Systems of Conservation Laws. *SIAM Reg. Ser. Appl. Math.* 1973b; **II**.

Lax PD and Wendroff B. Systems of Conservation Laws. *Commun. Pure. Appl. Math.* 1960; **13**:217–237.

Leoviriyakit K and Jameson A. *Aerodynamic shape optimization of wings including planform variations*. AIAA Paper 2003-0210. In 41st Aerospace Sciences Meeting & Exhibit, Reno, 2003.

Leoviriyakit K and Jameson A. *Aero-structural wing planform optimization*. AIAA Paper 2004-0029. In 42nd Aerospace Sciences Meeting & Exhibit, Reno, 2004.

Leoviriyakit K, Kim S and Jameson A. *Viscous aerodynamic shape optimization of wings including planform variables*. AIAA Paper 2003-3498. In 21st Applied Aerodynamics Conference, Orlando, 2003.

Leschziner MA. Turbulence modeling for aeronautical flows. Von Karman Institure Lecture Series 2003 02, 2003.

Liebeck RH. *Design of the blended-wing-body subsonic transport*. AIAA Paper 2002-0002. In Wright Brothers Lecture, Reno, 2002.

Liepmann HW and Roshko A. *Elements of Gas Dynamics*. Wiley, 1957. Reprinted by Dover, 2001.

Lighthill MJ. A new method of two dimensional aerodynamic design. R and M 1111, Aeronautical Research Council, 1945.

Lions JL. *Optimal Control of Systems Governed by Partial Differential Equations*. Springer-Verlag: New York, 1971 Translated by S.K. Mitter.

Liou M-S and Steffen CJ. A new flux splitting scheme. *J. Comput. Phys.* 1993; **107**:23–39.

Liu F and Jameson A. *Multigrid Navier–Stokes calculations for three-dimensional cascades*. AIAA Paper 92-0190. In AIAA 30th Aerospace Sciences Meeting, Reno, 1992.

Liu XD, Osher S and Chan T. Weighted essentially schemes. *J. Comput. Phys.* 1994; **115**:200–212.

Lohner R and Parikh P. Generation of three-dimensional unstructured grids by the advancing front method. AIAA Paper 88-0515. In *26th Aerospace Sciences Meeting*, Reno, January, 1988.

MacCormack RW. *Current status of numerical solutions of the Navier–Stokes equations*. AIAA Paper 85-0032. In AIAA 23rd Aerospace Sciences Meeting, Reno, 1985.

MacCormack RW. *A new implicit algorithm for fluid flow*. AIAA Paper. In Proceedings of AIAA 13th CFD Conference, Snowmass, 1997.

MacCormack RW and Paullay AJ. *Computational efficiency achieved by time splitting of finite difference operators*. AIAA Paper 72-154. In AIAA 33rd Aerospace Sciences Meeting, 1972.

Majda A and Osher S. Numerical viscosity and the entropy condition. *Commun. Pure Appl. Math.* 1979; **32**:797–838.

Martinelli L and Jameson A. Validation of a multigrid method for the Reynolds averaged equations. AIAA Paper 88-0414. In *26th Aerospace Sciences Meeting & Exhibit*, Reno, January, 1988.

Martinelli L, Jameson A and Malfa E. Numerical simulation of three-dimensional vortex flows over delta wing configurations. In *Proceedings of the 13th International Conference on Numerical Methods in Fluid Dynamics*, Napolitano M and Solbetta F (eds). Rome, Italy; Springer-Verlag, 1993; 534–538.

Mavriplis DJ. *Multigrid strategies for viscous flow solvers on anisotropic unstructured meshes*. AIAA Paper 97-1952. In AIAA 13th Computational Fluid Dynamics Conference, Snowmass, 1997.

Mavriplis DJ and Jameson A. Multigrid solution of the Navier–Stokes equations on triangular meshes. *AIAA J.* 1990; **28**(8):1415–1425.

Mavriplis DJ and Martinelli L. *Multigrid solution of compressible turbulent flow on unstructured meshes using a two-equation model*. AIAA Paper 91-0237. In AIAA 29th Aerospace Sciences Meeting, Reno, 1991.

Mavriplis DJ and Venkatakrishnan V. A 3D Agglomeration Multigrid Solver for the Reynolds-Averaged Navier–Stokes Equations on Unstructured Meshes. *Int. J. Numer. Methods Fluids* 1996; **23**:1–18.

McFadden GB. An Artificial Viscosity Method for the Design of Supercritical Airfoils. Internal Report, and PhD thesis C00-3077-158, New York University, 1979.

McMullen MS. The Application of Non-Linear Frequency Domain Methods to the Euler and Navier–Stokes Equations. PhD thesis, Stanford University, Stanford, 2003.

McMullen MS, Jameson A and Alonso JJ. *Application of nonlinear frequency domain solver to the Euler and Navier–Stokes equations*. AIAA Paper 2002-0120. In 40th Aerospace Sciences Meeting & Exhibit, Reno, 2002.

Melson ND, Sanetrik MD and Atkins HL. *Time-accurate Navier–Stokes calculations with multigrid acceleration*. In Proceedings of the Sixth Copper Mountain Conference on Multigrid Methods, Copper Mountain, 1993.

Melton JE, Pandya SA and Steger JL. 3D Euler flow solutions using unstructured Cartesian and prismatic grids. AIAA Paper 93-0331. In *31st Aerospace Sciences Meeting*, Reno, January, 1993.

Morawetz CS. On the non-existence of continuous transonic flows past profiles: Part 1. *Pure Appl. Math.* 1956; **9**:45–68.

Mulder WA. A new multigrid approach to convection problems. *J. Comput. Phys.* 1989; **83**:303–323.

Mulder WA. A high-resolution Euler solver based on multigrid, semi-coarsening, and defect correction. *J. Comput. Phys.* 1992; **100**:91–104.

Murman EM. Analysis of Embedded shocks waves calculated by relaxation methods. *AIAA J.* 1974; **12**:626–633.

Murman EM and Cole JD. Calculation of plane, steady, transonic flows. *AIAA J.* 1971; **9**:114–121.

Ni RH. A multiple grid scheme for solving the Euler equations. *AIAA J.* 1982; **20**:1565–1571.

Obayashi S and Kuwakara K. *LU factorization of an implicit scheme for the compressible Navier–Stokes equations*. AlAA Paper 84-1670. In AIAA 17th Fluid Dynamics and Plasma Dynamics Conference, Snowmass, 1984.

Obayashi S, Matsukima K, Fujii K and Kuwakara K. *Improvements in efficiency and reliability for Navier–Stokes computations using the LU-ADI factorization algorithm*. AlAA Paper 86-0338. In AIAA 24th Aerospace Sciences Meeting, Reno, 1986.

Osher S. Riemann solvers, the entropy condition, and difference approximations. *SIAM J. Numer. Anal.* 1984; **121**:217–235.

Osher S and Chakravarthy S. High resolution schemes and the entropy condition. *SIAM J. Numer. Anal.* 1984; **21**:955–984.

Osher S and Solomon F. Upwind difference schemes for hyperbolic systems of conservation laws. *Math. Comp.* 1982; **38**:339–374.

Osher S and Tadmor E. On the convergence of difference approximations to scalar conservation laws. *Math. Comp.* 1988; **50**:19–51.

Paillère H and Deconinck H. 1995 A Review of Multi-Dimensional Upwind Residual Distribution Schemes for the Euler Equations. In Hafez M and Oshima K (eds.), *Computational Fluid Dynamics Review 1995*, pp. 141–160. Wiley.

Parthasarathy V, Kallinderis Y and Nakajima K. *A hybrid adaptation method and directional viscous multigrid with prismatic-tetrahedral meshes*. AIAA Paper 95-0670. In AIAA 33rd Aerospace Sciences Meeting, Reno, 1995.

Peraire J, Peirö J and Morgan K. *A 3D finite-element multigrid solver for the Euler equations*. AIAA Paper 92-0449. In AIAA 30th Aerospace Sciences Conference, Reno, 1992.

Pierce NA and Giles MB. *Preconditioning compressible flow calculations on stretched meshes*. AIAA Paper 96-0889. In AIAA 34th Aerospace Sciences Meeting, Reno, 1996.

Pierce NA and Giles MB. Preconditioning compressible flow calculations on stretched meshes. *J. Comput. Phys.* 1997; **136**:425–445.

Pierce NA, Giles MB, Jameson A and Martinelli L. Accelerating three-dimensional Navier–Stokes calculations. AIAA Paper 97-1953. In AIAA 13th Computational Fluid Dynamics Conference, Snowmass, 1997.

Pironneau O. *Optimal Shape Design for Elliptic Systems*. Springer-Verlag: New York, 1984.

Pironneau O. *Optimal Shape Design for Aerodynamics*. AGARD FDP/Von Karman Institute Lecture Notes on Optimum Design Methods in Aerodynamics. AGARD Report 803, 1994; 6-1–6-40.

Powell KG and van Leer B. *A genuinely multidimensional upwind cell-vertex scheme for the Euler equations*. AIAA Paper 89-0095. In AIAA 27th Aerospace Sciences Meeting, Reno, 1989.

Prandtl L. *On Fluid Mothion with Very Small Friction*. Heidelberg Mathematical Congress: Heidelberg, 1904.

Prandtl L and Tietjens OG. *Applied Hydro and Aerodynamics*. Dover Publications, 1934. Reprinted by Dover, 1987.

Pulliam TH and Steger JL. *Recent improvements in efficiency, accuracy and convergence for implicit approximate factorization algorithms*. AIAA Paper 85-0360. In AIAA 23rd Aerospace Sciences Meeting, Reno, 1985.

Radespiel R, Rossow C and Swanson RC. *An efficient cell-vertex multigrid scheme for the three-dimensional Navier–Stokes equations*. AIAA Paper 89-1953-CP. In Proceedings of AIAA 9th Computational Fluid Dynamics Conference, Buffalo, 1989; 249–260.

Rao SV and Deshpande SM. *A Class of Efficient Kinetic Upwind Methods for Compressible Flows*. Report 91 FM 11, Indian Institute of Science, 1991.

Reuther J and Jameson A. *Aerodynamic shape optimization of wing and wing-body configurations using control theory*. AIAA Paper 95-0213. In AIAA 33rd Aerospace Sciences Meeting and Exhibit, Reno, 1995.

Rieger H and Jameson A. *Solution of steady three-dimensional compressible Euler and Navier–Stokes equations by and implicit LU scheme*. AIAA Paper 88-0619. In AIAA 26th Aerospace Sciences Meeting, Reno, 1988.

Rizzi A and Viviand H. *Numerical methods for the computation of inviscid transonic flows with shock waves*. In Proceedings of GAMM Workshop, Stockholm, 1979.

Roberts TW, Sidilkover D and Swanson RC. *Textbook multigrid efficiency for the steady Euler equations*. AIAA Paper 97-1949. In AIAA 13th Computational Fluid Dynamics Conference, Snowmass, 1997.

Roe PL. Approximate Riemann Solvers, Parameter Vectors, and Difference Schemes. *J. Comput. Phys.* 1981; **43**:357–372.

Roman DL, Allen JB and Liebeck RH. *Aerodynamic design challenges of the blended-wing-body subsonic transport*. AIAA Paper 2000-4335, Denver, 2000.

Rubbert PE. In *The Boeing Airplanes that have benefited from Antony Jameson's CFD Technology*, Caughey DA and Hafez MM (eds). John Wiley and Sons, 1994.

Rubbert PE and Saaris GR. 1968 A general three dimensional potential flow method applied to V/STOL aerodynamics. SAE Paper 680304.

Samant SS, Bussoletti JE, Johnson FT, Burkhart RH, Everson BL, Melvin RG, Young DP, Erickson LL and Madson MD. TRANAIR: A computer code for transonic analyses of arbitrary configurations. AIAA Paper 87-0034. In *25th Aerospace Sciences Meeting*, Reno, January, 1987.

Sawada K and Takanashi S. A numerical investigation on wing/nacelle interferences of USB configuration. AIAA Paper 87-0455. In *AIAA 25th Aerospace Sciences Meeting*, Reno, 1987.

Schlichting H and Gersten K. *Boundary Layer Theory*. Springer-Verlag, 1999 eight english edn.

Sears WD. On projectiles of minimum drag. *Q. Appl. Math.* 1947; **4**:361–366.

Shu CW and Osher S. Efficient implementation of essentially non-oscillatory shock-capturing schemes. *J. Comput. Phys.* 1988; **77**:439–471.

Sidilkover D. *Multi-dimensional Upwinding and Multigrid*. AIAA Paper 95-1759. In AIAA 12th Computational Fluid Dynamics Conference, San Diego, 1995.

Sidilkover D. *Some Approaches Towards Constructing Optimally Efficient Multigrid Solvers for the Inviscid Flow Equations*. ICASE Report 97-39, ICASE, 1997.

Smith RE. *Three-dimensional algebraic mesh generation*. AIAA Paper 83-1904. In Proceedings of AIAA 6th Computational Fluid Dynamics Conference, Danvers, 1983.

Sorenson RL. Elliptic generation of compressible three-dimensional grids about realistic aircraft. In *International Conference on Numerical Grid Generation in Computational Fluid Dynamics*, Hauser J and Taylor C (eds). Landshut, F.R.G., 1986.

Sorenson RL. Three-dimensional elliptic grid generation for an F-16. In *Three-Dimensional Grid Generation for Complex Configurations: Recent Progress*, Steger JL and Thompson JF (eds). AGARDOGRAPH AG 309, 1988.

Steger JL and Chaussee DS. Generation of body-fitted coordinates using hyperbolic partial differential equations. *SIAM J. Sci. Stat. Comput.* 1980; **1**:431–437.

Steger JL and Warming RF. Flux vector splitting of the inviscid gas dynamic equations with applications to finite difference methods. *J. Comput. Phys.* 1981; **40**:263–293.

Swanson RC and Turkel E. On central-difference and upwind schemes. *J. Comput. Phys.* 1992; **101**:297–306.

Sweby PK. High resolution schemes using flux limiters for hyperbolic conservation laws. *SIAM J. Numer. Anal.* 1984; **21**:995–1011.

Ta'asan S. *Canonical Forms of Multidimensional, Steady Inviscid Flows*. ICASE Report 93-34, Institute for Computer Applications in Science and Engineering: Hampton, 1993.

Ta'asan S, Kuruvila G and Salas MD. 1992 *Aerodynamic Design and Optimization in One Shot*. AIAA Paper 92-005, 30th Aerospace Sciences Meeting and Exibit, Reno, NV.

Tadmor E. 1984 Numerical Viscosity and the Entropy Condition for Conservative Difference Schemes. *Math. Comp.* **32**:369–382.

Tatsumi S, Martinelli L and Jameson A. *A new high resolution scheme for compressible viscous flows with shocks*. AIAA Paper to appear. In AIAA 33nd Aerospace Sciences Meeting, Reno, 1995.

Theodorsen T. Theory of Wing Sections of Arbitrary Shape, NACA TR 411, 1931.

Thompson JF, Thames FC and Mastin CW. Automatic numerical generation of body-fitted curvilinear coordinate system for field containing any number of arbitrary two-dimensional bodies. *J. Comput. Phys.* 1974; **15**:299–319.

Thompson JF, Warsi ZUA and Mastin CW. Boundary-fitted coordinate systems for numerical solution of partial differential equations: a review. *J. Comput. Phys.* 1982; **47**:1–108.

Turkel E. Preconditioned methods for solving the incompressible and low speed equations. *J. Comput. Phys.* 1987; **72**:277–298.

Turkel E. Preconditioning-squared methods for multidimensional aerodynamics. AIAA Paper 1997-2025. In *AIAA 13th Computational Fluid Dynamics Conference*, Snowmass Village, June, 1997.

Van Dyke MD. *Perturbation Methods in Fluid Mechanics*. Academic Press, 1964.

Van Leer B. Towards the ultimate conservative difference scheme. II. Monotonicity and conservation combined in a second order scheme. *J. Comput. Phys.* 1974; **14**:361–370.

Van Leer B. Flux Vector splitting for the Euler equations. In *Proceedings of the 8th International Conference on Numerical Methods in Fluid Dynamics*, Krause E (ed.). Springer-Verlag: Aachen, 1982; 507–512.

Van Leer B. Progress in multi-dimensional upwind differencing. In *Proceeding of the 13th International Conference on Numerical Methods in Fluid Dynamics*, Rome, Napolitano M and Solbetta F (eds.). Springer-Verlag, Rome, 1993; 1–26.

Van Leer B, Lee WT and Roe PL. Characteristic time stepping or local preconditioning of the Euler equations. AIAA Paper 91-1552. In *AIAA 10th Computational Fluid Dynamics Conference*, Honolulu, 1991.

Vassberg J. *A fast surface-panel method capable of solving million-element problems*. AIAA Paper 1997-0168. 35th AIAA Aerospace Sciences Meeting & Exhibit, Reno, 1997.

Venkatakrishnan V. *Newton Solution of Inviscid and Viscous Problems*. AIAA Paper 88-0413. AIAA 26th Aerospace Sciences Meeting, Reno, 1988.

Venkatakrishnan V. *Convergence to steady state solutions of the Euler equations on unstructured grids with limiters*. AIAA Paper 93-0880. In AIAA 31st Aerospace Sciences Meeting, Reno, 1993.

Venkatakrishnan V. A perspective on unstructured grid flow solvers. *AIAA J.* 1996; **34**:533–547.

Venkatakrishnan V and Mavriplis DJ. Implicit method for the computation of unsteady flows on unstructured grids. *J. Comput. Phys.* 1996; **127**:380–397.

Volpe G and Melnik RE. The design of transonic aerofoils by a well posed inverse method. *Int. J. Numer. Methods Eng.* 1986; **22**:341–361.

Voronoi G. Nouvelles applications des parametres continus a la theorie des formes quadratiques. Deuxieme Memoire: recherches sur les parallelloedres primitifs. *J. Reine Angew. Math.* 1908; **134**:198–287.

Wada Y and Liou M-S. *A flux splitting scheme with high-resolution and robustness for discontinuities*. AIAA Paper 94-0083. In AIAA 32nd Aerospace Sciences Meeting, Reno, 1994.

Warming RF, Beam RM and Hyett BJ. Diagonalization and simultaneous symmetrization of the gas dynamic equations. *Math. Comp.* 1975; **29**:1037–1045.

Weatherill NP and Forsey CA. Grid generation and flow calculations for aircraft geometries. *J. Aircraft* 1985; **22**:855–860.

Weiss JM and Smith WA. Preconditioning applied to variable and constant density flows. *AIAA J.* 1995; **33**(11):2050.

Whitcomb RT. *A Study of the Zero Lift Drag-Rise Characteristics of Wing-Body Combinations Near the Speed of Sound*. NACA Report TR 1273, 1956.

Whitcomb RT. *Review of NASA supercritical airfoils*. In 9th ICAS Congress, No. 74-10, Haifa, 1974.

Whitcomb RT. *A Design Approach and Selected Wind Tunnel Results at High Subsonic Speeds for Wing-Tip Mounted Winglets*. NASA Report TN D8260, 1976.

Wilcox DC. *Turbulence Modelling of CFD*. DCW Industries: La Canada, 1998.

Woodward P and Colella P. The numerical simulation of two-dimensional fluid flow with strong shocks. *J. Comput. Phys.* 1984; **54**:115–173.

Yee HC. *On symmetric and upwind TVD schemes*. In Proceedings of the 6th GAMM Conference on Numerical Methods in Fluid Mechanics, Gottingen, 1985a.

Yee HC. *On symmetric and upwind TVD schemes*. Proceedings of the 6th GAMM Conference on Numerical Methods in Fluid Mechanics, Gottingen, 1985b.

Yoon S and Jameson A. *Lower-upper symmetric-Gauss-Seidel method for the Euler and Navier–Stokes equations*. AIAA Paper 87-0600. In AIAA 25th Aerospace Sciences Meeting, Reno, 1987.

Zalesak ST. Fully multidimensional flux-corrected transport algorithms for fluids. *J. Comput. Phys.* 1979; **31**:335–362.